

**Novel Double Cantilever Beam experiments and related evaluation
methods to investigate the fracture behaviour of adhesive layers in
modes I and III**

Dissertation

zur

Erlangung des akademischen Grades des
Doktors der Ingenieurwissenschaften (Dr.-Ing.)

dem

Promotionszentrum für Ingenieurwissenschaften
des Forschungscampus Mittelhessens

vorgelegt von

Peer Schrader, M.Sc.

aus Rabenau

Gießen 2022

Abstract

This cumulative dissertation consists of four manuscripts dealing with the fracture mechanics testing of adhesive layers in pure loading modes I and III. Different Double Cantilever Beam (DCB) test specimens are used to investigate the energy release rate and cohesive traction of rigid, epoxy-based and soft, rubber-based adhesive systems under different boundary conditions. New test setups and evaluation methods are developed to gain a better understanding of the fracture behaviour of these adhesive joints and to investigate the influence of different evaluation methods on the results.

In order to investigate the fracture behaviour of epoxy-based bonded joints, the Out-of-plane Loaded Double Cantilever Beam (ODCB) test was extended to higher loading rates, which, with the help of a local strain measurement, allowed the determination of fracture energy and cohesive traction in mode III at increased loading rates for the first time. However, it became apparent that ODCB tests, which have to be carried out in a bi-axial testing machine, are probably not suitable for testing under impact. Hence, uni-axial test rigs were developed to enable mode III testing of such adhesive joints. These were carried out quasi-statically to investigate the influence of different evaluation methods in more detail.

The rate-dependent fracture behaviour of soft, rubber-like adhesives was also investigated, which includes both a creep load in pure mode I and an investigation at increased loading rates in modes I and III. For the investigation under creep loading, a method is proposed which allows the control of the tests on constant J -integral. In addition, the influence of the material behaviour within the process zone is examined in more detail, as this influences both the creep behaviour and the cohesive stresses and their evaluation methods. For the determination of the cohesive traction, a new method is developed within the scope of the work, which is based on the strain measurement along with the adherends and thereby enables a determination of the dependence of the cohesive stresses on the loading rate along the entire adhesive layer. A comparison with the conventional method of determining the cohesive traction from the derivative of the energy release rate with respect to the crack opening displacement showed that the currently applied method may deliver inadequate results.

The results of this work thus extend the state of the state of research and in doing so demonstrate new methods that can be used in DCB tests in modes I and III to provide new insights into the fracture behaviour of adhesively bonded joints.

Kurzfassung

Die vorliegende kumulative Dissertation besteht aus vier Manuskripten, welche sich mit der bruchmechanischen Prüfung von Klebschichten in den reinen Belastungsmoden I und III beschäftigen. Es werden unterschiedliche Double Cantilever Beam (DCB) Prüfkörper verwendet, um damit die Energiefreisetzungsrate und die kohäsiven Spannungen von steifen, epoxidharzbasierten und weichen, gummiartigen Klebstoffsystemen unter verschiedenen Randbedingungen zu untersuchen. Dabei werden neue Versuchsaufbauten und Auswertemethoden entwickelt, um ein besseres Verständnis für das Bruchverhalten dieser Klebverbindungen zu erhalten und den Einfluss von verschiedenen Auswertemethoden auf die Ergebnisse zu untersuchen.

Um das Bruchverhalten von epoxybasierten Klebverbindungen zu untersuchen, wurde der Out-of-plane loaded Double Cantilever Beam (ODCB) Versuch auf höhere Belastungsraten erweitert, was die Bestimmung von Bruchenergie und kohäsiven Spannungen im Mode III bei höheren Belastungsraten unter Zuhilfenahme einer lokalen Dehnungsmessung erstmals ermöglichte. Da sich hierbei aber zeigte, dass der ODCB Versuch, welcher in einer bi-axialen Prüfmaschine durchgeführt werden muss, für eine Untersuchung unter Impakt vermutlich nicht geeignet ist, wurden uniaxiale Versuchsstände entwickelt, die eine Mode III Prüfung solcher Klebverbindungen ermöglichen sollen. Zunächst wurden diese quasi-statisch durchgeführt und der Einfluss von verschiedenen Auswertemethoden genauer untersucht.

Ebenso wurde das ratenabhängige Bruchverhalten von weichen, gummiartigen Klebstoffen untersucht, was sowohl eine Untersuchung unter Kriechbelastung im reinen Mode I als auch eine Untersuchung bei höheren Belastungsraten in den Moden I und III beinhaltet. Für die Untersuchung unter Kriechbelastung wird eine Methode vorgeschlagen, welche eine Regelung der Versuche auf ein konstantes J -integral ermöglicht. Zudem wird der Einfluss des Materialverhaltens innerhalb der Prozesszone näher beleuchtet, da diese sowohl das Kriechverhalten als auch die kohäsiven Spannungen und deren Evaluierungsmethoden beeinflusst. Zur Bestimmung der kohäsiven Spannungen wird im Rahmen der Arbeit eine neue Methode entwickelt, die auf der Dehnungsmessung entlang der Fügeiteile beruht und dabei eine Bestimmung der Abhängigkeit der kohäsiven Spannungen von der Belastungsrate entlang der ganzen Klebschicht ermöglicht. Ein Vergleich mit der konventionellen Methode zur Bestimmung der kohäsiven Spannungen über die Ableitung der Energiefreisetzungsrate nach der Rissöffnungsverschiebung zeigte, dass diese zur Zeit gängige Methode unzureichende Ergebnisse liefern könnte.

Die Ergebnisse dieser Arbeit erweitern also den Stand der Forschung und zeigen dabei neue Methoden auf, mit denen in DCB Versuchen in den Moden I und III neue Einblicke in das Bruchverhalten von Klebverbindungen ermöglicht werden.

Acknowledgements

This doctoral thesis was written at the Doctoral Center for Engineering Science of the Research Campus of Central Hessen under the supervision of the Justus-Liebig-University Gießen in cooperation with the University of Applied Sciences of Central Hessen (Technische Hochschule Mittelhessen) during my employment as a research associate at the Institute of Mechanics and Materials. I wish to briefly thank all those who have accompanied me on this journey:

Firstly, I wish to express my gratitude towards Prof. Dr.-Ing. Stephan Marzi, who gave me the chance to pursue a doctorate in the first place and has always supported and challenged me to improve professionally. I want to thank Prof. Dr. Sangam Chatterjee for his supervision and support of the PhD project. I wish to also express my gratitude towards the members of the audit committee, namely Prof. Dr.-Ing. Beate Lauterbach and Prof. Dr. André Schirmeisen. I would also like to thank the team of the Research Campus of Central Hessen – particularly Dr. Janina Rojek –, who provided help and advice with all organisational questions regarding the doctorate.

I'm really grateful for all my former supervisors, collaborators, and colleagues at the Institute of Mechanics and Materials, who were generally supportive, open for discussion, and fun to work with. My special thanks go to my peers at the work group of Prof. Marzi: Thank you Christopher, Dennis, Felix, Ihssane, Lukas, and Niklas – I enjoyed your company!

Finally, I would like to thank my friends and family for their understanding, solidarity and constant encouragement – especially my fiancé Svenja, who provided me with loving support during times of exhaustion. You all having my back and offering me places to retreat to means a lot to me!

Cheers!

Peer Schrader

Rabenau, November 2022

Affidavit

I declare that I have completed this dissertation single-handedly without the unauthorized help of a second party and only with the assistance acknowledged therein. I have appropriately acknowledged and cited all text passages that are derived verbatim from or are based on the content of published work of others, and all information relating to verbal communications. I consent to the use of an anti-plagiarism software to check my thesis. I have abided by the principles of good scientific conduct laid down in the regulations of the leading University which were delivered to me in carrying out the investigations described in the dissertation.

Rabenau, 2022

Peer Schrader

List of appended papers

This cumulative dissertation is based on the following scientific papers:

- **Paper A:**

P. Schrader, C. Schmand, S. Marzi: *Mode I creep fracture of rubber-like adhesive joints at constant crack driving force*. International Journal of Adhesion and Adhesives 113, <https://doi.org/10.1016/j.ijadhadh.2021.103079>, 2022.

- **Paper B:**

P. Schrader, S. Marzi: *Mode III testing of structural adhesive joints at elevated loading rates*. International Journal of Adhesion and Adhesives 113, <https://doi.org/10.1016/j.ijadhadh.2021.103078>, 2022.

- **Paper C:**

P. Schrader, D. Domladovac, S. Marzi: *Influence of loading rate on the cohesive traction for soft, rubber-like adhesive layers loaded in modes I and III*. Preprint submitted to International Journal of Adhesion and Adhesives, submitted April 21st, 2022.

- **Paper D:**

P. Schrader, S. Marzi: *Novel mode III DCB test setups and related evaluation methods to investigate the fracture behaviour of adhesive joints*. Preprint submitted to Theoretical and Applied Fracture Mechanics, submitted August 25th, 2022.

Contributions to co-authored papers

All papers were prepared in collaboration with co-authors. The author's contributions to the performed studies are detailed below:

- **Paper A:**

The specimens were manufactured by C. Schmandt and the author. The experiments were conducted by C. Schmandt and the author; the author was particularly responsible for the planning of the visual crack tip detection as well as the set-up and operation of the camera systems. All experimental results were solely evaluated by the author, including conceptualization and implementation of the image processing algorithms. The paper was planned and written by C. Schmandt and the author. S. Marzi was responsible for funding acquisition, supervised the work and proofread the paper.

- **Paper B:**

The author conceptualized, designed and built the test setup, manufactured the tested specimens, and planned and conducted the experiments. The development of the evaluation methods as well as the evaluation of the test data was performed by the author. The author planned and wrote the paper. S. Marzi was responsible for funding acquisition, supervised the work and proofread the paper.

- **Paper C:**

D. Domladovac and the author contributed equally to the work and share first authorship. The experimental setup was conceptualized and planned by D. Domladovac and the author. The author was responsible for specimen manufacturing. The optical fibres for the backface strain measurements were prepared by D. Domladovac. The experiments were performed by D. Domladovac and the author. The approach to the evaluation of the backface strain measurements was developed together with D. Domladovac, who then evaluated the backface strain measurements. The remaining data was analysed by the author. The paper was planned and written by D. Domladovac and the author. S. Marzi was responsible for funding acquisition, supervised the work and proofread the paper.

- **Paper D:**

The author conceptualized, designed and built the test setup, manufactured the tested specimens, and planned and conducted the experiments. The development of the evaluation methods as well as the evaluation of the test data was performed by the author. The author planned and wrote the paper. S. Marzi was responsible for funding acquisition, supervised the work and proofread the paper.

Contents

Abstract / Kurzfassung	I
Acknowledgements	III
Affidavit	IV
List of appended papers	V
Contributions to co-authored papers	VI
1 Introduction	1
1.1 Motivation	1
1.2 State of research	1
1.3 Achievements of this work	5
2 Theory	7
2.1 Irwin-Kies Equation	7
2.2 J-integral	8
2.3 Evaluation of the ERR in Double Cantilever Beam Tests	9
2.3.1 Double Cantilever Beam Test	9
2.3.2 Tapered Double Cantilever Beam Test	11
2.3.3 Out-of-plane loaded Double Cantilever Beam Test	12
2.4 Determination of cohesive laws in single mode loading	13
2.4.1 J-integral approach	13
2.4.2 Beam theory evaluation	14
3 Summary of appended papers	16
3.1 Paper A	16
3.2 Paper B	17
3.3 Paper C	19
3.4 Paper D	21
4 Conclusions and perspectives	24
References	26
Appended papers	34
Paper A	34
Paper B	44
Paper C	54
Paper D	70

1 Introduction

In the mobility sector, the design goal of weight reduction to improve the fuel efficiency of vehicles has become particularly important in recent years. One option of reducing weight that is increasingly being implemented in series-produced vehicles is the use of adhesive joints instead of conventional mechanical fasteners. Next to weight reduction possibilities, adhesive joints have some additional advantages: Because of their ability of joining dissimilar materials cost effectively, according to a white paper of the Center for Automotive Research [1], adhesive joints may even overtake the percentage of all other joints, e.g., spot welds, screws, bolting, or rivets, in a vehicle by the mid-to-late 2020's. Furthermore, the increased energy dissipation of adhesive layers during fracture in comparison to other mechanical fasteners, which potentially increases the passenger safety in the event of a crash, is a considerable advantage. For the extensive use of adhesively bonded joints in industrial practice and the prediction of component failure, their fracture behaviour must be thoroughly investigated and prepared for use in numerical simulations.

1.1 Motivation

As an elementary prerequisite for the failure prediction of adhesive joints in industrial practice, suitable experimental methods are necessary that both allow fracture mechanical testing under different load conditions and the abstraction of relevant data such as fracture energy or traction separation relations. For the fracture modes I and II in particular, a significant number of methods are available which have been applied primarily to epoxy-based adhesives. So far, comparatively fewer methods have been proposed for the investigation in pure mode III. Furthermore, soft, rubber-like adhesive joints have so far been investigated rarely, although it is argued that these have important advantages in comparison to epoxy-based adhesive joints concerning damping, fatigue, crack resistance, and impact [2]. Considering flexible adhesives, it also must be clarified to what extent the established methods predominantly developed for epoxy-based adhesives can be applied to such more ductile and rate-sensitive adhesive systems.

For fracture mechanical investigations of adhesive layers in mode I, Double Cantilever Beam (DCB) specimens are used very commonly as there exist standardised testing procedures akin to ISO 25217 [3]. Generally, DCB specimens are easy to manufacture and offer many loading configurations that, depending on the case of use, bare experimental advantages for testing both epoxy-based and rubber-like adhesive systems. Furthermore, as will be summarized shortly, there exist some methods that also allow mode III testing using DCB specimens. Therefore, the main focus of this work is the further development of experimental and evaluation methods that allow the characterisation of the fracture mechanical behaviour of adhesively bonded joints using DCB specimens in fracture modes I and III.

1.2 State of research

In the following, the state of research shall be highlighted briefly, with an emphasis on fracture mechanical testing of adhesive layers in peel and shear. Furthermore, the state of research regarding the extraction of cohesive laws, i.e., the nominal stresses at the crack tip, from the experimental data, and the influence of data reduction schemes on the obtained results shall be addressed:

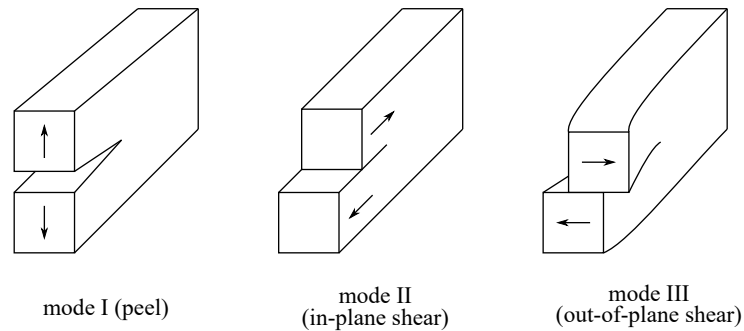


Figure 1.1 – Classical fracture modes I, II, and III that can be applied to a crack

Fracture modes. A crack can experience three types of loading (and combinations thereof), which are illustrated in Fig. 1.1. In mode I, the load is applied normal to the crack plane, opening the crack (peel loading). An in-plane shear deformation is denoted as mode II loading, leading to the crack planes sliding with respect to another. Out-of-plane shear is referred to as mode III loading. As stated by Chaves et al. [4], for a bulk material, the crack will tend to grow in mode I regardless of original orientation, whereas, when investigating adhesive layers, the crack growth will be constrained by the adherends, forcing the crack to propagate in mixed-mode (or shear, respectively).

Concepts of fracture mechanics. Generally, fracture mechanics offers various concepts to investigate the fracture behaviour of materials, oftentimes aiming to describe the loading state at the crack tip using single parameters. To put it briefly, such parameters can be obtained from concepts of Linear Elastic Fracture Mechanics (LEFM) under the assumption of linear-elastic material behaviour, e.g., the stress intensity factors from the K -concept or the critical Griffith strain Energy Release Rate (ERR) from the G -concept, or Non-Linear Elastic Fracture Mechanics (NLEFM) under the assumption of non-linear elastic material behaviour, e.g., via the J -integral. It shall be noted that, in the following, the term LEFM generally refers to the G -concept for the sake of brevity. The usage of the K -concept is more common in the fracture mechanical investigation of bulk materials but rarely employed during the investigation of adhesives because the energetic criterion G , according to Kinloch [5], has physical meaning related to the energy absorption during fracture and the stress intensity factors are difficult to obtain experimentally for adhesive layers, especially when the crack grows near the interface.

Testing in pure mode I. Mode I loading is generally considered as the critical load case for adhesive joints – and is also most practicable to investigate experimentally –, wherefore mode I fracture of adhesive joints is studied in most cases, with the DCB, Tapered Double Cantilever Beam (TDCB) and wedge tests being abundantly used in practice and standardised in ISO 25217 [3] and ISO 11343 [6], respectively. This leads to a large variety of studies quasi-statically investigating mode I fracture using both evaluation methods of LEFM, e.g., [7], and NLEFM, e.g., [8–11]. As will be shown shortly, creep and impact fracture behaviour are also investigated in mode I most commonly.

Quasi-static testing under shear loads. For shear testing, mode II fracture is most commonly examined in recent literature. According to Banea et al. [12], the most suitable mode II test is the End-notched Flexure (ENF) test, which is standardised for composite materials in ASTM D 7905 [13] and prominently used in literature for testing adhesives, both employing data reduction schemes from LEFM, e.g., [14], and NLEFM, e.g., [9, 15–17]. Next to the ENF tests, the End-loaded split test, e.g., [18], the End-Loaded shear joint [19, 20] or the test setup by Watson et al. [21] shall be mentioned. Chavez et al. [4] note a general lack in the fracture mechanics characterization of mode II. The lack of research is certainly even more severe considering the pure mode III fracture of adhesive layers, as only few studies are available: After

the pioneering works of Mai [22], Chai [23], and Donaldson [24] in the 1970s and 80s, mode III testing fell out of experimental focus. The mode III failure of wood and composites began being re-investigated by, e.g., Yoshihara [25], Davidson and Sediles [26], and Johnston [27], with all of the mentioned studies employing data reduction schemes based on LEFM or finite element analysis. Stigh et al. [28] developed the Split double Cantilever Beam (SCB) test, with which they were able to investigate the mode III fracture of a structural adhesive tape using a J -integral evaluation method and obtained cohesive laws from the measurements for the first time. Shortly thereafter, Loh and Marzi [29] presented the Out-of-plane loaded Double Cantilever Beam (ODCB) test setup for investigating the mode III fracture of adhesive layers using the J -integral. Being designed for use in a bi-axial testing machine, the ODCB test was later adapted to also enable the investigation of arbitrary mixed-mode I+III loads [30–32] with the development of the so-called Mixed-Mode-Controlled Double Cantilever Beam (MC-DCB) test.

Mode II contributions in mode III testing. The works of Mai [22] and Donaldson [24] were criticised by Kinloch [5] and Martin [33], respectively, because the crack tip is influenced by mode II loads due to the out-of-plane width of the adhesive layer. This was also acknowledged by Loh and Marzi [30–32] when they expanded the ODCB test to mixed-mode investigations. They estimated this influence from a mode-decomposition of the external loads in their MC-DCB tests and found that the influence was of negligible magnitude in the experimental investigations at the start of crack propagation for both epoxy-based and rubber-like adhesive layers. Bödeker and Marzi [34] investigated the influence of the mode II contribution in a simulative study and found that the mode II contribution in the MC-DCB experiments does not influence the obtained cohesive traction significantly. Just recently, Biel et al. [35] also investigated this effect for SCB tests on wider paperboard layers and derived a method to adjust the mode III ERR for the mode II shear contribution from the initial shear stiffness of the material, width of the layer, and applied load point rotation. Their results also imply that, for small layer widths, this contribution can reasonably be assumed as negligible.

Comparability of mode II and mode III fracture. The experimental results of some studies, e.g., Fernlund et al. [36] and Chai [37], suggest that there may be no strict necessity of differentiating between mode II and mode III regarding the fracture behaviour of thin, isotropic materials such as adhesive layers in the first place. However, it should be highlighted that the mode III examination may be more suitable in some cases, especially when investigating the ductile adhesive layers that exhibit finite deformations at the crack tip before the initiation of crack growth. This is undermined by the results of Boutar et al. [14], who, when investigating a flexible adhesive system with layer thicknesses up to 2 mm, had to rely on a graphical evaluation of the failure load to estimate the ERR in ENF tests due to plastification of the adherends and limited visibility of the propagating crack. In contrast, using the ODCB test setup, Loh and Marzi [31] were able to directly measure the ERR and observe crack growth even for thicker rubber-like adhesive joints.

Creep fracture. Currently, there exists a limited amount of fracture mechanical studies about the creep rupture of adhesive bonds, whereas the bulk behaviour is investigated comparatively more often, e.g., [38, 39]. In the available studies in which the creep behaviour is investigated using fracture mechanics tests the mode I DCB test is used commonly. In DCB experiments, however, the Griffith ERR G depends on the current crack length. Hence, to achieve a constant ERR, in most of the conducted studies, the DCB specimens were geometrically modified and loaded using dead weights, or complex spring and wire constructions [40–42]. Notably, Plausinis and Spelt [43] loaded the DCB specimens with pure external bending moments, making G independent of crack length. The advantage of a constant ERR during crack growth can also be achieved in TDCB tests, which was employed by Moutou Pitti et al. [44] to investigate the mixed-mode I+II creep rupture of wood. Carneiro Neto et al. [45, 46] recently investigated the mode II creep fracture using ENF tests. A mathematical description of the rate-dependent mode I creep fracture under steady-state

crack propagation was recently developed by Márquez Costa et al. [47]. The mentioned experimental studies were exclusively conducted using LEFM data reduction schemes, making it more difficult to account for non-linearities related to the fracture behaviour of ductile adhesive layers. Furthermore, the fracture mechanical creep behaviour of soft, rubber-like adhesive layers has rarely been addressed experimentally.

Fracture at increased loading rates. According to Machado et al. [48], a considerable amount of studies has investigated the strain rate sensitivity of adhesives in bulk form. According to Borges et al. [49], the rate-dependency of the fracture energy of adhesive joints presents limited research, with an increased amount of studies investigating mode I fracture, e.g., [50–60]. Considering pure shear fracture of adhesive layers at increased loading rates, mode II investigations are available predominantly [61–64]. Sato and Marzi [65] state that conducting ENF tests under impact conditions is almost impossible and advocate for using the End-loaded shear joint for impact testing akin to Bas et al. [66]. Pennas et al. [67] investigated the rate-dependency of the critical mode III ERR of a composite material using LEFM data reduction schemes. Only recently, Borges et al. [49] and Dagorn et al. [68] were able to develop methods for the investigation of mixed-mode loading under impact. The pure mode III fracture behaviour of adhesive layers at increased loading rates including the extraction of cohesive laws, however, remained to be examined to the author’s knowledge.

Influence of data reduction schemes and crack length measurements. In most of the studies mentioned thus far, methods from LEFM were employed to investigate the fracture behaviour of adhesive joints. According to the findings of Stamoulis and Carrere [69], data reduction schemes based on LEFM could be problematic when investigating adhesive systems because of possibly non-negligible influences of viscoelastic and viscoplastic effects on the adhesives’ fracture behaviour. Furthermore, as found by Pérez-Galméz et al. [70] when testing composite materials using different experimental techniques in mode II, the obtained critical ERR from LEFM data reduction schemes varies depending on the test setup and evaluation method, whereas the J -integral evaluation was found to deliver a method-independent critical ERR. They mainly attributed this discrepancy to difficulties with crack length monitoring, which is often mandatory for applying LEFM data reduction schemes. It shall be noted that crack length monitoring, to this date, is often performed visually by the examiner, which, depending on the specimen configuration and loading mode, may introduce additional inaccuracies. To overcome this issue, some authors have already proposed methods to determine crack lengths automatically from captured images in mode I testing, e.g., [57, 71, 72], or measurements of the backface strain of the adherends, e.g., [73–76]. These solutions, however, come with increased experimental effort and rely on expensive equipment, making them problematic for usage in industrial practice. Sun and Blackman [72] concluded that, during mode I testing, the critical ERR determined by LEFM was in good agreement with the J -integral approach for brittle, toughened epoxy adhesive systems, whereas for a ductile adhesive, the critical ERR determined from LEFM was considered invalid by the authors due to a large discrepancy with the J -integral approach. In a later study [77], they found that a closer agreement between the LEFM and J -integral evaluation of the critical ERR is obtained if, for the evaluation of G , the crack length is extended to the position in the process zone of the adhesive where the beam root rotation becomes naught, which, however, is difficult to determine without using, e.g., digital image correlation techniques or backface strain measurements.

Experimental investigation of soft, rubber-like adhesive joints. In most of the mentioned studies, epoxy-based adhesives were investigated. The fracture mechanical behaviour of soft, polyurethane-based adhesive systems has been investigated much less, although these, as stated earlier, have advantages in comparison to epoxy-based adhesive joints concerning damping, fatigue, crack resistance, and impact [2]. Whereas the advantages of rubber-like adhesive layers may be beneficial in practical application, the finite deformations that these adhesives exhibit prior to fracture as well as their rate-dependent material and

fracture behaviour complicate the experimental investigation, requiring the development of suitable testing and evaluation methods. Probably because of these issues, rubber-like adhesive joints are, so far, almost exclusively investigated quasi-statically in pure mode I, e.g., [11, 78–80], with the exception of the works of Hasegawa et al. [81], Boutar et al. [14], Loh and Marzi [31], and Rosendahl [82], who also investigated pure shear and mixed-mode loading. The work of Rosendahl [82] additionally provides a holistic investigation of the bulk and fracture mechanical properties of rubber-like adhesives and develops a failure model using finite fracture mechanics. The rate-dependency of the ERR of rubber-like adhesive layers was investigated in mode I by Schmandt and Marzi [83, 84] and Sun et al. [59]. Under shear loads, the rate-dependent fracture behaviour of such adhesives remained to be addressed.

Extraction of traction separation relations. Generally, traction separation relations or cohesive laws are extracted from experimental data by taking the derivative of the measured ERR with respect to the Crack Opening Displacement (COD). This approach is deemed very pragmatic and has been employed in many of the aforementioned studies investigating epoxy-based adhesives in peel, shear, and mixed-mode testing, e.g., [8, 10, 28, 29]. The approach was also used for the mode I investigation of soft, rubber-like adhesive joints [11, 83, 84]. An extraction of the cohesive laws from shear tests on rubber-like adhesive layers has not been achieved as of yet. Additionally, the approach of Khayer Dastjerdi et al. [85] shall be mentioned, who developed a rigid DCB specimen that allows a direct measurement of cohesive laws in mode I. However, their approach is limited to thin adhesive layers, wherefore it is not deemed suitable for testing soft, rubber-like adhesive layers of larger thicknesses. As will be discussed later, especially for soft, rubber-like adhesive layers, the underlying theoretical assumptions for determining cohesive laws from the derivative of the ERR with respect to the COD could potentially be violated because of energy dissipation outside of the crack tip. Hence, an investigation of this issue is deemed beneficial for gaining a better insight into the fracture behaviour of such adhesive layers.

1.3 Achievements of this work

Building on the previous section, demand for research in the following topics can be extracted, which was addressed within the framework of this dissertation:

- The mentioned studies investigating creep fracture were exclusively conducted using LEFM data reduction schemes. To investigate the creep fracture of, e.g., soft, rubber-like adhesives, non-linearities in the fracture behaviour should be accounted for. Motivated by this, in **Paper A**, an experimental investigation of the creep fracture of a soft, rubber-like adhesive layer under constant applied J -integral was conducted for the first time.
- Considering rate-dependent shear fracture, experimental methods are needed for the evaluation of the ERR at increased loading rates for both testing of epoxy-based and rubber-like adhesive layers. Using ODCB setups in a bi-axial testing machine, **Paper B** and **Paper C** are the first works to develop evaluation methods for investigating the rate-dependency of mode III ERR and cohesive laws for an epoxy-based and a soft, rubber-like adhesive, respectively.
- Cohesive laws are generally evaluated by taking the derivative of the ERR with respect to the COD. Due to energy dissipation inside the process zone, underlying theoretical assumptions of this approach may be violated. In **Paper C**, a method is developed to, for the first time, measure the cohesive traction along with the complete adhesive layer under both peel and shear loading at various external loading rates. The proposed method allows determining rate-dependent traction separation laws along with the complete specimen, which, to the authors knowledge, has not yet been achieved elsewhere.

1 Introduction

- The experimental setup of the ODCB test requires a complex setup in a bi-axial testing machine. To overcome this issue, in **Paper D**, two mode III setups based on the DCB and TDCB tests are presented that can be performed in a uni-axial testing machine. Furthermore, the influence of the J -integral and LEFM data reduction schemes on the obtained ERR and cohesive laws is investigated holistically for mode III shear loading.

Hence, the results of this work expand the state of research in many respects and, in doing so, reveal novel mode I and mode III DCB testing and evaluation methods, which will certainly allow gaining further insight into the fracture behaviour of epoxy-based and rubber-like adhesive joints.

2 Theory

The present work is concerned with fracture mechanical testing of adhesive joints using DCB specimens in modes I and III, relying both on evaluation methods from LEFM and NLEFM. The following section shall provide a brief introduction into the basic concepts and the methods of evaluation used within the context of this work. Firstly, the Irwin-Kies equation (LEFM) shall be derived for an ideally brittle, linear elastic material, followed by the introduction of the non-linear elastic J -integral (NLEFM). Then, the application of these concepts to DCB specimens shall be discussed, allowing for a determination of the ERR from the load configurations applied to the specimens. At last, the theoretical background behind the determination of cohesive laws in single mode loading is presented.

2.1 Irwin-Kies Equation

The Griffith ERR G is defined as a measure for the energy causing an increment of crack extension in an ideally brittle, linear elastic material, which is given by the rate of change in potential energy Π with crack area A :

$$G = -\frac{d\Pi}{dA} \quad (2.1)$$

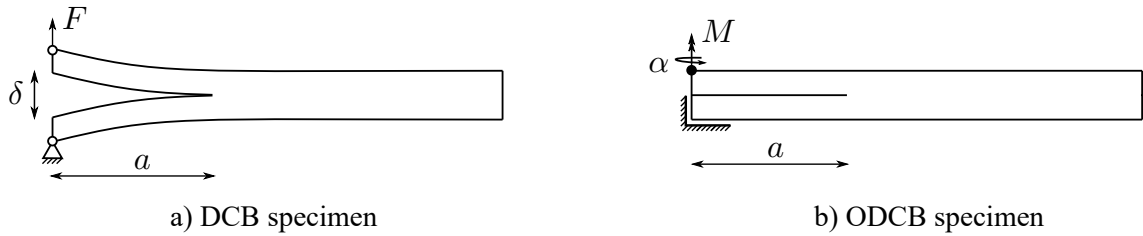


Figure 2.1 – DCB specimens loaded by external in-plane force and out-of-plane moment

Consider a DCB specimen with thickness b and an initial crack of length a that is loaded by constant external force F , i.e., under load control, leading to a displacement δ of the load introduction point as shown in Fig. 2.1a. The potential energy of the elastic body is given by the elastic energy stored in the body U and the work done by the external load W_{ext} as

$$\Pi = U - W_{\text{ext}} = \frac{1}{2}F\delta - F\delta = -\frac{F\delta}{2}. \quad (2.2)$$

Assuming that the crack extends infinitesimally by da under the constant applied force yielding a change in potential $d\Pi$ with the displacement $d\delta$, Eq. (2.1) yields:

$$G = \frac{F}{2b} \left(\frac{d\delta}{da} \right)_{F=\text{const.}} \quad (2.3)$$

2 Theory

By introducing the compliance C as the inverse of the specimens stiffness, i.e., $\delta = CF$, this can be rewritten as

$$G = \frac{F^2}{2b} \frac{dC}{da}, \quad (2.4)$$

yielding the well-known Irwin-Kies Equation [86]. Although omitted here, it can be shown that a generalised loading condition accounting for the compliance of the test machine also leads to Eq. (2.4). From the Irwin-Kies equation, the critical ERR can be determined experimentally from a measurement of the applied force F and the width of the adhesive layer b . However, the change of compliance with crack length dC/da cannot be determined easily without beam theory assumptions on the adherends' behaviour, which shall be briefly discussed in Sec. 2.3 and investigated in **Paper D**. It shall also be noted that dC/da is not constant during crack growth for most specimen configurations if loaded by an external force, necessitating a measurement of the current crack length.

It is also possible to compute the ERR for a specimen that is loaded by a constant applied moment M , leading to a load point rotation α (cf. Fig. 2.1b). In this case, the potential energy equates to

$$\Pi = W - W_{\text{ext}} = \frac{1}{2}M\alpha - M\alpha = -\frac{M\alpha}{2}, \quad (2.5)$$

which ultimately yields an ERR of

$$G = \frac{M}{2b} \left(\frac{d\alpha}{da} \right)_{M=\text{const.}} = \frac{M^2}{2b} \frac{dC}{da}. \quad (2.6)$$

This approach bears the significant advantage that, because the bending stiffness EI and, hence, the compliance are independent of crack length for a linear elastic beam, the change in compliance with crack length is constant when the specimen is loaded by a pure bending moment and only dependent on the elastic modulus and the geometry of the lever arms, i.e. $dC/da = 2/(EI)$.

It must generally be stated that LEFM ceases to be valid when plastic deformations of significant magnitude occur during fracture initiation. To correct for yielding at the crack tip, analyses were developed by, e.g., Dugdale [87] and Barenblatt [88], who established models based on narrow strips of yielded material at the crack tip and, as will be described later, provided the theoretical foundation for cohesive zone modeling.

2.2 J-integral

The J -integral, which was independently proposed by Rice [89] and Cherepanov [90] in the late 1960's, represents an alternative approach of determining the ERR. As they showed, the J -integral may also consider non-linear mechanical behaviour at the crack tip during fracture initiation.

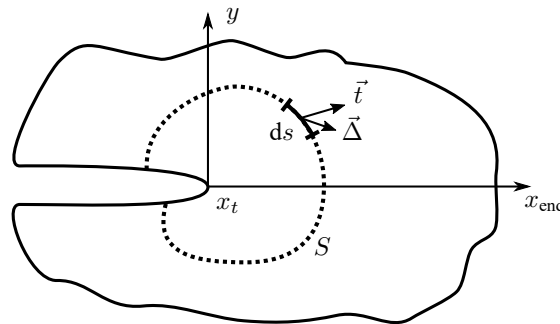


Figure 2.2 – Flat surfaced notch in two-dimensional deformation field

Following Rice's [89] notation, the J -integral of an arbitrary non-linear elastic body containing a crack tip that is subjected to a two-dimensional deformation field (cf. Fig. 2.2) is given as

$$J = \int_S \left(W dy - t_i \frac{\partial \Delta_i}{\partial x} ds \right) \quad (2.7)$$

where $W = \hat{W}(y)$ is the elastic energy density, t_i are the components of the (nominal) traction vector, and Δ_i are the components of the displacement vector. The coordinate axes x and y denote the direction of crack propagation and the normal to the direction of crack propagation, respectively. The J -integral is evaluated in the reference configuration along an arbitrary path S in counter-clockwise direction around the crack tip, with ds being an infinitesimal element of arc length on S . Generally, when applying the J -integral to a non-linear material to determine the ERR, the integration is performed over all inhomogeneities in the body. Hence, for non-linear-elastic media in which a crack tip of point-like shape is the only inhomogeneity, J is path-independent, yielding $J = 0$ for a closed integration curve S . Rice [89] showed in his paper that, by ideally treating elastic-plastic deformation as non-linear elastic, the J -integral can also be applied to elastic-plastic materials, provided that the material is loaded monotonically and plasticity occurs solely at the point-like crack tip. Hutchinson [91] and Rice and Rosengren [92] later showed that path-independence can also be proven for a plastic zone in which the stress and strain decrease hyperbolically with the distance to the crack tip, which retains validity if a power-law relationship between plastic strain and stress can be assumed.

The path-independence of the J -integral yields significant advantages in testing of adhesive layers in comparison to the LEFM approaches: The main experimental advantage of the J -integral approach is, as will become more evident later, that the current crack tip position is generally not required for the evaluation of the ERR, rendering crack length measurements during testing superfluous. Additionally, as will be shown later, if the integration path S is chosen around the outer bounds of the tested specimen excluding the crack tip, the J -integral value at the crack tip J_{tip} is obtained from the equilibrium with the applied loads acting on the integration path S ; the position of the points of load introduction are arbitrary due to the path-independence of J . It shall also be noted that, as the elastic energy density may explicitly depend on the material coordinate y , material changes such as the transition between the adhesive layer and the adherend as well as notches or other geometric features that shall ensure straight crack growth or prevent plastic deformations of the adherends do not influence the J -integral obtained from the applied loads.

However, some restrictions of the J -integral evaluation can be extracted from the underlying assumptions: Generally, an elastic energy density W must exist, which strictly must not depend explicitly on the material coordinates in crack growth direction x . Especially for materials that exhibit viscoelastic or viscoplastic behaviour, the assumption of $W = \hat{W}(y)$ may be violated, as rate-effects on the material behaviour are neglected. Furthermore, care must be taken as energy dissipation outside the crack tip, e.g., due to plastic deformations and damage in a process zone of extended length, may lead to J being path-dependent. This could be particularly problematic for soft, rubber-like adhesive systems which develop large process zones prior to fracture. Hence, when investigating such materials, energy dissipation inside the process zone may be falsely ascribed to the crack tip when experimentally evaluating the critical ERR or, as will be shown in Sec. 2.4.1, determining cohesive laws.

2.3 Evaluation of the ERR in Double Cantilever Beam Tests

2.3.1 Double Cantilever Beam Test

Consider a bonded DCB specimen as shown in Fig. 2.3 with out-of-plane thickness b and an applied load point displacement δ , leading to a reaction force F_y and rotations of the load introduction points θ .

2 Theory

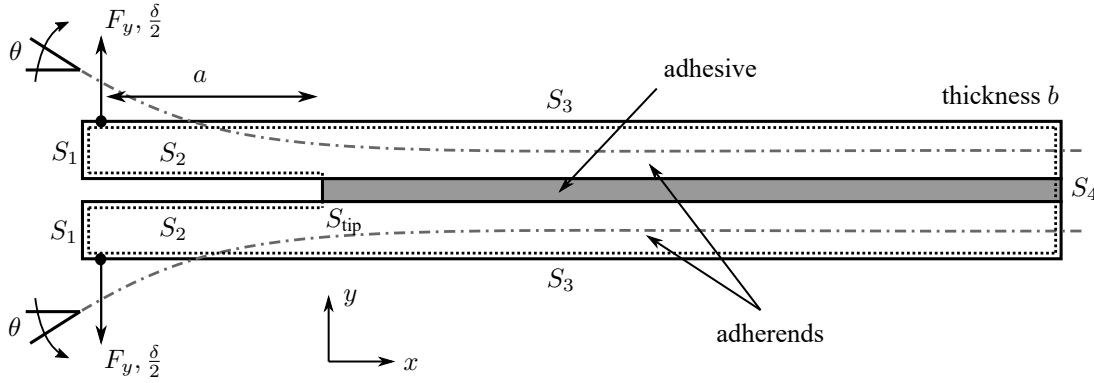


Figure 2.3 – Schematic representation of a loaded DCB specimen

For an experimental determination of the ERR using LEFM data reduction schemes, the Irwin-Kies Equation, Eq. (2.4), is commonly employed. For this approach, assumptions have to be made on the compliance of the adherends $C = \hat{C}(a)$ to compute the ERR, which are briefly summarised in the following:

1. The adherends behave as linear-elastic Euler-Bernoulli beams (no shear deformations) with bending stiffness EI_z that are perfectly built-in at the current crack tip, which is commonly referred to as Simple Beam Theory (SBT).

$$C_{\text{SBT,E}}(a) = \frac{2a^3}{3EI_z} \quad \Rightarrow \quad G_{\text{SBT,E}} = \frac{F_y^2 a^2}{bEI_z} \quad (2.8)$$

2. The adherends behave as Timoshenko beams with shear modulus μ , shear factor κ and cross-sectional area A that are perfectly built-in at the crack tip.

$$C_{\text{SBT,T}}(a) = \frac{a^3}{3EI_z} + \frac{a}{\mu\kappa A} \quad \Rightarrow \quad G_{\text{SBT,T}} = \frac{F_y^2}{b} \left(\frac{a^2}{3EI_z} + \frac{2}{\mu\kappa A} \right) \quad (2.9)$$

3. The adherends behave as linear-elastic Euler-Bernoulli beams but the crack length is virtually extended by $|\Delta|$ to accompany for the finite compliance of the adhesive layer and beam root rotation. The virtual crack extension $|\Delta|$ is determined from a linear regression between the cube root of the experimentally measured compliance and the crack length, yielding the so-called Corrected Beam Theory (CBT) approach.

$$C_{\text{CBT}}(a) = \frac{2(a + |\Delta|)^3}{3EI_z} \quad \Rightarrow \quad G_{\text{CBT}} = \frac{F_y^2 (a + |\Delta|)^2}{bEI_z} \quad (2.10)$$

4. The compliance of the adherend beams is assumed to be an exponential equation that can be obtained from the experimental data, yielding the so-called Experimental Compliance Method (ECM) or Berry's method [93]. The value for n is determined from the slope of a linear regression between the logarithms of the measured compliance and crack length, respectively.

$$C_{\text{ECM}}(a) = ka^n \quad \Rightarrow \quad G_{\text{ECM}} = \frac{nF_y^2 \delta}{2ba} \quad (2.11)$$

These (and additional) approaches are discussed more thoroughly for a DCB specimen loaded in mode III in **Paper D**, however, it can already be observed that the measurement of crack length and the assumptions on the behaviour of the adherend beams will inevitably have an influence on the obtained ERR, which was already shown by Blackman et al. [7] in an international round robin.

To determine the ERR by means of the J -integral according to Eq. (2.7) from the applied loads, the integration path $S = S_1 + S_2 + S_3 + S_4$ is chosen as the outer boundary of the specimen excluding the crack tip (cf. Fig. 2.3). As stated earlier, the value for J_{tip} evaluated along S_{tip} shall be in equilibrium with the contributions from S_1 to S_4 from the external loads. As the path S_1 is unloaded, i.e., $W = 0$ and $t_i = 0$, its contribution to J according to Eq. (2.7) is zero. For the horizontal path S_2 , $dy = 0$. Furthermore, the boundary on S_2 is not loaded by external tractions, wherefore $t_i = 0$, also rendering its contribution to J zero. The path S_3 is also horizontal, wherefore $dy = 0$. The loads applied at the load introduction points lead to a contribution J_{S_3} . Here, Eq. (2.7) yields

$$J_{S_3} = \int_{S_3} -t_i \frac{\partial \Delta_i}{\partial x} ds. \quad (2.12)$$

As long as the specimen is sufficiently large, the end of the specimen along S_4 is unloaded, yielding $W = 0$ and $t_i = 0$. Hence, the only contribution to J is the traction applied at the load introduction point in y -direction, which is given by $t_y = -F_y/b$. Furthermore, $\partial \Delta_y / \partial x$ gives the rotation of the specimen at the load introduction point θ . Inserting this into Eq. (2.12) and taking into account the symmetry of the specimen, the well-known equation for J for the DCB specimen as proposed by Paris and Paris [94] is obtained:

$$J = -2J_{S_3} = \frac{2F_y\theta}{b} \quad (2.13)$$

Evidently, as hinted at earlier, the presented J -integral approach is independent of the current crack length, making crack length measurements during testing superfluous and, in effect, reducing corresponding measurement uncertainties. Additionally, neither must assumptions be made on the compliance of the adherends nor must dC/da be experimentally determined to obtain the ERR, which reduces potential sources of error during the evaluation of the experiments.

It shall briefly be noted that the above relationship is also obtained from the Irwin-Kies Equation under SBT assumptions for both Euler-Bernoulli or Timoshenko beams if the equivalent crack length a_{eq} calculated from applied force F_y and rotational angle θ is used for evaluation instead of the measured crack length. For both beam theory approaches, the rotational angle at the load introduction point of a cantilever beam is given as

$$\theta = \frac{F_y a_{\text{eq}}^2}{2EI_y}. \quad (2.14)$$

Rearranging for a_{eq} and inserting into Eq. (2.8) yields

$$G = \frac{2F_y\theta}{b}, \quad (2.15)$$

which coincides with the J -integral solution from Eq. (2.13).

2.3.2 Tapered Double Cantilever Beam Test

Consider a TDCB specimen as shown in Fig. 2.4 with the applied load point displacement δ , leading to a reaction force F_y . Following the original proposal of the TDCB specimen by Mostovoy [95], the height of the specimen changes in such a way that the value for $dC(a)/da$ remains constant during crack propagation. Under the assumption that LEFM retains validity for the tested material, this experimental setup bares the advantage that the ERR is independent of crack length, ideally leading to a constant force F_y during crack propagation. The critical ERR is then obtained from the Irwin-Kies Equation, Eq. (2.4), using the measured plateau force.

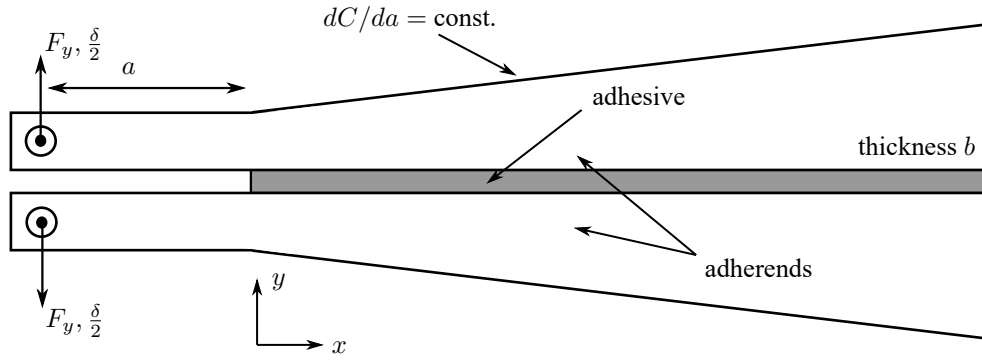


Figure 2.4 – Schematic representation of loaded TDCB specimen

2.3.3 Out-of-plane loaded Double Cantilever Beam Test

The ODCB specimen, which was initially proposed by Loh and Marzi in 2018 [29], is a modification to the DCB test in which, as shown in Fig. 2.5, the specimen is loaded by an out-of-plane rotation α , resulting in a reaction moment M_y instead of a force. Again, the out-of-plane thickness of the specimen is given by b . As derived in Sec. 2.1, the Irwin-Kies equation for an applied moment gives a mode III ERR of

$$G = \frac{M_y^2}{b} \frac{1}{EI_y}. \quad (2.16)$$

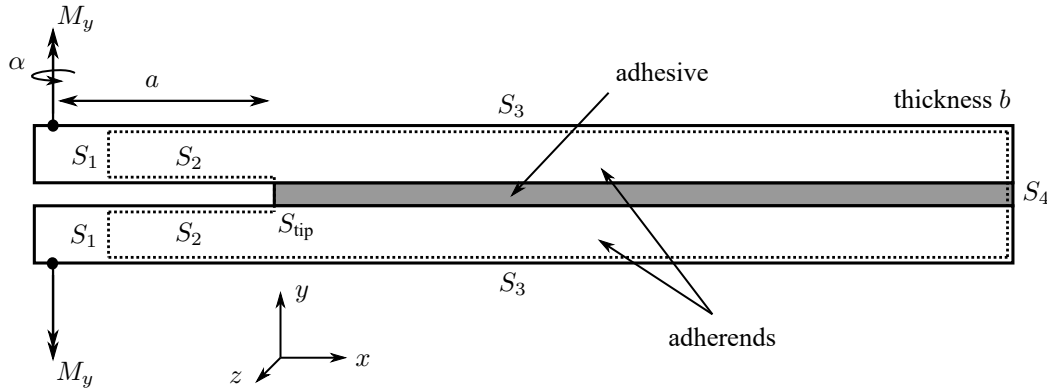


Figure 2.5 – Schematic representation of a loaded ODCB specimen

Loh and Marzi [29] derived the J -integral of the ODCB specimen by idealising the applied moment as a set of two opposing external forces from an integration along a path including the load introduction points. Comparatively, the J -integral for the ODCB specimen can also be determined from the integration path highlighted in Fig. 2.5 using the bending moment in the adherend beam similar to the approaches of Fernlund et al. [96] and Rosendahl [82]. As for the DCB specimen, the contributions to J along the paths S_2 , and S_4 vanish. As the load introduction points are excluded from the evaluation paths, the contributions along S_3 also become naught. Assuming that the adherend beams consist of a linear elastic material, the only contributions to J occur along S_1 due to normal stresses σ_x in the x -direction of the beam induced by the bending deformation. Using Hooke's law $\sigma_x = E\varepsilon_x$, a strain energy density of

$$W = \frac{1}{2} \sigma_x \varepsilon_x = \frac{\sigma_x^2}{2E} \quad (2.17)$$

is obtained. Furthermore,

$$t_x \frac{\partial \Delta_x}{\partial x} = \sigma_x \varepsilon_x = \frac{\sigma_x^2}{E}. \quad (2.18)$$

The normal stresses under pure bending within the beam depend on the coordinate z and are obtained via $\sigma_x = M_y z / I_y$. Inserting this into Eq. (2.7) then gives the J -integral

$$J_{S_1}(z) = \int_{S_1} \left(W - t_x \frac{\partial \Delta_x}{\partial x} \right) dy = \left(\frac{\sigma_x^2}{2E} - \frac{\sigma_x^2}{E} \right) [y]_0^h = -\frac{hM_y^2}{2EI_y^2} z^2 \quad (2.19)$$

where h denotes the height of the specimen. Hence, strictly speaking, a dependency on the out-of-plane position in the specimen can be observed. Expediently, the J -integral is obtained by averaging over the width:

$$\bar{J}_{S_1} = \frac{1}{b} \int_{-b/2}^{b/2} J_{S_1}(z) dz = -\frac{hM_y^2}{2bEI_y^2} \left[\frac{z^3}{3} \right]_{-b/2}^{b/2} = -\frac{M_y^2}{2bEI_y^2} \frac{hb^3}{12} \quad (2.20)$$

Inserting the adherends' moment of inertia for a rectangular specimen $I_y = hb^3/12$ and taking into account the symmetry of the specimen then gives the total J -integral

$$J = -2\bar{J}_{S_1} = \frac{M_y^2}{b} \frac{1}{EI_y}, \quad (2.21)$$

coinciding with the solution according to the Irwin-Kies equation. Hence, it can be observed that the differences between the LFM and J -integral approach vanish if a rotational rather than an axial displacement is applied and the applied moment is used for evaluating the ERR.

To experimentally load the specimens by a pure bending moment, the ODCB test necessitates a floating bearing of one side of the specimen, e.g., with linear slides. Furthermore, due to lateral contraction of the adhesive, a mode I loading is induced when applying an external rotation. Hence, the ODCB test must be performed in a bi-axial loading machine, which allows both loading the specimen with an external moment while simultaneously being able to control axial forces to naught, requiring expensive equipment and large experimental effort. In the hopes of overcoming these issues with the ODCB test setup, the uni-axial test setups proposed in **Paper D** were developed.

For the sake of completeness it shall be noted that, as found and investigated by Loh and Marzi [30–32] when expanding the ODCB test to mixed-mode loading (MC-DCB test), unintended contributions to J can occur, which, however, do not have a significant influence during pure mode III investigations and, according to Bödeker and Marzi [34], do not significantly influence the obtained cohesive laws. It is referred to the publication by Loh and Marzi [31] for more information on the derivation of these contributions.

2.4 Determination of cohesive laws in single mode loading

2.4.1 J-integral approach

Building on the works of Dugdale [87] and Barenblatt [88], Rice [89] was able to relate the cohesive traction at the crack tip for pure mode I loading with the J -integral, which is the currently established approach to experimentally obtain parameters for cohesive zone modelling. The following derivations are performed under the assumption of path-independence of J and a symmetric specimen with identical adherends and shall briefly highlight issues with the evaluation method, which, as of yet, have not been distinctly addressed by the current state of research to the author's knowledge. For more detailed explanations on the determi-

2 Theory

nation of the cohesive traction from the J -integral evaluation, the publication of Bödeker and Marzi [34] is recommended.

Consider Eq. (2.7) and choose a J -integral evaluation path around the boundary between the adherend and adhesive layer parallel to the x -coordinate, i.e., $dy = 0$, from the (unloaded) end of the adhesive layer x_{end} to the crack tip position x_t . This yields

$$J = 2 \int_{x_{\text{end}}}^{x_t} t_i(x) \frac{\partial \Delta_i(x)}{\partial x} dx = \int_{x_{\text{end}}}^{x_t} t_i(x) \frac{\partial \delta_i(x)}{\partial x} dx, \quad (2.22)$$

where $\delta_i = 2\Delta_i$ are the components of the separation vector in the respective loading mode denoted by i , i.e., the relative displacement of the upper and lower boundary. The assumption of non-linear elastic behaviour of the adhesive layer implies that the cohesive traction must depend solely on the deformation state, $t_i(\delta_i(x))$. Integration by substitution can now be applied by replacing the integration variable x with $\delta_i(x)$ using $d\delta_i(x) = \frac{\partial \delta_i(x)}{\partial x} dx$, giving

$$J = \int_{\delta_i(x_{\text{end}})}^{\delta_i(x_t)} t_i(\delta_i(x)) d\delta_i(x) = \int_0^{\delta_i(x_t)} t_i(\delta_i(x)) d\delta_i(x). \quad (2.23)$$

In the latter equation, $\delta_i(x_{\text{end}}) = 0$ is inserted because of the assumption of an unloaded end of the specimen. Furthermore, given that the traction depends solely on the deformation state, the adhesive exhibits the same behaviour along the complete adhesive layer, enabling the use of the COD $\delta_{t,i} = \delta_i(x_t)$ as the integration variable. Therefore, the solution from Rice's original paper [89]

$$J = \int_0^{\delta_{t,i}} t_i(\delta'_{t,i}) d\delta'_{t,i} \quad (2.24)$$

is obtained, which can then be written in differential form and rearranged for the cohesive traction, thus yielding the cohesive law

$$t_i(\delta_i) = \frac{dJ}{d\delta_{t,i}}. \quad (2.25)$$

This, in effect, allows the determination of the traction separation laws from the externally measured J -integral and the COD, which is a straightforward method as the cohesive traction at the crack tip can be determined directly by derivation of the measured quantities. It shall be noted that the derivation of the measured quantities can be numerically problematic due to measurement noise in both J and COD. To overcome this issue, the data is often fitted with analytical functions before taking the derivative. Likewise, filtering, smoothing or thinning out the data before taking the derivative is commonly employed as well.

Depending on the tested adhesive, it is possible that some of the underlying assumptions may be contravened: If the material exhibits viscoelastic or viscoplastic behaviour, the assumption that the cohesive traction depends solely on the deformation state is violated if rate-effects on the material behaviour cannot be deemed negligible. Furthermore, it is assumed that plastic and viscous effects as well as damage processes in an extended process zone, i.e., outside the vicinity of the crack tip, may contribute to the externally measured value of J and would, hence, falsely be ascribed to the crack tip if the cohesive traction is calculated via Eq. (2.25). Especially for soft, rubber-like adhesive layers, care should be exercised as these assumptions may not certainly be deemed valid.

2.4.2 Beam theory evaluation

Building on these issues, an additional method of determining the cohesive traction is developed in **Paper C** to obtain the cohesive traction along with the complete adhesive layer in pure mode I and III loading from

a measurement of the adherends' backface strain $\varepsilon(x)$ using Euler-Bernoulli beam theory. To put it briefly, by measuring the strain along with adherend in the direction of crack propagation x , given the distance c between the position of strain measurement and the marginal fibre of the adherend, the curvature $\kappa(x)$ of the beam and the resulting bending moment $M_b(x)$ are obtained via

$$M_b(x) = -\kappa(x)EI = -\frac{\varepsilon(x)}{c}EI, \quad (2.26)$$

with EI as the bending stiffness around the bending axis of interest (y -axis in ODCB and z -axis in DCB tests, respectively). This allows determining the transverse force and line load through differentiation of the bending moment. Assuming that the load is distributed equally on the width of the adhesive layer for both peel and shear loading, the cohesive traction can be calculated by dividing the line load by the adhesive layer width, ultimately yielding

$$t(x) = \frac{EI}{bc} \frac{d^2\varepsilon(x)}{dx^2}. \quad (2.27)$$

Furthermore, it shall be noted that the slope $\varphi(x)$ of the beam and the separation of the adhesive layer $\delta(x)$ are obtained by integrating the measured $\kappa(x)$ along with the adherends from the (unloaded) end of the adhesive layer x_{end} up to the crack tip position x_t , i.e.,

$$\varphi(x) = - \int_{x_{\text{end}}}^{x_t} \frac{\varepsilon(x)}{c} dx \quad \text{and} \quad \delta(x) = 2 \int_{x_{\text{end}}}^{x_t} \varphi(x) dx, \quad (2.28)$$

also allowing the determination of the separation (and separation rate) along with the specimen. Next to the possibility of obtaining rate-dependent traction separation relations, this approach also allows investigating the development of the cohesive traction inside the process zone. Additionally, following this approach, the J -integral can be computed with Eq. (2.22). As $\partial\Delta_i(x)/\partial(x) = \varphi(x)$, this yields the total J -integral at the crack tip from beam theory:

$$J = 2 \int_{x_{\text{end}}}^{x_t} t(x)\varphi(x) dx \quad (2.29)$$

3 Summary of appended papers

In this section, a brief summary for each of the manuscripts of which this dissertation is composed shall be given. Both the used methods as well as the most important findings of each of the individual manuscripts shall be addressed, discussed, and placed in the overarching context of this work. The works are sorted according to the chronological order of their submission date.

3.1 Paper A

Mode I creep fracture of rubber-like adhesive joints at constant crack driving force

This paper addresses the time-dependent mode I creep fracture of soft, rubber-like adhesive layers under finite deformations. The DCB tests performed on a 3 mm thick and 5 mm wide soft, rubber-like adhesive layer were externally controlled on a constant value of the J -integral, which was calculated in-situ from the measured data with Eq. (2.13), rendering crack length measurements superfluous for the determination of the ERR. Throughout the experiments, the fracture process was captured with one high-resolution camera on each side of the specimen to gain insight into the dependency of crack resistance and resulting crack propagation rate on the forming of secondary cracks on the outer surface of the adhesive layer beside the macroscopic major crack tip. Two methods of obtaining the current crack extension and crack propagation rate, one based on image processing and one based on the adherends' beam compliance according to Škec et al. [97], were applied to the measured data and thoroughly compared. Furthermore, the growth of secondary cracks on the outer surfaces of the adhesive layer was quantified using an image processing algorithm by, in layman's terms, counting the amount of pixels in visibly damaged areas of the adhesive layer.

As displayed in Fig. 3.1, distinct phenomena were observed during crack propagation under constant J . Most importantly, finite deformations and necking at the crack tip were seen. Furthermore, minor cracks besides the macroscopic crack tip occurred, which were manifested through surface tearing and yielded a complex geometric shape of the macroscopic crack front. It was suspected that the forming of the secondary minor cracks was due to the necking processes causing increased stresses at the outer surfaces of the adhesive layer. These phenomena complicate the detection of the current crack tip position, wherefore it was concluded in the manuscript that other mechanically motivated methods of crack length determination should be employed in future studies. Building on this, a possibility to determine the crack length during experiments on soft, rubber-like adhesive layers by measuring the strain of the adherends is proposed in **Paper C**.

Generally, differences between the optically determined crack extension and the equivalent crack extension from beam theory assumptions were obtained, which arose from the observed micro-damage and viscous softening of the adhesive layer. As was found in the work, the differences between the optically determined crack extension and the crack extension obtained from the specimen compliance correlated with the damage processes visible through surface tearing. Typically, one would expect a constant crack propagation rate, i.e., steady-state crack propagation, under constant applied J , which could not be observed during the study. However, a correlation between the crack propagation rate and the size of the damaged areas was observed, implying that the growth of the damaged areas may reduce the macroscopic crack propagation rate. Hence, it could be concluded that minor cracking reduced the stress intensity for the macroscopic

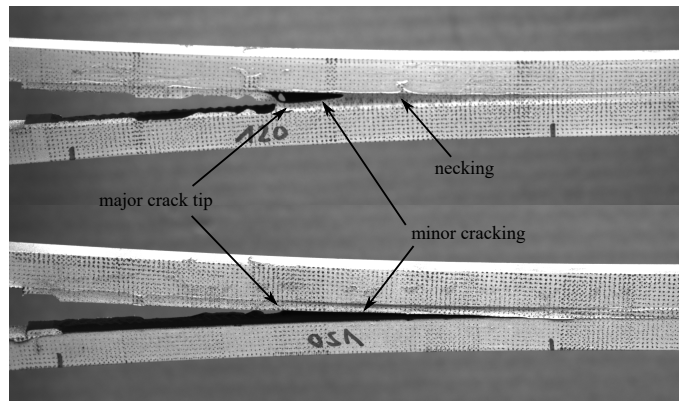


Figure 3.1 – Phenomena observed during crack propagation under constant applied J

major crack tip, resulting in a higher macroscopic crack resistance and, ultimately, lower crack propagation rates. The observed minor cracking also heavily implied that the material behaviour and energy dissipation in the process zone may have a significant influence on the obtained results when investigating soft, rubber-like adhesive layers. Motivated by this observation, the influence of energy dissipation in the process zone behind the macroscopic major crack tip and related implications for the determination of cohesive laws is investigated more thoroughly in **Paper C**.

Discussion. In comparison to the previous works of, e.g., Lefebvre et al. [40], Dillard [41], Dillard et al. [42], or Plausinis and Spelt [43], in which tapered specimen geometries or complex load rigs were used to achieve a constant ERR during creep fracture, the method of computer-controlling the tests on the in-situ value of J allowed testing without any prior knowledge of the material behaviour for the design of the specimens. Furthermore, through the in-situ calculation of J via Eq. (2.13), a crack length measurement became superfluous for obtaining the fracture energy, which is an experimental advantage for fracture processes in which the current crack length cannot be easily identified. The results clearly indicated that damage processes behind the macroscopic crack tip govern the macroscopic fracture behaviour of the tested adhesive. Hence, a future in-depth investigation of these processes, e.g., with a backface strain measurement procedure akin to the approach presented in **Paper C**, is deemed crucial. As, under ideal conditions, a constant J should ideally result in a steady-state crack propagation, it might also be worth linking the results from this study with the recently published work of Márquez Costa et al. [47] in future investigations. Furthermore, the proposed method may be extended to experiments under constant C^* -integral [98], which is also commonly used to study materials that undergo steady-state creep.

3.2 Paper B

Mode III testing of structural adhesive joints at elevated loading rates

In this paper, it was investigated whether the ODCB test proposed by Loh and Marzi [29] can also be used to determine the ERR and cohesive laws of adhesive layers at elevated loading rates. The ODCB setup was modified and the rotational degree of freedom around the upper load introduction point was constrained to reduce the mass of the clamping devices, which shall minimise transient effects during testing at increased loading rates. Additionally, the specimens were – under ideal conditions, i.e., when the friction in the lateral slides is negligible and the axial force is successfully controlled to naught – purely loaded by external bending moments, simplifying the determination of the J -integral through strain gauge measurements. Experiments were performed on an epoxy-based adhesive under quasi-static conditions and at two increased external loading rates (applied angle rates of 0.05 deg/s, 10 deg/s, and 120 deg/s). The crack tip kinematics

3 Summary of appended papers

were investigated using digital image correlation, allowing a determination of the COD components in both mode I and mode III direction.

By measuring the strain ε at the marginal fibres of the (T-shaped) adherends of width w , the mode III contribution to the J -integral, Eq. (2.21), was reworked as

$$J_{III,loc} = \frac{4\varepsilon^2 EI_y}{bw^2}, \quad (3.30)$$

yielding a possibility of locally determining the mode III ERR from strain gauge measurements. As was found during the experimental investigation, this local measurement of the applied J -integral was mandatory, because, with increasing loading rates, the external moment measurements could not be considered reliable due to pronounced oscillations in the load signals. The observed good correspondence between the externally measured ERR and the strain gauge measurements indicated that the results were not influenced significantly by friction in the linear slides or contributions in modes other than mode III. The local strain measurements also showed that the specimen was loaded symmetrically, indicating that the inertia of the specimen did not significantly influence the obtained results.

An investigation of the crack tip kinematics with digital image correlation showed that, at increased loading rates, the mode III COD increased linearly until a point of sudden acceleration, which could be correlated with the damage onset according to the cohesive law. Linear regressions of the mode III COD in this linear region yielded equivalent crack opening velocities between approx. $1.6 \cdot 10^{-3}$ mm/s and 2.5 mm/s, corresponding to nominal strain rates between $5.4 \cdot 10^{-3}$ 1/s and 8.7 1/s. Whereas the mode I component of the COD was of negligible magnitude under quasi-static conditions, it increased with loading rate, indicating that a small amount of mixed-mode loading is present at increased loading rates. However, the results showed that the mode III component of the COD still dominated the deformation at the initial crack tip, allowing the conclusion that the traction separation laws could be determined from Eq. (2.25) with a minor error.

One of the most significant results of the study is shown in Fig. 3.2. Here it can be observed that the critical ERR was independent of loading rate for the tested adhesive in view of material scattering. In contrast, the cohesive laws varied significantly with loading rate, changing from a trilinear to a more bilinear shape, implying that the failure became more brittle with less energy dissipation through plastic flow during fracture initiation. This finding was also undermined by the fracture surfaces, which, only for the quasi-static tests, showed signs of plastic deformations through crazing. At increased loading rates, after initial failure close to the interface, the fracture surfaces even showed partly adhesive failure.

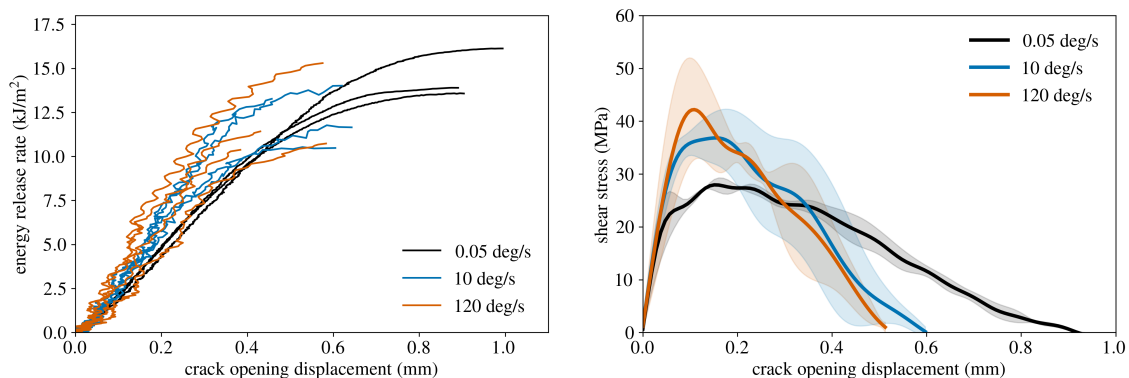


Figure 3.2 – ERR and cohesive traction (mean curves with corresponding standard deviation) over mode III COD at different loading rates

Discussion. From the results it could be concluded that the ODCB test could indeed be successfully extended to testing at increased loading by locally measuring the strain of the adherend beams, allowing the determination of mode III ERR and, for the first time, also of the cohesive traction. It shall be noted that, during ENF tests at increased loading rates, the adherends tend to deform plastically as for example in the study of Borges et al. [49], wherefore Sato and Marzi [65] advise not to use ENF specimens for testing under impact conditions. In this paper, experimental problems such as plastically deforming adherends could not be observed. Hence, it was concluded that mode III testing could, indeed, be more practical especially for testing rubber-like adhesive layers, which are already difficult to test in mode II under quasi-static conditions. If higher loading rates shall be achieved during mode III testing in the future, as the necessity of controlling external forces to zero requires a bi-axial testing machine, it was concluded that a uni-axial setup akin to the works of Mai [22], Chai [23], Donaldson [24], or Stigh [28] may be advantageous for testing under impact conditions. A test setup which may be suitable for this application was later developed in **Paper D**. The approach of determining ERR and cohesive traction from strain measurements was refined in **Paper C**, in which the strain along with the complete adherend beams was used to investigate the mode I and III fracture behaviour of a soft, rubber-like adhesive system.

3.3 Paper C

Influence of loading rate on the cohesive traction for soft, rubber-like adhesive layers loaded in modes I and III

This paper addressed the rate-dependent fracture behaviour of a soft, rubber-like adhesive system loaded in pure modes I and III, considering both the determination of the critical ERR and the determination of the nominal cohesive traction. For this reason, DCB and ODCB tests were performed on a 1 mm thick adhesive layer at three external loading velocities (mode I: 0.05 mm/s, 0.5 mm/s, 5 mm/s; mode III: 0.05 deg/s, 0.5 deg/s, 5 deg/s). The approach of locally measuring the strain of the adherends from **Paper B** was extended to allow the measurement of the cohesive traction as described in Sec. 2.4.2 along with the complete specimen using fibre-optics measurements and Euler-Bernoulli Beam theory. As stated, the separation (and, hence, the separation rate of the adherends) can also be obtained at each position of strain measurement, allowing the determination of rate dependent traction separation laws from the deflection curve of the specimen. The COD was monitored using digital image correlation. As highlighted in Sec. 2.4.1, underlying assumptions for the determination of the cohesive traction by taking the derivative of the measured J with respect to the COD, Eq. (2.25), may be violated for soft, rubber-like adhesive joints. The paper compared the evaluation methods, with the conclusion that the method according to the state of research delivered inadequate results. Additionally, the strain measurements also allowed a determination of the current crack tip position and process zone length, the latter of which was also rarely investigated thus far.

In all experiments, large displacements at the initial crack tip were observed before the start of crack propagation. The large displacements lead to interesting mode III fracture surfaces during the two lower loading rates, as, after crack initiation, the crack propagated perpendicular to the bonding surface, accompanied by partly adhesive failure on one of the outer edges of the adhesive layer and plastic shear deformations at the other. The fracture perpendicular to the bonding surface indicated local mode I peel load at the crack tip during fracture initiation, which was undermined by a comparable rate-dependency of the ERR in both modes I and III (cf. Fig. 3.3).

The strain measurements along with the adherends showed large process zones in all cases, which implied a possible violation of the underlying assumptions behind the conventional method of deriving cohesive laws via Eq. (2.25). Generally, the process zone – which, in the context of this work, was defined as the loaded region within the adhesive layer – obtained in mode I was significantly smaller than in mode III, which

was attributed to the reduced stiffness of the adhesive layer under shear loads. For both loading modes, the process zone grew until the start of crack propagation, after which the process zone length remained approximately constant. The crack lengths obtained from the strain measurements and analytical solutions following Euler-Bernoulli beam theory were in good agreement despite a constant offset of 160 mm in the mode I and 180 mm in the mode III experiments. It was argued that, due to this constant offset, the crack extension could still be approximated relatively accurately with beam theory assumptions even for a soft, rubber-like adhesive system. Furthermore, the bending strain measurements unexpectedly revealed that lateral forces in the linear slides due to friction influenced the mode III ERR obtained from the externally applied moment for the soft adhesive layer. Nevertheless, a comparison between the externally measured loads and COD with the values obtained from beam theory assumptions and the bending strain measurements along with the specimen showed a good agreement.

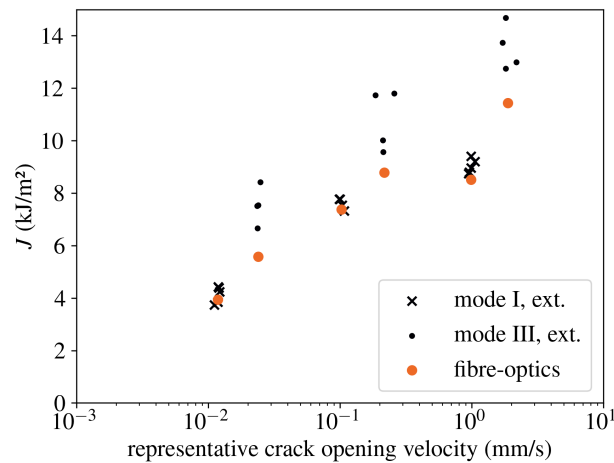


Figure 3.3 – Influence of loading mode and representative crack opening velocity on the ERR

For both mode I and mode III, a significant increase of the critical ERR with loading rate was observed. In Fig. 3.3, the externally measured mode I and mode III are displayed over the representative crack opening velocity alongside the J -integral value obtained from the deflection curve of the adherends, Eq. (2.27). The similar results between the mode I and III experiments implied that, considering material scattering, the ERR might be independent of loading mode for the tested adhesive. For the mode I experiments, no significant resistance curve behaviour was observed. For the two lower loading velocities in mode III, however, the resistance curve behaviour was significant, which was attributed to the complex fracture behaviour described earlier during these tests. It shall be noted that the unintended contributions to the mode III ERR were well below 1% of the critical mode III ERR at the start of crack propagation, wherefore they were considered negligible.

In Fig. 3.4, the conventional method of determining traction separation laws (bold lines), Eq. (2.25), was compared to the scatter band obtained from the strain measurements of the adherends, Eq. (2.27), showing large discrepancies and, hence, demonstrating that the conventional method of determining cohesive laws must not necessarily be considered accurate for soft, rubber-like adhesive layers. The rate-dependent cohesive traction was obtained from the strain measurements as shown in Fig. 3.5, which, to the authors knowledge, has not been achieved elsewhere.

Discussion. As described earlier during the mode III experiments, lateral forces due to friction in the floating bearing of the ODCB experiments influenced the mode III ERR significantly. Whereas the results of previous studies on stiff epoxy-based adhesive layers were likely not influenced by these, the frictional forces must definitely be considered in the evaluation of the ERR for soft adhesive layers, necessitating a measurement of the frictional work in future studies. Additionally, it should be stated that due to the

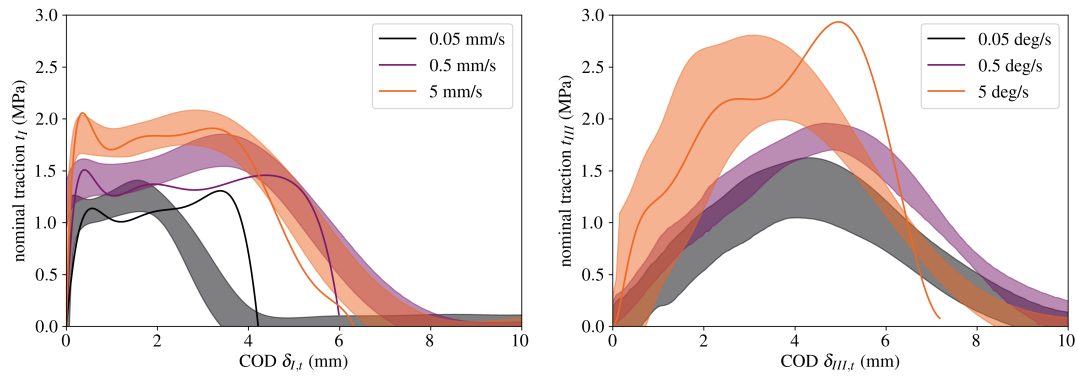


Figure 3.4 – Comparison between traction separation laws obtained from J -integral approach (bold lines), Eq. (2.25), and strain measurements (scatter bands), Eq. (2.27)

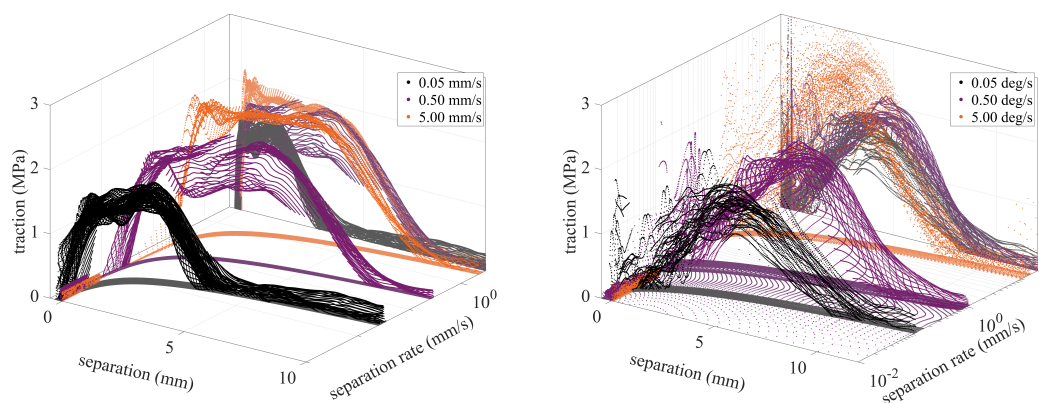


Figure 3.5 – Rate-dependent cohesive traction for all measurement points along with the adherends: mode I (left) and mode III (right)

large out-of-plane deformations of the specimens under mode III loading, measuring the COD becomes increasingly involved due to lack of depth of view of the digital image correlation system. By achieving a uni-axial setup, it could be argued that the floating bearing could be omitted in the first place and the COD could be measured in-plane, motivating the development of the test setups proposed in **Paper D**. Overall, the results of this study heavily implied that the strain measurements along with the adherends, although requiring large efforts in experimental preparation and evaluation, provide valuable insight into the fracture behaviour of adhesive joints and have significant benefits considering the determination of crack tip position, process zone length, and cohesive traction. Whereas, unfortunately, it was not possible to implement the traction obtained from the fibre-optics measurements into a cohesive zone model within this dissertation, a future implementation is deemed worthwhile.

3.4 Paper D

Novel mode III DCB test setups and related evaluation methods to investigate the fracture behaviour of adhesive joints

In this paper, the Uni-axial Out-of-plane loaded Double Cantilever Beam (UODCB) and Tapered Out-of-plane loaded Double Cantilever Beam (TODCB) specimens are presented, which are based on the previous works of Mai [22], Chai [23], Donaldson [24], and Stigh et al. [28] and shall allow the determination of critical ERR and cohesive traction for adhesive systems under mode III loading. The aim of the study was to

3 Summary of appended papers

holistically compare the evaluation methods based on J -integral and Irwin-Kies Equation and to determine the experimental advantages and disadvantages of the different evaluation methods for the investigation of an epoxy-based adhesive system. Furthermore, next to familiar data reduction schemes following ISO 25217 [3], crack length independent and CBT approaches that incorporate the rotational angle of the load introduction points were developed. Akin to **Paper C**, backface strain measurements were conducted to monitor crack growth and process zone length, i.e., the length of the loaded region in the adhesive layer, during the experiments.

In Fig. 3.6, the obtained ERR and cohesive laws for the J -integral evaluation of the UODCB and the LEFM evaluation for the TODCB specimens are compared until the start of crack propagation, showing good agreement. The J -integral evaluation of the UODCB specimens was considered the experimental benchmark, as the evaluation does not rely on any assumptions about the adherend beams other than that they do not exhibit plastic deformations. After the start of crack propagation, for the UODCB specimens, a falling ERR was observed, which could be attributed to a rising mode I influence on the overall fracture behaviour due to the boundary conditions, i.e., the floating bearing of the lower clamping and the rotational degree of freedom around the axis of load introduction. This was not observed for the TODCB experiments, because, as was shown, the mode I influence remained relatively constant throughout the experiments.

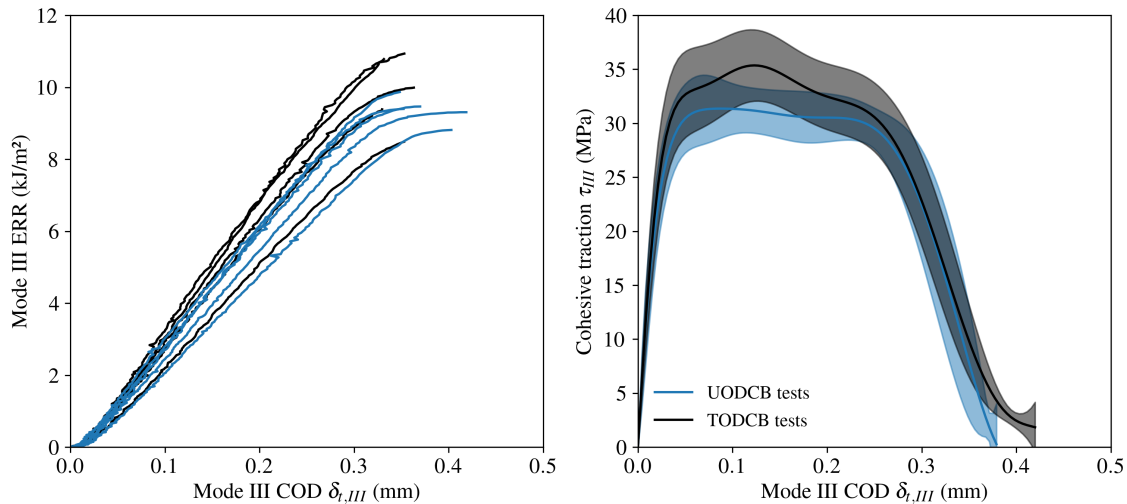


Figure 3.6 – ERR and cohesive traction determined from the UODCB and TODCB tests over mode III COD

A comparison between the analytically determined crack lengths from beam theory assumptions for the UODCB tests showed that, despite a constant offset, the methods of obtaining equivalent crack lengths match well with the measured crack extension. Especially the equivalent crack extension obtained from the rotation of the load introduction points agreed extremely well with the measured crack extension. The measured process zone length exceeded 100 mm in both the UODCB and TODCB experiments.

The comparison between the determined critical ERR and plateau stress of the traction separation laws following the J -integral and LEFM data reduction schemes revealed that the LEFM methods relying on equivalent crack lengths, with exception of a data reduction method in which the external force was substituted by other measured quantities, gave results comparable to the J -integral benchmark. Furthermore, under beam theory assumptions, the J -integral and Griffith ERR were found to coincide in the case where the equivalent crack length obtained from the measured load point rotation was inserted. The methods relying on CBT also deliver satisfactory results, with the best performing method being the CBT approach standardised in ISO 25217 [3]. For the CBT and ECM approaches, a multi-specimen compliance calibration was performed and compared with the simultaneous crack length measurements, giving equivalent results. For the determination of the ERR, it was generally concluded that the J -integral approach, Eq. (2.13), has to

be considered the most advisable, as the least assumptions have to be made on the behaviour of the adherends and the least measured quantities contribute to the obtained ERR, reducing measurement uncertainties. The influence of the crack length measurement was generally deemed problematic, as a (visual) measurement is difficult or, depending on adhesive system or specimen configuration, possibly even inaccurate.

Discussion. A clear disadvantage of the proposed test setups is the complex specimen kinematics due to the floating bearing of the lower clamping device to avoid damaging the testing machine. This was accepted, however, as in comparison to the aforementioned studies [22–24, 28] narrower adhesive layers could be tested with the designed specimens in a uni-axial mode III test setup for the first time. A reconsideration of the proposed UODCB and TODCB test setups with a positionally fixed lower clamping is nevertheless deemed worthwhile. It is argued that the proposed setups are better suited for testing at increased loading rates than the setup presented in **Paper B**, as a uni-axial test setup may allow future testing in drop towers or other high-speed load rigs. Unfortunately, it was not possible to apply the measurement techniques for the cohesive traction developed in **Paper C** within the scope of this work due to lack of time and funding. For future testing of soft, rubber-like adhesive layers, it must be noted that much larger specimens would be needed, which likely complicates machining the adherends and specimen preparation. Furthermore, due to the specimens being loaded in-plane, a measurement of the COD is simplified in this case. As stated earlier, the results of the study heavily imply that a J -integral evaluation of fracture mechanics tests is of large experimental advantage, as only force and rotational angles at the load introduction points have to be measured to obtain the ERR, which, in both cases, is generally possible with a very high accuracy.

4 Conclusions and perspectives

In this thesis, various scientific contributions were made to the topic of fracture mechanics testing of adhesively bonded joints using DCB experiments. The most important findings and suggestions for future research are summarised below:

Creep investigations. The mode I creep fracture of a rubber-like adhesive joint was, for the first time, successfully investigated in **Paper A** by means of NLEFM in the context of this work. The proposed methodology of controlling the test on the in-situ J -integral value offers interesting possibilities for future investigations. As stated earlier, due to J being controlled to be constant throughout the experiments, steady-state crack propagation should be provoked, which may also be of interest for experimentally investigating and numerically modelling adhesive layers other than the tested soft, rubber-like adhesive. The methodology of determining the crack length using strain measurements along with the specimen developed in **Paper C** is also deemed a worthwhile extension for future creep experiments to gain better insight into the fracture behaviour of adhesive layers under constant ERR and the development of damaged areas in the process zone.

Pure mode III testing. According to the current state of research it is not often differentiated between the loading modes II and III. The combined results of this work indicate that, in comparison to mode II testing, the fracture mechanical investigation of the shear behaviour of adhesive layers using mode III test setups may be beneficial for experimentally investigating soft, rubber-like adhesive layers and/or testing at increased loading rates. However, using a bi-axial test setup as in **Paper B** is likely problematic under impact conditions, as the axial force on the specimen has to be externally controlled to naught, because, otherwise, mode I contributions to the ERR cannot be deemed negligible. Using uni-axial setups akin to the ones proposed in **Paper D** is assumed to be advantageous for this purpose, but remains to be addressed experimentally. The quasi-static results, however, already imply that the critical ERR and traction separation relations may be obtained for epoxy-based adhesive systems with these test configurations. Hence, employing these test setups at increased loading rates should definitely be considered in future investigations.

Influence of data reduction schemes. The increasing use of soft, rubber-like adhesive systems in industrial practice will also require suitable testing methods that can take into account finite deformations and material non-linearities and inhomogeneities of the adhesive layers. Hence, although the approaches based on LEFM and the Irwin-Kies Equation are well established in the current state of research, due to the increasing importance of ductile adhesive systems, J -integral testing of adhesive layers in future investigations is generally advised. The J -integral evaluation method generally provides the ERR without the necessity of measuring the crack length, resulting in less measurement uncertainties in determining the ERR; a measurement of the current crack length, however, is still considered reasonable, as it allows determining resistance curves.

Testing of soft, rubber-like adhesive layers. Within this work, the rate-dependent mode I and mode III fracture behaviour of a soft, rubber-like adhesive layer was investigated in **Paper C** for the first time. The results implied that the ERR may have been independent of loading mode in view of material scattering. The cohesive traction, in contrast, changed significantly, which means that simulative modelling of such layers

cannot be achieved from mode I experiments, solely. It is advised that future studies investigate this more in-depth, because, due to an increasing interest in rubber-like adhesive joints in structural applications, this necessitates suitable models for finite element analysis.

Determination of the cohesive traction. As was shown, for soft, rubber-like adhesive layers, the approach of taking the derivative of the measured J -integral with respect to the COD does not yield reliable results for determining the cohesive traction. The method of using the backface strain of the adherends to determine the cohesive traction developed in **Paper C** is considered superior, although the experimental effort is heavily increased. The combined results of this work clearly indicate that a measurement of the bending strain of the adherends may, next to a more accurate determination of the crack tip position, provide both more accurate results and give additional insight into the rate-dependency of the cohesive traction and its development along with the process zone. In future investigations, this approach shall be improved further to gain more insight into the rate-dependent fracture behaviour of adhesive layers – especially soft, rubber-like adhesive systems. Furthermore, an implementation of the results in a cohesive zone model is deemed worthwhile to enable finite element analyses of such joints.

In summary, various aspects in fracture mechanical testing of adhesive joints were experimentally investigated in this dissertation using DCB specimens loaded in modes I and III. Each of the conducted studies presents innovative experimental setups, results, and novel evaluation methods based on fracture mechanics. Creep fracture, the fracture of stiff, epoxy-based and soft, rubber-like adhesive joints at increased loading rates, and the extraction of cohesive laws from the measured data are examined. Furthermore, novel mode III DCB specimens are presented and LEFM and J -integral data reduction schemes are holistically compared. With rising interest in using adhesive joints in industrial practice, fracture mechanics testing of adhesive layers will likely gain more industrial relevance, wherefore this dissertation thus makes a significant contribution to the future of adhesive testing.

References

- [1] B. Smith, A. Spulber, S. Modi, and T. Fiorelli. *[White paper] Technology Roadmaps: Intelligent Mobility Technology, Materials and Manufacturing Processes, and Light Duty Vehicle Propulsion*. Ed. by Center for Automotive Research, Ann Arbor, MI. 2017. URL: https://www.cargroup.org/wp-content/uploads/2017/07/Technology_Roadmaps.pdf (visited on 07/24/2022).
- [2] A. L. Loureiro, L. F. M. Da Silva, C. Sato, and M. A. V. Figueiredo. “Comparison of the Mechanical Behaviour Between Stiff and Flexible Adhesive Joints for the Automotive Industry”. In: *The Journal of Adhesion* 86.7 (2010), pp. 765–787. ISSN: 0021-8464. DOI: 10.1080/00218464.2010.482440.
- [3] International Organization for Standardization. *ISO 25217, Adhesives — Determination of the mode I adhesive fracture energy of structural adhesive joints using double cantilever beam and tapered double cantilever beam specimens*. 2009.
- [4] F. J. P. Chaves, L. F. M. Da Silva, M. F. S. F. de Moura, D. A. Dillard, and V. H. C. Esteves. “Fracture Mechanics Tests in Adhesively Bonded Joints: A Literature Review”. In: *The Journal of Adhesion* 90.12 (2014), pp. 955–992. ISSN: 0021-8464. DOI: 10.1080/00218464.2013.859075.
- [5] A. J. Kinloch. *Adhesion and Adhesives*. Dordrecht: Springer Netherlands, 1987. ISBN: 978-90-481-4003-9. DOI: 10.1007/978-94-015-7764-9.
- [6] International Organization for Standardization. *ISO 11343:2019-10, Adhesives - Determination of dynamic resistance to cleavage of high-strength adhesive bonds under impact wedge conditions - Wedge impact method (ISO 11343:2019); German version EN ISO 11343:2019*. Berlin. DOI: 10.31030/3051445.
- [7] B. Blackman, A. J. Kinloch, M. Paraschi, and W. S. Teo. “Measuring the mode I adhesive fracture energy, GIC, of structural adhesive joints: the results of an international round-robin”. In: *International Journal of Adhesion and Adhesives* 23.4 (2003), pp. 293–305. ISSN: 0143-7496. DOI: 10.1016/S0143-7496(03)00047-2.
- [8] A. Biel, T. Walander, and U. Stigh. “Influence of Edge-Boundaries on the Cohesive Behaviour of an Adhesive Layer”. In: *Proceedings of the ASME 2012 International Mechanical Engineering Congress & Exposition* (2012).
- [9] T. Walander, A. Biel, and U. Stigh. “Temperature dependence of cohesive laws for an epoxy adhesive in Mode I and Mode II loading”. In: *International Journal of Fracture* 183.2 (2013), pp. 203–221. ISSN: 0376-9429. DOI: 10.1007/s10704-013-9887-3.
- [10] A. Biel. *Constitutive behaviour and fracture toughness of an adhesive layer*. 2019.
- [11] P. L. Rosendahl, Y. Staudt, C. Odenbreit, J. Schneider, and W. Becker. “Measuring mode I fracture properties of thick-layered structural silicone sealants”. In: *International Journal of Adhesion and Adhesives* 91 (2019), pp. 64–71. ISSN: 0143-7496. DOI: 10.1016/j.ijadhadh.2019.02.012.
- [12] M. D. Banea, L. F. M. Da Silva, and R. D. S. G. Campilho. “Mode II Fracture Toughness of Adhesively Bonded Joints as a Function of Temperature: Experimental and Numerical Study”. In: *The Journal of Adhesion* 88.4-6 (2012), pp. 534–551. ISSN: 0021-8464. DOI: 10.1080/00218464.2012.660835.

- [13] D30 Committee. *Test Method for Determination of the Mode II Interlaminar Fracture Toughness of Unidirectional Fiber-Reinforced Polymer Matrix Composites*. West Conshohocken, PA. DOI: 10.1520/D7905_D7905M-19E01.
- [14] Y. Boutar, S. Naïmi, S. Mezlini, L. F. da Silva, and M. Ben Sik Ali. “Characterization of aluminium one-component polyurethane adhesive joints as a function of bond thickness for the automotive industry: Fracture analysis and behavior”. In: *Engineering Fracture Mechanics* 177 (2017), pp. 45–60. ISSN: 0013-7944. DOI: 10.1016/j.engfracmech.2017.03.044.
- [15] K. Leffler, K. S. Alfredsson, and U. Stigh. “Shear behaviour of adhesive layers”. In: *International Journal of Solids and Structures* 44.2 (2007), pp. 530–545. ISSN: 00207683. DOI: 10.1016/j.ijsolstr.2006.04.036.
- [16] U. Stigh, K. S. Alfredsson, and A. Biel. “Measurement of cohesive laws and related problems”. In: *Proceedings of the ASME 2009 International Mechanical Engineering Congress & Exposition* (2009).
- [17] U. Stigh, A. Biel, and T. Walander. “Shear strength of adhesive layers – Models and experiments”. In: *Engineering Fracture Mechanics* 129 (2014), pp. 67–76. ISSN: 0013-7944. DOI: 10.1016/j.engfracmech.2014.07.033.
- [18] B. Blackman, A. J. Kinloch, and M. Paraschi. “The determination of the mode II adhesive fracture resistance, GIIC, of structural adhesive joints: an effective crack length approach”. In: *Engineering Fracture Mechanics* 72.6 (2005), pp. 877–897. ISSN: 0013-7944. DOI: 10.1016/j.engfracmech.2004.08.007.
- [19] S. Marzi, O. Hesebeck, M. Brede, and F. Kleiner. “An End-Loaded Shear Joint (ELSJ) Specimen to Measure the Critical Energy Release Rate in Mode II of Tough, Structural Adhesive Joints”. In: *Journal of Adhesion Science and Technology* 23.15 (2009), pp. 1883–1891. ISSN: 0169-4243. DOI: 10.1163/016942409X12508517390716.
- [20] S. Marzi, A. Biel, and U. Stigh. “On experimental methods to investigate the effect of layer thickness on the fracture behavior of adhesively bonded joints”. In: *International Journal of Adhesion and Adhesives* 31.8 (2011), pp. 840–850. ISSN: 0143-7496. DOI: 10.1016/j.ijadhadh.2011.08.004.
- [21] B. Watson, M. J. Worswick, and D. S. Cronin. “Quantification of mixed mode loading and bond line thickness on adhesive joint strength using novel test specimen geometry”. In: *International Journal of Adhesion and Adhesives* 102 (2020), p. 102682. ISSN: 0143-7496. DOI: 10.1016/j.ijadhadh.2020.102682.
- [22] Y. W. Mai. “Quasi-Static Adhesive Fracture”. In: *The Journal of Adhesion* 7.2 (1975), pp. 141–153. ISSN: 0021-8464. DOI: 10.1080/00218467508075046.
- [23] H. Chai. “Shear fracture”. In: *International Journal of Fracture* 37.2 (1988), pp. 137–159. DOI: 10.1007/BF00041716.
- [24] S. L. Donaldson. “Mode III interlaminar fracture characterization of composite materials”. In: *Composites Science and Technology* 32.3 (1988), pp. 225–249. ISSN: 02663538. DOI: 10.1016/0266-3538(88)90022-X.
- [25] H. Yoshihara. “Examination of the 4-ENF test for measuring the mode III R-curve of wood”. In: *Engineering Fracture Mechanics* 73.1 (2006), pp. 42–63. ISSN: 0013-7944. DOI: 10.1016/j.engfracmech.2005.06.008.
- [26] B. D. Davidson and F. O. Sediles. “Mixed-mode I–II–III delamination toughness determination via a shear–torsion–bending test”. In: *Composites Part A: Applied Science and Manufacturing* 42.6 (2011), pp. 589–603. ISSN: 1359-835X. DOI: 10.1016/j.compositesa.2011.01.018.

References

- [27] A. L. Johnston, B. D. Davidson, and K. K. Simon. “Assessment of split-beam-type tests for mode III delamination toughness determination”. In: *International Journal of Fracture* 185.1-2 (2014), pp. 31–48. ISSN: 0376-9429. DOI: 10.1007/s10704-013-9897-1.
- [28] U. Stigh, A. Biel, and D. Svensson. “Cohesive zone modelling and the fracture process of structural tape”. In: *Procedia Structural Integrity* 2 (2016), pp. 235–244. ISSN: 24523216. DOI: 10.1016/j.prostr.2016.06.031.
- [29] L. Loh and S. Marzi. “An Out-of-plane Loaded Double Cantilever Beam (ODCB) test to measure the critical energy release rate in mode III of adhesive joints: Special issue on joint design”. In: *International Journal of Adhesion and Adhesives* 83 (2018), pp. 24–30. ISSN: 0143-7496. DOI: 10.1016/j.ijadhadh.2018.02.021. URL: <http://www.sciencedirect.com/science/article/pii/S014374961830054X>.
- [30] L. Loh and S. Marzi. “A Mixed-Mode Controlled DCB test on adhesive joints loaded in a combination of modes I and III”. In: *Procedia Structural Integrity* 13 (2018), pp. 1318–1323. ISSN: 24523216. DOI: 10.1016/j.prostr.2018.12.277.
- [31] L. Loh and S. Marzi. “Mixed-mode I+III tests on hyperelastic adhesive joints at prescribed mode-mixity”. In: *International Journal of Adhesion and Adhesives* 85 (2018), pp. 113–122. ISSN: 0143-7496. DOI: 10.1016/j.ijadhadh.2018.05.024. URL: <http://www.sciencedirect.com/science/article/pii/S0143749618301519>.
- [32] L. Loh and S. Marzi. “A novel experimental methodology to identify fracture envelopes and cohesive laws in mixed-mode I + III”. In: *Engineering Fracture Mechanics* 214 (2019), pp. 304–319. ISSN: 0013-7944. DOI: 10.1016/j.engfracmech.2019.03.011.
- [33] R. H. Martin. “Evaluation of the Split Cantilever Beam for Mode III Delamination Testing”. In: *Composite Materials: Fatigue and Fracture (Third Volume)*. Ed. by T. K. O’Brien. 100 Barr Harbor Drive, PO Box C700, West Conshohocken, PA 19428-2959: ASTM International, 1991, pp. 243-243–24. ISBN: 978-0-8031-1419-7. DOI: 10.1520/STP17722S.
- [34] F. Bödeker and S. Marzi. “Applicability of the mixed-mode controlled double cantilever beam test and related evaluation methods”. In: *Engineering Fracture Mechanics* 235 (2020), p. 107149. ISSN: 0013-7944. DOI: 10.1016/j.engfracmech.2020.107149.
- [35] A. Biel, J. Tryding, M. Ristinmaa, M. Johansson-Näslund, O. Tuveesson, and U. Stigh. “Experimental evaluation of normal and shear delamination in cellulose-based materials using a cohesive zone model”. In: *International Journal of Solids and Structures* 252 (2022), p. 111755. ISSN: 00207683. DOI: 10.1016/j.ijsolstr.2022.111755.
- [36] G. Fernlund, H. Lanting, and J. K. Spelt. “Mixed Mode II-Mode III Fracture of Adhesive Joints”. In: *Journal of Composites Technology and Research* 17.4 (1995), p. 317. ISSN: 08846804. DOI: 10.1520/CTR10452J.
- [37] H. Chai. “Bond thickness effect in mixed-mode fracture and its significance to delamination resistance”. In: *International Journal of Solids and Structures* 219-220 (2021), pp. 63–80. ISSN: 00207683. DOI: 10.1016/j.ijsolstr.2021.03.006.
- [38] I. Costa and J. A. O. Barros. “Creep of structural adhesives: an overview”. In: (2012).
- [39] R. A. Queiroz, E. M. Sampaio, V. J. Cortines, and N. R. F. Rohem. “Study on the creep behavior of bonded metallic joints”. In: *Applied Adhesion Science* 2.1 (2014), p. 8. ISSN: 2196-4351. DOI: 10.1186/2196-4351-2-8.
- [40] D. R. Lefebvre, D. A. Dillard, and H. F. Brinson. “The development of a modified double-cantilever-beam specimen for measuring the fracture energy of rubber to metal bonds”. In: *Experimental Mechanics* 28.1 (1988), pp. 38–44. ISSN: 0014-4851. DOI: 10.1007/BF02328994.

- [41] D. A. Dillard. “Stresses between Adherends with Different Curvatures”. In: *The Journal of Adhesion* 26.1 (1988), pp. 59–69. ISSN: 0021-8464. DOI: 10.1080/00218468808071274.
- [42] D. A. Dillard, J. Z. Wang, and H. Parvatareddy. “A Simple Constant Strain Energy Release Rate Loading Method for Double Cantilever Beam Specimens”. In: *The Journal of Adhesion* 41.1-4 (1993), pp. 35–50. ISSN: 0021-8464. DOI: 10.1080/00218469308026553.
- [43] D. Plausinis and J. K. Spelt. “Application of a new constant G load-jig to creep crack growth in adhesive joints”. In: *International Journal of Adhesion and Adhesives* 15.4 (1995), pp. 225–232. ISSN: 0143-7496. DOI: 10.1016/0143-7496(96)83703-1.
- [44] R. Moutou Pitti, F. Dubois, and O. Pop. “A proposed mixed-mode fracture specimen for wood under creep loadings”. In: *International Journal of Fracture* 167.2 (2011), pp. 195–209. ISSN: 0376-9429. DOI: 10.1007/s10704-010-9544-z.
- [45] R. M. Carneiro Neto, A. Akhavan-Safar, E. M. Sampaio, J. T. Assis, and L. F. M. Da Silva. “Effect of creep on the mode II residual fracture energy of adhesives”. In: *Journal of Applied Polymer Science* 138.47 (2021), p. 51387. ISSN: 00218995. DOI: 10.1002/app.51387.
- [46] R. M. Carneiro Neto, A. Akhavan-Safar, E. M. Sampaio, J. T. Assis, and L. Da Silva. “Assessment of the creep life of adhesively bonded joints using the end notched flexure samples”. In: *Engineering Failure Analysis* 133 (2022), p. 105969. ISSN: 13506307. DOI: 10.1016/j.engfailanal.2021.105969.
- [47] J. P. Márquez Costa, J. Jumel, C. Badulescu, and G. Stamoulis. “Self-similar crack propagation along a viscoelastic interface in a double-cantilever beam test”. In: *Mechanics of Time-Dependent Materials* (2022). ISSN: 1385-2000. DOI: 10.1007/s11043-022-09559-8.
- [48] J. J. M. Machado, E. A. S. Marques, and L. F. M. Da Silva. “Adhesives and adhesive joints under impact loadings: An overview”. In: *The Journal of Adhesion* 94.6 (2018), pp. 421–452. ISSN: 0021-8464. DOI: 10.1080/00218464.2017.1282349.
- [49] C. Borges, P. Nunes, A. Akhavan, E. Marques, R. Carbas, L. Alfonso, and L. Silva. “Influence of mode mixity and loading rate on the fracture behaviour of crash resistant adhesives”. In: *Theoretical and Applied Fracture Mechanics* 107 (2020), p. 102508. ISSN: 01678442. DOI: 10.1016/j.tafmec.2020.102508.
- [50] S. Xu and D. A. Dillard. “Determining the impact resistance of electrically conductive adhesives using a falling wedge test”. In: *IEEE Transactions on Components and Packaging Technologies* 26.3 (2003), pp. 554–562. ISSN: 1521-3331. DOI: 10.1109/TCAPT.2003.817646.
- [51] B. Blackman, A. J. Kinloch, F. S. Rodriguez Sanchez, W. S. Teo, and J. G. Williams. “The fracture behaviour of structural adhesives under high rates of testing”. In: *Engineering Fracture Mechanics* 76.18 (2009), pp. 2868–2889. ISSN: 0013-7944. DOI: 10.1016/j.engfracmech.2009.07.013.
- [52] S. H. Marzi. *Ein ratenabhängiges, elasto-plastisches Kohäsivzonenmodell zur Berechnung struktureller Klebverbindungen unter Crashbeanspruchung: Zugl.: Aachen, Techn. Hochsch., Diss., 2010*. Stuttgart: Fraunhofer-Verl., 2010. ISBN: 978-3-8396-0161-7. URL: <http://publica.fraunhofer.de/dokumente/N-139053.html>.
- [53] A. Karac, B. Blackman, V. Cooper, A. J. Kinloch, S. Rodriguez Sanchez, W. S. Teo, and A. Ivankovic. “Modelling the fracture behaviour of adhesively-bonded joints as a function of test rate”. In: *Engineering Fracture Mechanics* 78.6 (2011), pp. 973–989. ISSN: 0013-7944. DOI: 10.1016/j.engfracmech.2010.11.014.

References

- [54] J. U. Cho, A. Kinloch, B. Blackman, F. S. Rodriguez Sanchez, and M. S. Han. “High-strain-rate fracture of adhesively bonded composite joints in DCB and TDCB specimens”. In: *International Journal of Automotive Technology* 13.7 (2012), pp. 1127–1131. ISSN: 1229-9138. DOI: 10.1007/s12239-012-0115-3.
- [55] T. Gao, A. J. Kinloch, B. R. K. Blackman, F. S. Rodriguez Sanchez, S.-k. Lee, C. Cho, H.-j. Bang, S. S. Cheon, and J. U. Cho. “A study of the impact properties of adhesively-bonded aluminum alloy based on impact velocity”. In: *Journal of Mechanical Science and Technology* 29.2 (2015), pp. 493–499. ISSN: 1738-494X. DOI: 10.1007/s12206-015-0109-y.
- [56] S. Marzi, A. Biel, and O. Hesebeck. “3D optical displacement measurements on dynamically loaded adhesively bonded T-peel specimens”. In: *International Journal of Adhesion and Adhesives* 56 (2015), pp. 41–45. ISSN: 0143-7496. DOI: 10.1016/j.ijadhadh.2014.07.013.
- [57] M. Isakov, M. May, P. Hahn, H. Paul, and M. Nishi. “Fracture toughness measurement without force data – Application to high rate DCB on CFRP”. In: *Composites Part A: Applied Science and Manufacturing* 119 (2019), pp. 176–187. ISSN: 1359-835X. DOI: 10.1016/j.compositesa.2019.01.030.
- [58] N. Dagorn, G. Portemont, V. Joudon, B. Bourel, and F. Lauro. “Fracture rate dependency of an adhesive under dynamic loading”. In: *Engineering Fracture Mechanics* 235 (2020), p. 107082. ISSN: 0013-7944. DOI: 10.1016/j.engfracmech.2020.107082.
- [59] F. Sun, R. Zhang, and B. R. Blackman. “Determination of the mode I crack tip opening rate and the rate dependent cohesive properties for structural adhesive joints using digital image correlation”. In: *International Journal of Solids and Structures* 217-218 (2021), pp. 60–73. ISSN: 00207683. DOI: 10.1016/j.ijsolstr.2021.01.034.
- [60] L. Škec and G. Alfano. “Experimental and numerical study of rate-dependent mode-I failure of a structural adhesive”. In: *The Journal of Adhesion* (2022), pp. 1–33. ISSN: 0021-8464. DOI: 10.1080/00218464.2022.2106132.
- [61] T. Carlberger, A. Biel, and U. Stigh. “Influence of temperature and strain rate on cohesive properties of a structural epoxy adhesive”. In: *International Journal of Fracture* 155.2 (2009), pp. 155–166. ISSN: 0376-9429. DOI: 10.1007/s10704-009-9337-4.
- [62] S. Marzi. “Measuring the critical energy release rate in mode II of tough, structural adhesive joints using the tapered end-notched flexure (TENF) test”. In: *The European Physical Journal Special Topics* 206.1 (2012), pp. 35–40. ISSN: 1951-6355. DOI: 10.1140/epjst/e2012-01584-4.
- [63] M. May, O. Hesebeck, S. Marzi, W. Böhme, J. Lienhard, S. Kilchert, M. Brede, and S. Hiermaier. “Rate dependent behavior of crash-optimized adhesives – Experimental characterization, model development, and simulation”. In: *Engineering Fracture Mechanics* 133 (2015), pp. 112–137. ISSN: 0013-7944. DOI: 10.1016/j.engfracmech.2014.11.006. URL: <http://www.sciencedirect.com/science/article/pii/S0013794414003804>.
- [64] M. Costa, R. Carbas, E. Marques, G. Viana, and L. Da Silva. “An apparatus for mixed-mode fracture characterization of adhesive joints”. In: *Theoretical and Applied Fracture Mechanics* 91 (2017), pp. 94–102. ISSN: 01678442. DOI: 10.1016/j.tafmec.2017.04.014.
- [65] C. Sato and S. Marzi. “High-rate loading and impact in adhesively bonding joints”. In: *Adhesive Bonding*. Elsevier, 2021, pp. 257–293. ISBN: 9780128199541. DOI: 10.1016/B978-0-12-819954-1.00015-0.
- [66] G. S. Baş and E. Sancaktar. “Mixed-mode fracture behavior of epoxy-based impact adhesives”. In: *International Journal of Adhesion and Adhesives* (2021), p. 103012. ISSN: 0143-7496. DOI: 10.1016/j.ijadhadh.2021.103012.

- [67] D. Pennas, W. J. Cantwell, and P. Compston. “The Influence of Loading Rate on the Mode III Fracture Properties of Adhesively Bonded Composites”. In: *Journal of Reinforced Plastics and Composites* 28.16 (2009), pp. 1999–2012. ISSN: 0731-6844. DOI: 10.1177/0731684408090716.
- [68] N. Dagorn, G. Portemont, J. Berthe, F. Rasselet, B. Bourel, and F. Lauro. “Development of a mixed mode double cantilever beam specimen for the fracture characterization of adhesives under high displacement rate”. In: *Engineering Fracture Mechanics* 242 (2021), p. 107467. ISSN: 0013-7944. DOI: 10.1016/j.engfracmech.2020.107467.
- [69] G. Stamoulis and N. Carrere. “Linear elastic analysis of the loading rate dependency of the fracture properties of structural adhesives in the mixed mode I+II plane”. In: *Engineering Fracture Mechanics* 225 (2020), p. 106840. ISSN: 0013-7944. DOI: 10.1016/j.engfracmech.2019.106840.
- [70] M. Pérez-Galmés, J. Renart, C. Sarrado, A. J. Brunner, and A. Rodríguez-Bellido. “Towards a consensus on mode II adhesive fracture testing: Experimental study”. In: *Theoretical and Applied Fracture Mechanics* 98 (2018), pp. 210–219. ISSN: 01678442. DOI: 10.1016/j.tafmec.2018.09.014.
- [71] F. Lahuerta, T. Westphal, R. Nijssen, F. P. van der Meer, and L. J. Sluys. “Measuring the delamination length in static and fatigue mode I tests using video image processing”. In: *Compos. Part B* 63.63 (2014), pp. 1–7. DOI: 10.1016/j.compositesb.2014.03.003.
- [72] F. Sun and B. Blackman. “A DIC method to determine the Mode I energy release rate G , the J -integral and the traction-separation law simultaneously for adhesive joints”. In: *Engineering Fracture Mechanics* 234 (2020), p. 107097. ISSN: 0013-7944. DOI: 10.1016/j.engfracmech.2020.107097.
- [73] N. Ben Salem, M. K. Budzik, J. Jumel, M. Shanahan, and F. Lavelle. “Investigation of the crack front process zone in the Double Cantilever Beam test with backface strain monitoring technique”. In: *Engineering Fracture Mechanics* 98.18 (2013), pp. 272–283. ISSN: 0013-7944. DOI: 10.1016/j.engfracmech.2012.09.028.
- [74] A. Bernasconi, M. Kharshiduzzaman, and L. Comolli. “Strain Profile Measurement for Structural Health Monitoring of Woven Carbon-fiber Reinforced Polymer Composite Bonded joints by Fiber Optic Sensing Using an Optical Backscatter Reflectometer”. In: *The Journal of Adhesion* 92.6 (2016), pp. 440–458. ISSN: 0021-8464. DOI: 10.1080/00218464.2015.1043005.
- [75] H. T. Truong, M. J. Martinez, O. O. Ochoa, and D. C. Lagoudas. “Mode I fracture toughness of hybrid co-cured Al-CFRP and NiTi-CFRP interfaces: An experimental and computational study”. In: *Composites Part A: Applied Science and Manufacturing* 135.2 (2020), p. 105925. ISSN: 1359-835X. DOI: 10.1016/j.compositesa.2020.105925.
- [76] R. Lima, R. Perrone, M. Carboni, and A. Bernasconi. “Experimental analysis of mode I crack propagation in adhesively bonded joints by optical backscatter reflectometry and comparison with digital image correlation”. In: *Theoretical and Applied Fracture Mechanics* 116.10 (2021), p. 103117. ISSN: 01678442. DOI: 10.1016/j.tafmec.2021.103117.
- [77] F. Sun and B. R. Blackman. “Using digital image correlation to automate the measurement of crack length and fracture energy in the mode I testing of structural adhesive joints”. In: *Engineering Fracture Mechanics* 255 (2021), p. 107957. ISSN: 0013-7944. DOI: 10.1016/j.engfracmech.2021.107957.
- [78] M. D. Banea, L. F. M. Da Silva, and R. D. S. G. Campilho. “The Effect of Adhesive Thickness on the Mechanical Behavior of a Structural Polyurethane Adhesive”. In: *The Journal of Adhesion* 91.5 (2015), pp. 331–346. ISSN: 0021-8464. DOI: 10.1080/00218464.2014.903802.
- [79] R. Campilho, D. C. Moura, M. D. Banea, and L. Da Silva. “Adhesive thickness effects of a ductile adhesive by optical measurement techniques”. In: *International Journal of Adhesion and Adhesives* 57 (2015), pp. 125–132. ISSN: 0143-7496. DOI: 10.1016/j.ijadhadh.2014.12.004.

References

- [80] M. Cabello, J. Zurbitu, J. Renart, A. Turon, and F. Martínez. “A non-linear hyperelastic foundation beam theory model for double cantilever beam tests with thick flexible adhesive”. In: *International Journal of Solids and Structures* 80 (2016), pp. 19–27. ISSN: 00207683. DOI: 10.1016/j.ijsolstr.2015.10.017.
- [81] K. Hasegawa, A. D. Crocombe, F. Coppuck, D. Jewel, and S. Maher. “Characterising bonded joints with a thick and flexible adhesive layer? Part 1: Fracture testing and behaviour”. In: *International Journal of Adhesion and Adhesives* 63 (2015), pp. 124–131. ISSN: 0143-7496. DOI: 10.1016/j.ijadhadh.2015.09.003.
- [82] P. L. Rosendahl. “From bulk to structural failure: fracture of hyperelastic materials”. PhD thesis. Technical University of Darmstadt, 2020. DOI: 10.25534/tuprints-00008693.
- [83] C. Schmandt and S. Marzi. “Effect of crack opening velocity on fracture behavior of hyperelastic semi-structural adhesive joints subjected to mode I loading”. In: *Procedia Structural Integrity* 13 (2018), pp. 799–805. ISSN: 24523216. DOI: 10.1016/j.prostr.2018.12.154.
- [84] C. Schmandt and S. Marzi. “Effect of crack opening velocity and adhesive layer thickness on the fracture behaviour of hyperelastic adhesive joints subjected to mode I loading: Special issue on joint design”. In: *International Journal of Adhesion and Adhesives* 83 (2018), pp. 9–14. ISSN: 0143-7496. DOI: 10.1016/j.ijadhadh.2018.02.028. URL: <http://www.sciencedirect.com/science/article/pii/S0143749618300678>.
- [85] A. Khayer Dastjerdi, E. Tan, and F. Barthelat. “Direct Measurement of the Cohesive Law of Adhesives Using a Rigid Double Cantilever Beam Technique”. In: *Experimental Mechanics* 53.9 (2013), pp. 1763–1772. ISSN: 0014-4851. DOI: 10.1007/s11340-013-9755-0.
- [86] G. R. Irwin and J. A. Kies. “Critical Energy Rate Analysis of Fracture Strength”. In: *Welding Journal, Research Supplement Vol. 33* (1954), p. 193s.
- [87] D. S. Dugdale. “Yielding of steel sheets containing slits”. In: *Journal of the Mechanics and Physics of Solids* 8.2 (1960), pp. 100–104. DOI: 10.1016/0022-5096(60)90013-2.
- [88] G. I. Barenblatt. “The Mathematical Theory of Equilibrium Cracks in Brittle Fracture”. In: *Advances in Applied Mechanics Volume 7*. Vol. 7. Advances in Applied Mechanics. Elsevier, 1962, pp. 55–129. ISBN: 9780120020072. DOI: 10.1016/S0065-2156(08)70121-2.
- [89] J. R. Rice. “A Path Independent Integral and the Approximate Analysis of Strain Concentration by Notches and Cracks”. In: *Journal of Applied Mechanics* 35.2 (1968), pp. 379–386. ISSN: 0021-8936. DOI: 10.1115/1.3601206.
- [90] G. P. Cherepanov. “Crack propagation in continuous media”. In: *Journal of Applied Mathematics and Mechanics* 31.3 (1967), pp. 503–512. ISSN: 00218928. DOI: 10.1016/0021-8928(67)90034-2.
- [91] J. W. Hutchinson. “Singular behaviour at the end of a tensile crack in a hardening material”. In: *Journal of the Mechanics and Physics of Solids* 16.1 (1968), pp. 13–31. DOI: 10.1016/0022-5096(68)90014-8. URL: <http://www.sciencedirect.com/science/article/pii/0022509668900148>.
- [92] J. R. Rice and G. F. Rosengren. “Plane strain deformation near a crack tip in a power-law hardening material”. In: *Journal of the Mechanics and Physics of Solids* 16.1 (1968), pp. 1–12. DOI: 10.1016/0022-5096(68)90013-6. URL: <http://www.sciencedirect.com/science/article/pii/0022509668900136>.
- [93] J. P. Berry. “Determination of Fracture Surface Energies by the Cleavage Technique”. In: *Journal of Applied Physics* 34.1 (1963), pp. 62–68. ISSN: 0021-8979. DOI: 10.1063/1.1729091.
- [94] A. J. Paris and P. Paris. “Instantaneous evaluation of J and C”. In: *International Journal of Fracture* 38 (1988), R19–R21.

- [95] S. Mostovoy and E. J. Ripling. “Fracture toughness of an epoxy system”. In: *Journal of Applied Polymer Science* 10.9 (1966), pp. 1351–1371. ISSN: 00218995. DOI: 10.1002/app.1966.070100913.
- [96] G. Fernlund, M. Papini, D. McCammond, and J. K. Spelt. “Fracture load predictions for adhesive joints”. In: *Composites Science and Technology* 51.4 (1994), pp. 587–600. ISSN: 02663538. DOI: 10.1016/0266-3538(94)90091-4.
- [97] L. Škec, G. Alfano, and G. Jelenić. “Enhanced simple beam theory for characterising mode-I fracture resistance via a double cantilever beam test”. In: *Composites Part B: Engineering* 167 (2019), pp. 250–262. ISSN: 13598368. DOI: 10.1016/j.compositesb.2018.11.099.
- [98] J. D. Landes and J. A. Begley. “A Fracture Mechanics Approach to Creep Crack Growth”. In: *Mechanics of Crack Growth*. Ed. by J. R. Rice and P. C. Paris. 100 Barr Harbor Drive, PO Box C700, West Conshohocken, PA 19428-2959: ASTM International, 1976, pp. 128-128–21. ISBN: 978-0-8031-0509-6. DOI: 10.1520/STP33943S.

Appended papers

Paper A:

Mode I creep fracture of rubber-like adhesive joints at constant crack driving force

Peer Schrader, Christopher Schmandt, Stephan Marzi

Reprinted from International Journal of Adhesion and Adhesives, Volume 113, P. Schrader, C. Schmandt, S. Marzi, *Mode I creep fracture of rubber-like adhesive joints at constant crack driving force*, 103079, 2022, <https://doi.org/10.1016/j.ijadhadh.2021.103079>, with permission from Elsevier

Author Contributions:

The specimens were manufactured by C. Schmandt and the author. The experiments were conducted by C. Schmandt and the author; the author was particularly responsible for the planning of the visual crack tip detection as well as the set-up and operation of the camera systems. All experimental results were solely evaluated by the author, including conceptualization and implementation of the image processing algorithms. The paper was planned and written by C. Schmandt and the author. S. Marzi was responsible for funding acquisition, supervised the work and proofread the paper.



Contents lists available at ScienceDirect

International Journal of Adhesion and Adhesives

journal homepage: www.elsevier.com/locate/ijadhadh

Mode I creep fracture of rubber-like adhesive joints at constant crack driving force

Peer Schrader, Christopher Schmandt, Stephan Marzi*

Institute of Mechanics and Materials, Technische Hochschule Mittelhessen, Wiesenstrasse 14, 35390, Giessen, Germany

ARTICLE INFO

Keywords:
Polyurethane
Aluminium and alloys
Peel
Creep
J-integral

ABSTRACT

This work contributes to the description of time-dependent mechanical mode I creep fracture of viscoelastic adhesive joints under pure peel loading at finite deformations. The focus is on the dependency of crack resistance and resulting crack propagation rate on the forming of minor cracks beside the macroscopic major crack tip. In this work, Double Cantilever Beam tests were carried out at polyurethane-based flexible adhesive joints. The experiments were externally controlled on a constant J -integral, which was calculated in-situ from measured data to obtain a constant crack driving force and a statically loaded crack tip, respectively. The resulting creep crack propagation was investigated using two cameras targeting both sides of the specimen. With help of image processing and the beam compliance method, crack extension and crack propagation rate were determined. The respective results were used to draw comparisons between these two methods. The slight difference between the methods was attributed to the appearance of minor cracks, which seemed to reduce the stress intensity at the macroscopic crack tip, yielding a lower crack propagation rate.

1. Introduction

The joining of various dissimilar types of materials is nowadays frequently realized by the usage of adhesion technologies, which have evolved to standard applications within various branches of industry in recent years. The literature contains many contributions dealing with stiff epoxy-based adhesives, but only few investigated rubber-like ones, although Loureiro et al. [1], amongst others, emphasized important advantages of very flexible joints concerning damping, fatigue, crack resistance, and impact.

Metal-glass-constructions are only practicable due to rubber-like adhesives because the bond line must provide soft coupling to avoid high stresses in the brittle glass plates that could lead to damage. In the field of civil engineering, natural influences like snow, gravity, wind, or vibrations can produce complex loading situations in the high-deforming adhesive layer, as experimentally investigated by Richter et al. [2] in component tests on multi-side-bonded steel-glass facade panels. However, the aforesaid quasi-static and dynamic loadings from natural influences can lead to creep fracture processes in the adhesive layer as well, whereby only contributions investigating stiff epoxy-based adhesives are available. Meshgin et al. [3] investigated the long-term behaviour of an epoxy-based interface between fibre-reinforced

polymers and concrete, while Puigvert et al. [4] studied tendons made of carbon-fibre-reinforced polymer, which were adhesively potted in a steel tube.

Regarding the long-term integrity of adhesive connections, peel loading is the most disadvantageous load case. Even shear loadings will mainly cause peel stresses in a thick and soft adhesive layer due to finite deformations. This is why investigating the peel fracture is essential if one wishes to describe fracture processes for flexible adhesives. The peel fracture behaviour can be studied using Double Cantilever Beam (DCB) tests, yielding the mode I critical energy release rate as the most important material parameter characterizing the damage process. A large number of publications exists trying to accomplish the investigation of adhesives under an approximately constant energy release rate. Next to the classical example of the Tapered Double Cantilever Beam test, as proposed by Mostovoy and Ripling [5] in the 1960s, a range of other intricate experimental techniques tried to approximate a constant energy release rate during peel debonding. Lefebvre et al. [6] used a spring device, whereas Dillard et al. [7] used a geometric arrangement of cables and a dead weight to load a modified DCB specimen on nearly constant energy release rate within certain test windows. Dillard [8] also proposed adherends of different curvatures as a possibility to investigate fracture processes under constant energy release rate resulting from

* Corresponding author.

E-mail address: stephan.marzi@me.thm.de (S. Marzi).<https://doi.org/10.1016/j.ijadhadh.2021.103079>

Received 15 October 2021; Accepted 16 December 2021

Available online 18 December 2021

0143-7496/© 2021 Elsevier Ltd. All rights reserved.

residual peel stresses. Chang et al. [9] as well as Dillard and Bao [10] obtained constant energy release rates during modified blister tests with large experimental effort. With the help of computer control, it is nowadays possible to control experiments on desired values of the energy release rate in-situ, using less intricate setups within the experimental investigation.

Apart from the energy release rate, the knowledge of the current crack length is of great relevance in the field of fracture testing and is still a topic of ongoing research. Srilakshmi et al. [11] used optical monitoring of the crack tip position via digital image correlation, while Eaton et al. [12] used acoustic emissions to locate the propagating crack, which is likely infeasible for rubber-like adhesives due to their damping properties. Anyway, determining a reliable value for the crack position is a challenging measurement task, especially if the crack front is uneven, finite deformations occur, or micro-cracked regions emerge ahead of the main crack, as observed from Blackman et al. [13], who determined the effective crack length with an analytical approach in consequence. Hence, the ability to investigate fracture processes without knowing the current crack length is of significant interest because it noticeably reduces the experimental effort and possible sources of measurement uncertainty.

With the setup presented in this study, it is possible to externally control a testing machine on an arbitrary prescribed crack driving force, opening up possibilities to characterize time-dependent crack growth. In the performed experiments, the J -integral according to Rice [14] is calculated in-situ from peel force and rotation of the load introduction points in DCB tests with a rubber-like thick adhesive. The crack position is optically determined by manually analysing images captured during crack growth from both sides of the specimen. The resulting value of crack position is compared to the equivalent crack extension obtained from enhanced simple beam theory, as proposed by Skec et al. [15]. Differences between these two methods, which occurred in some cases, can be related to the formation of minor cracks in the vicinity of the major crack tip in direction of crack propagation, which was observed similarly by Blackman et al. [13]. This phenomenon correlates with a reduction of stress intensity at the crack tip, yielding lower crack propagation rates.

Throughout this paper, we will mostly rely on showing representative measurements of only one specimen for reasons of clarity. The evaluations of all experiments will be provided individually in the supplementary materials.

2. Methods

2.1. Experimental setup

Consider a DCB specimen of width b loaded with a force F as sketched in Fig. 1. The applied force F introduces a mode I peel loading into the adhesive layer, resulting in a bending of the adherends. Assuming linear deformation of the adherends with θ_1 and θ_2 as the rotational angles at the force introduction points being small (cf. Fig. 7b), the J -Integral according to Rice [14] for mode I loading can be calculated directly from measured data using an approach as proposed by Paris and Paris [16]:

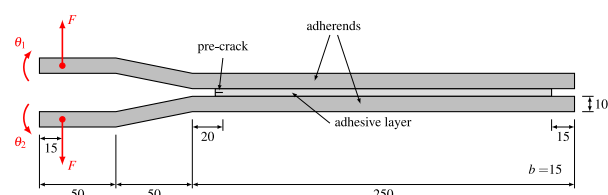


Fig. 1. Schematic representation of the used DCB specimens (all dimensions in millimetres).

$$J = \frac{F(\theta_1 + \theta_2)}{b} \quad (1)$$

More details on the approach and the derivation from the original definition of the J -integral resulting from the equilibrium of energetic forces can be found in the paper of Andersson and Stigh [17]. F , θ_1 , and θ_2 can be easily measured during the experiments, allowing an in-situ calculation of J . This enables the possibility of controlling DCB tests on specific values of J .

The experimental setup is depicted in Fig. 2. The tests were performed in an electro-mechanical testing machine with a load cell of 500 N capacity (inspekt table 5 kN, Hegewald & Peschke, Nossen, Germany). To measure the adherends' rotation at the points of load introduction, incremental high-resolution rotary encoders (BDH 1P.05A320000-L0-5, Baumer AG, Frauenfeld, Switzerland) were used. Two 12 MP cameras (acA4112-20 μ m, Basler AG, Ahrensburg, Germany) were set up to capture the crack propagation during the experiments, with one camera being placed on each side of the specimen. We want to note that end-blocks were used to accommodate for the rotary encoders in the setup.

Before testing, the specimens were coated with white water-based lacquer. Thereafter, a black speckle pattern, which was necessary to determine the rigid body motion of the specimens, was applied with a speckle roller (Correlated Solutions Inc., Irmo, USA). A reference length of 120 mm was marked on the adherends to be used later as a scale for conversion from pixels to length in millimetres.

2.2. Controlling the load frame on J -Integral

Using an external measuring software (DASYLab 13, National Instruments, Texas, USA) the analogue signal of the peel force F was multiplied with the sum of the digital signals containing the rotational angles of the force introduction points θ_1 and θ_2 to calculate the current value of J as a process variable in-situ according to Eq. (1). Besides this, a setpoint generator module within the DASYLab software was used to generate the setpoint value of J . The difference between the current and the setpoint value as the error value of J was corrected by a PID controller module within the DASYLab software and transferred from the analogue output of the measuring card (Goldammer GOA-1024-3, Goldammer GmbH, Wolfsburg, Germany) to an analogue input of the testing machine. The driving command of the testing machine was set to

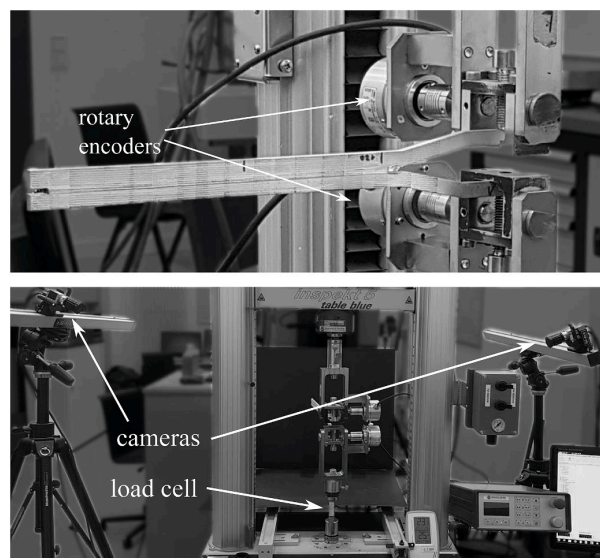


Fig. 2. Experimental setup with DCB specimen, testing machine, rotary encoders, cameras and load cell.

hold the input to be nought over the whole test. For a better overview, the procedure is highlighted in Fig. 3.

In effect, if the current value of J according to Eq. (1) was below the setpoint value of J , a positive voltage was supplied to the analogue input of the testing machine, causing the crosshead to drive upwards until the in-situ value of J was equal to the desired setpoint value. If the current value was above the setpoint, a negative voltage was supplied to the analogue input of the testing machine, causing the crosshead to drive downwards.

2.3. Specimen manufacturing

The DCB tests performed in this study were conducted on the rubber-like adhesive Sikaflex® –521 UV, a one-component polyurethane-hybrid sealant, curing under exposure to atmospheric humidity. According to the manufacturer's specifications, the adhesive provides a tensile strength of 1.8 MPa and a strain at failure of about 400%. To obtain an indication of the materials viscoelastic response, the relaxation behaviour under an uniaxial tensile stress state was investigated in four relaxation tests using a digital image correlation system (GOM Aramis 3D Motion and Deformation Sensor, GOM GmbH, Braunschweig, Germany) and the above mentioned electro-mechanical testing machine. The tensile specimens were elongated to 100% engineering strain and the strain state was then controlled to be constant over time, yielding the curves for the relaxation modulus (calculated from true stress divided by true strain) shown in Fig. 4.

The adherends were made of an aluminium alloy (AlZn5.5MgCu, material grade number 3.4365) with an elastic modulus of (70 ± 1) GPa. Before applying the adhesive with an electric caulking gun, the bonding surfaces of the adherends were sandblasted with corundum (grain size of 100–150 μm) and cleaned with methylethylketone. To adjust the adhesive layer thickness, Teflon spacers (nominal thickness of 3 mm) were placed at the beginning and the end of the adhesive layer. During the curing process, the substrates were held in place with screw clamps. The spacers were removed after a curing time of 10 weeks at room climate (around 22 °C, relative humidity of approximately 30–40%). The adhesive layer thickness of (2.96 ± 0.05) mm was determined after curing by calliper measurements at three different positions and subsequent averaging. Before testing, a sharp pre-crack was introduced at the beginning of the adhesive layer by inserting a razor blade parallel to the bonding surfaces, yielding an initial crack length of (100.2 ± 0.7) mm.

2.4. Equivalent crack extension measurement by use of enhanced simple beam theory

To obtain an equivalent crack extension based on the compliance of the DCB specimen, we will rely on the enhanced simple beam theory approach as proposed by Skec et al. [15], which is based on Timoshenko beam theory. According to their work, the equivalent crack length can be computed via

$$a_c = \sqrt[3]{\left(\sqrt{\frac{6EI}{5\mu wh}}\right)^3 + \frac{3EI\delta}{2F}} - \sqrt{\frac{6EI}{5\mu wh}} \quad (2)$$

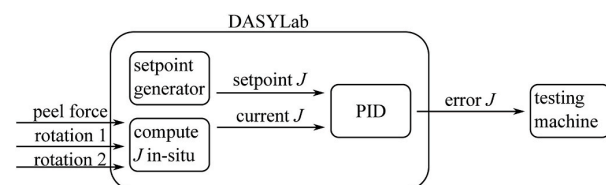


Fig. 3. Schematic representation of the control loop used to achieve a constant crack driving force during testing.

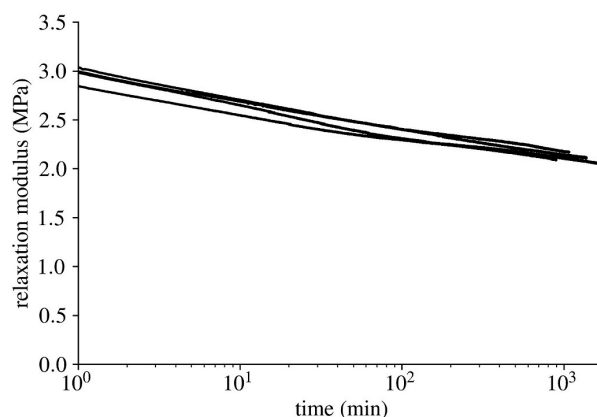


Fig. 4. Relaxation modulus of four tensile specimens of the selected adhesive.

allowing the consideration of beam root rotation. EI , μ , w , and h denote the bending stiffness, the shear modulus, and width and height of the adherends, respectively. δ is the machine displacement, which was corrected with the experimentally determined compliance of the load train without the DCB specimen mounted ($0.61 \mu\text{m}/\text{N}$) before the analysis. To obtain the equivalent crack extension for each experiment, the initial value of the computed equivalent crack length at constant J is subtracted from the subsequent measurement.

We are aware that different effects could influence the computed crack extension, including the usage of end blocks to accommodate for the used rotary encoders, the presence of beam root deflection, or a finite process zone length. However, we assume that these effects are of negligible magnitude due to the small angles θ at the load introduction points (cf. Fig. 7b), comparatively small loads acting on the specimen (cf. Fig. 6a), and, hence, small deformations in the adherends.

2.5. Crack extension measurement by image processing

For the optical determination of the crack length, the crack tip position was evaluated with an image processing algorithm (realized in Python 3). By using the reference length of 120 mm marked on the adherends, scale factors of $(48.84 \pm 0.02) \mu\text{m}/\text{px}$ (left camera) and $(55.61 \pm 0.02) \mu\text{m}/\text{px}$ (right camera) were determined to convert between the number of pixels in the images and the length in millimetres on the specimen. Thereafter, the crack tip position was manually located in each captured image on both sides of the specimen. The rigid body motion of the adherends, which was calculated from the displacement of the whole speckle pattern in the direction of crack extension using the trackpy module [18], was added to the measured crack length to accompany for the relative motion between the deforming DCB specimen and the cameras.

2.6. Optical evaluation of visible damage processes away from the macroscopic crack tip

As we will present later, during the DCB tests under creep load, fracture processes in the adhesive layer away from the macroscopic major crack tip in direction of crack propagation were observed, which was evidenced by tearing on the side surface of the adhesive layer during finite deformations. In the images captured from each side of the specimen, this was manifested by intensive black areas due to the black colour of the adhesive layer, which got visible underneath the white water-based lacquer after damage occurred.

Image processing was used to investigate these damage processes as forming minor cracks away from the major crack tip. Firstly, the images were filtered using a mean filter (kernel size of 5 pixels) to already

attenuate the visibility of the speckle pattern or breakage of the background lacquer. Then, a threshold was applied to the grayscale images, yielding binary images with the detected intensive black areas. As special care was taken in the illumination of the specimens, the selection of the background colour and the selection of white lacquer on a black adhesive layer, a threshold of a grey value of 45 was found to be sufficient for detecting the intensive dark areas in the captured images during the evaluation of all conducted experiments. To reduce errors that could occur due to the speckle pattern being falsely identified as damaged areas, the images were eroded for two iterations and dilated for three iterations (kernel sizes of 5 pixels), making smaller black areas disappear within the image. To then quantify the visible damage processes, the remaining pixels in the binary image with a value of 1 away from the manually located major crack tip in direction of crack propagation were counted, yielding a possibility to quantify the presence of minor cracks away from the major crack tip.

The described procedure ensured that small cracks on the surface of the applied paint as well as the speckle pattern were not detected as damaged areas, whereas larger cracks of the adhesive surface were considered. Hence, it can be assumed that the influences of both breakage of the applied lacquer and the speckle pattern can be considered negligible.

3. Results and discussion

3.1. Fracture behaviour

Representative images of the fracture process with its uneven crack front are shown in Fig. 5, captured from both sides of the specimen. The rubber-like adhesive is subjected to finite deformations and distinctive necking occurs before the crack propagation starts. The large deformations lead to surface tearing on the sides of the specimen, which is visible through intensive black areas away from the crack tip in the direction of crack propagation. Within this study, we refer to the tearing process as minor cracking, occurring in the adhesive layer in direction of crack propagation before macroscopic total fracture takes place through the propagation of the major crack tip. The entirety of these processes yields a complex geometric shape of the developing crack front, which makes it difficult to accurately determine a certain value for the crack tip position.

Although the crack often progressed near the interfaces on the sides of the specimens, it should be noted that the specimens failed cohesively in all cases. It is assumed that the fracture near the interface can be attributed to finite deformations within the adhesive layer and the necking processes, yielding increased stresses at the outer surface of the adhesive layer and hence, inducing the observed minor cracking.

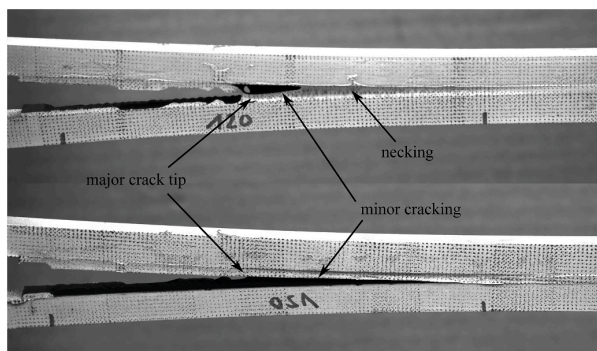


Fig. 5. Example of visible crack propagation phenomena during the experiments.

3.2. Control on constant J

The difference between the desired setpoint and the measured process variable is displayed in Fig. 6a. The setpoint of 2.2 kJ/m^2 was reached within 8 s, which is considered a small fraction of the tests' runtimes. An averaged absolute controller deviation of $(1.99 \pm 1.23) \text{ J/m}^2$ was achieved during the complete measurement. As this deviation is deemed insignificant, it can be stated that the crack propagation took place under constant crack driving force. It should be mentioned that the achieved controller deviation is of such a small value that the bit depth in the measurement becomes visible in the curves in Fig. 6a, leading to a "pixelated" appearance.

Remember at this point, that a viscoelastic material always reacts with deformation-dependent equilibrium stress and a rate-dependent non-equilibrium overstress. The setpoint of 2.2 kJ/m^2 was iteratively chosen from pretests to obtain crack propagation under a quasi-static loading state with strain rates and resulting viscous overstresses being as small as possible for the test setup used. Some pretests with a value of J below 2.2 kJ/m^2 were stopped after days without any further crack propagation. A value of J above 2.2 kJ/m^2 yielded higher crack propagation rates with increased crack opening velocities. In a former publication [19], the rate-dependent fracture process of the investigated adhesive was examined, finding that the materials' resistance against crack propagation rises with the applied loading rate. Higher setpoint values for J would therefore cause additional viscous effects, which are undesirable for those creep fracture investigations. The setpoint of 2.2 kJ/m^2 was, hence, chosen for reasons of practicability and to obtain complete fracture of all specimens at long last under almost quasi-static conditions without temporarily stopped crack propagation or test times of multiple days or even weeks.

It should also be noted that, towards the end of the experiments, the controller deviation increases rapidly, because the remaining adhesive layer was not able to transfer the peel force necessary for the desired J any longer. This yields a sudden acceleration of the crosshead, which can be observed in Fig. 6b.

We want to point out that, within the context of this study, we will refer to the crack driving force being constant as long as the controller deviation is below the value of 5 J/m^2 , which roughly corresponds to

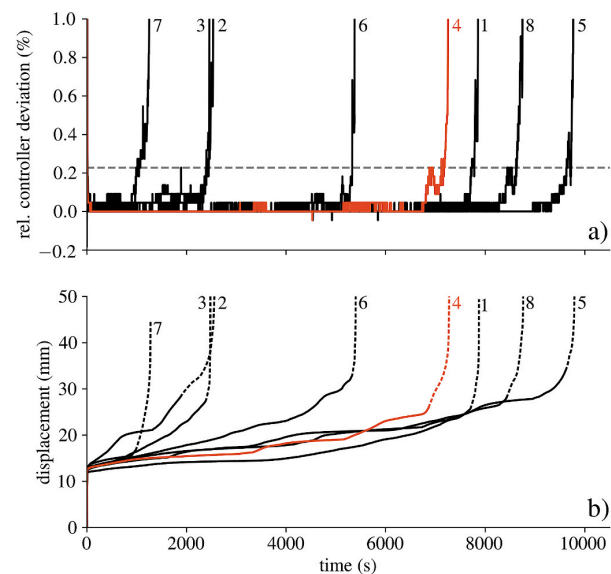


Fig. 6. a) Relative controller deviation with accepted deviation tolerance (dashed line), b) Crosshead displacement under constant crack driving force; displayed numbers correspond to the specimen IDs.

0.2% of the J -setpoint. In the following illustrations, the range of constant crack driving force is either highlighted using solid lines (as in Fig. 6b), or the display range of the graphs is limited to the range of constant crack driving force, respectively. As stated earlier, we will present our findings on one representative specimen, which is highlighted in colour in Fig. 6a and b.

3.3. Measured force and rotational angle

The measured values of force and rotational angle of all tested specimens are displayed in Fig. 7. The maximum forces are similar for the performed trials, varying between 102 and 110 N. Although the measured force decrease shows a common trend for all specimens, the instant at which the measured force starts to decrease rapidly, varies significantly. This point in time marks the end of the controlled iso- J -state, resulting from a rising crack propagation rate, and can correspondingly be observed in the angle measurements, coinciding with the start of increasing controller deviation above 5 J/m^2 . It can be stated here, that large scattering occurred between the individual samples regarding the total test time and that each sample had a different crack resistance to withstand the constant crack driving force. In other words, the loading input of constant J yields a large scatter in the output of machine displacement, coming from the individual fracture resistance of each specimen. This was already observed vice versa in a former publication [19] for the investigated adhesive, where tests at constant machine velocities yielded high scatter in the resulting energy release rates.

3.4. Crack extension measurements

As stated previously, the crack extension measurement was corrected for the motion of the DCB specimens relative to the used cameras. The measured specimen translation for the selected representative specimen is plotted in Fig. 8 with the display range being limited to the region of constant crack driving force.

In Fig. 9, the crack extension according to the optical measurement on both sides of the specimen and to the compliance method is displayed over time. As can be observed, the crack extension determined from the compliance method a_c is larger than, but generally similar to the one observed from optical measurements anytime. This may be attributed to

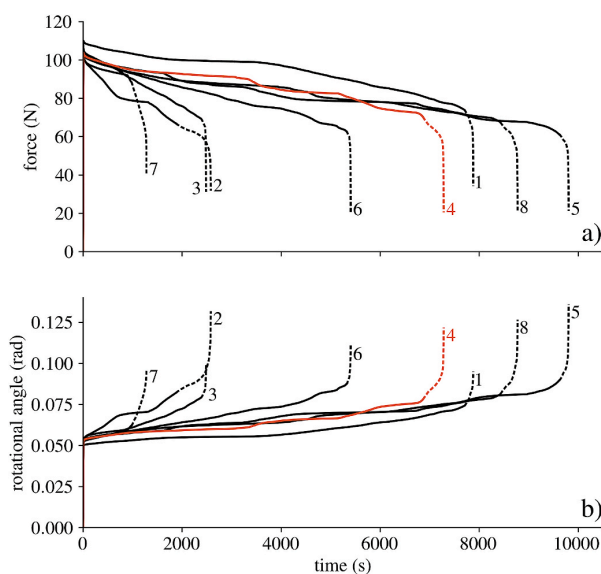


Fig. 7. a) Measured force and b) rotational angle during the experiments; displayed numbers correspond to the specimen IDs.

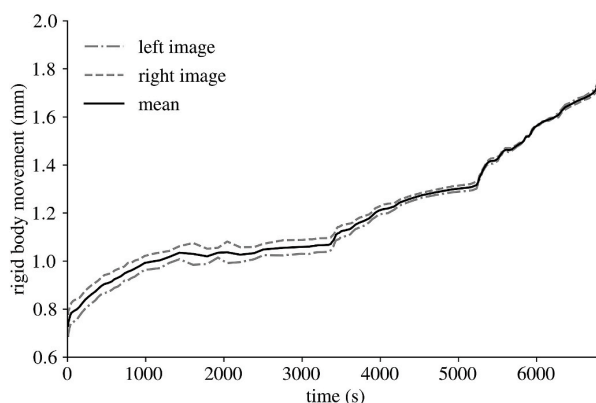


Fig. 8. Rigid body motion of the representative specimen (specimen 4) in the range of constant crack driving force.

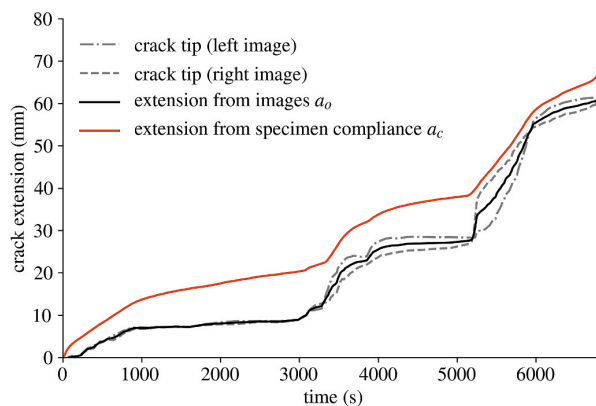


Fig. 9. Determination of crack extension, comparison between optical and compliance-based method (specimen 4).

the fact that a_c is derived from the specimen compliance, which increases due to viscous softening and ongoing fracture of the adhesive layer, even if softening or micro-damage is not visually recognizable. Therefore, the optical method of crack extension measurement leads to smaller values for crack extension, taking only externally visible material separation into account.

Furthermore, the optically determined crack extension on the left and right sides of the specimen is not necessarily equal at all times. This can be attributed to general difficulties with a manual human choice at determining a certain position for the crack with its uneven and complex geometric shape. Anyway, for this reason, the mean value of the optical determination a_o will be used from now on, which is estimated to be the best approximation for the position of the visible crack tip.

We want to point out that, despite finite deformations of the soft adhesive layer, the crack extension obtained from enhanced simple beam theory and optical measurement is at least qualitatively similar. The difference between both methods is noticeable but not substantial to such an extent, that the use of the enhanced simple beam theory approach could not serve as an adequate estimation tool for determining crack extension without optical measurements, which seems difficult especially in the case of large deformations of a very flexible adhesive layer. Furthermore, the enhanced simple beam theory approach takes effects like micro-damage or viscous softening into account by definition, which are not visible in image processing. Hence, it is not evident, which method is better suited to give a reliable value for the crack tip position concerning thick and flexible adhesive joints.

The crack extension for all tested specimens is displayed in Fig. 10. Again, large scatter within the fracture process can be observed.

3.5. Crack propagation rate

The crack propagation rate, i.e. the time-derivative of crack extension, is displayed in Fig. 11. The derivative of the crack propagation rate from the optical measurements was computed using the difference quotient between obtained crack extension and the time of image acquisition. To obtain the crack propagation rate from the compliance measurement and simultaneously reduce measurement noise, a floating average filter over a time frame of 20 s was applied to the measured crack extension before taking the derivative. It can be observed that both the crack propagation rate from optical measurement and the one from the compliance method are similar. This supports the findings that the determination of crack extension with enhanced simple beam theory can be an adequate method for non-optically determining crack propagation rates in rubber-like media. It is noticeable, however, that the propagation rate derived from the optical investigation is subject to larger measurement noise. This is attributed to the fact that the rate of image acquisition was much smaller than the sample rate from the measuring card due to limited hard disk space.

3.6. Damage processes

As described above, damaged areas on the side surfaces of the specimens could be observed as intensive black areas within the images. The affected „damaged pixels“ below a certain grey value threshold were counted by the image processing algorithm described in Section 2.6. An example of the areas detected by the algorithm is given in Fig. 12 with both the original image and the highlighted damaged areas. The vertical line indicates the manually located major crack tip position in the image, the horizontal lines indicate the boundaries between which the damaged pixels are counted. It can be observed that the damaged areas as minor cracks are reliably detected with the proposed methodology.

In Fig. 13, the number of damaged pixels is displayed for a representative specimen together with the crack extension difference. As can be seen, the crack extension difference can be correlated to the

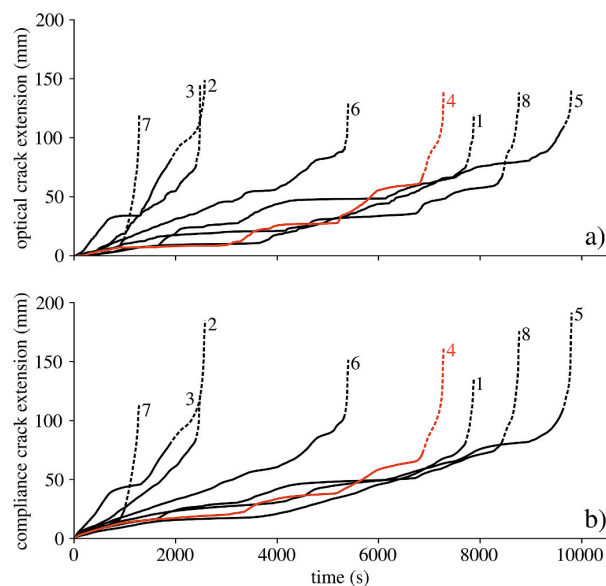


Fig. 10. a) Optical and b) compliance crack extension measurements for all tested specimens; displayed numbers correspond to the specimen IDs.

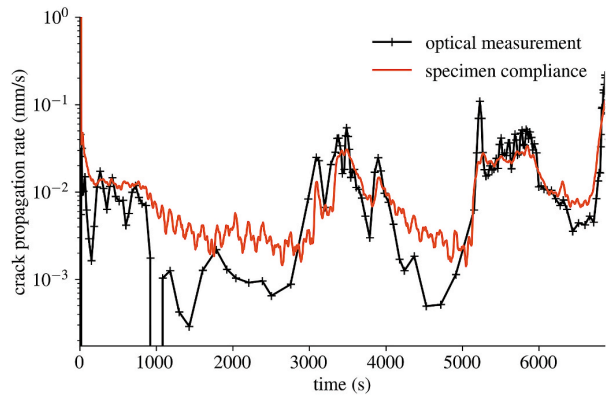


Fig. 11. Crack propagation rate in the range of constant crack driving force (specimen 4), comparison between optical and compliance-based method.

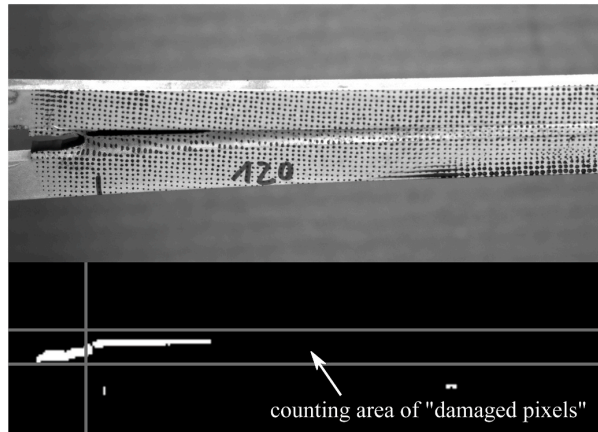


Fig. 12. Sideview on damaged DCB specimen, determination of “damaged pixels” within the captured images via image processing.

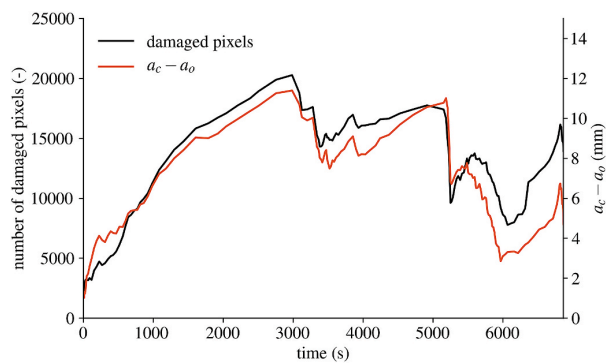


Fig. 13. Comparison between the number of observed damaged pixels and crack extension difference (specimen 4).

appearance of pre-damage away from the crack tip in direction of crack propagation. The forming of minor cracks was expected, because pre-damage does not affect the position of the manually selected major crack position, but shows up in a softening of the adhesive layer, which yields increasing specimen compliance. Hence, the crack extension difference can be correlated to the appearance of minor cracks away from

the crack tip in direction of crack propagation.

The forming of minor cracks enables material motion in its vicinity in the direction of the heavily loaded macroscopic major crack tip. The material movement towards the macroscopic major crack changes the geometric shape and reduces the stress intensity. This effect can further be increased by viscous effects in the material as time-dependent softening.

A reduced stress intensity for the macroscopic major crack should therefore result in a higher macroscopic crack resistance, yielding lower crack propagation rates. Fig. 14, in which the inverse of crack extension difference is correlated with the crack propagation rate, confirms this assumption. Hence, a decrease in the crack propagation rate, even if not measured optically but solely by using the compliance method, might indicate forming of minor cracks beside the macroscopic major crack.

3.7. Fracture patterns

The fracture surfaces of all eight specimens are shown in Fig. 15. The red solid lines mark the crack extension path (optical measurement) under constant J . The crack starts on the left side of the picture and propagates to the right side in each case. Consequently, the areas to the right of the red lines mark crack propagation after the end of the experiments with J not being constant anymore, accompanied by an accelerating testing machine (cf. Fig. 6b).

It can be observed that specimen No. 7, which fractured relatively early and showed a distinct drop of the load curve, shows a tendency to exhibit a more flat fracture surface. In addition, a relatively short distance of crack propagation that happened under constant crack driving force can be noticed here. Therefore, it is suspected that the crack path has early approached the adherend's interface, yielding a lower crack resistance of the adhesive layer. This is why specimen No. 7 was almost completely incapable to withstand the adjusted crack driving force, so the testing machine accelerated early without reaching the setpoint of J later again.

The other specimens show rougher fracture surfaces and chevron patterns, which are especially pronounced in the regions of constant J . At this point, it is unclear why these patterns emerge. However, we suspect that the effect could be related to fillers within the adhesive layer deflecting the propagating crack. Specimens No. 2 and 3 fractured relatively early as well, but in contrast to specimen No. 7 the fracture surfaces have evolved distinctly rougher under the formation of chevron patterns. Furthermore, a distinct region of constant crack driving force can be observed. However, specimens No. 2 and 3 fractured with a relatively high crack propagation rate, indicating higher strain rates, and with this, higher viscous overstresses compared to the other samples. Regarding sample No. 6, a relatively long distance of crack propagation under constant crack driving force can be noticed in combination with a rather high crack propagation rate. Samples No. 1,

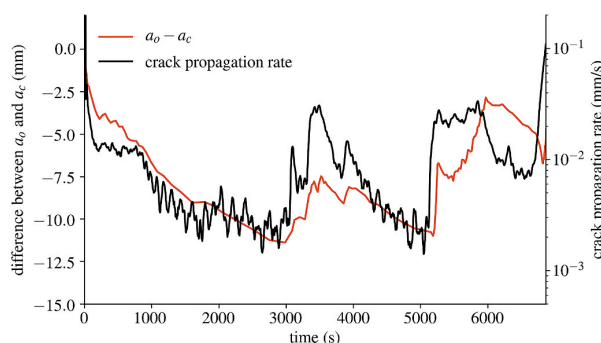


Fig. 14. Comparison between negative value of crack extension difference and crack propagation rate (specimen 4).

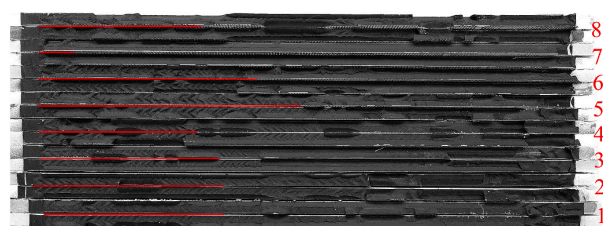


Fig. 15. Fracture patterns of the tested specimens with marked (optical) crack extension under constant crack driving force; displayed numbers correspond to the specimen IDs.

4, 5 and 8 fractured similarly with low average crack propagation rates, though sample No. 5 showed the longest distance of crack propagation under constant crack driving force and the longest total test time. Regarding sample No. 8, no chevron patterns could be observed at all.

It can be assumed here, that quasi-static creep fracture under constant J control can be correlated with rather rough fracture surfaces, whereas more flat fracture surfaces can be correlated with higher crack propagation rates. Similar results were found in a former publication [20], where the stick-slip fracture process of a rather stiff semi-structural polyurethane adhesive was investigated. It was observed that an over-critical crack jump with very high crack propagation rates yields flat fracture patterns, whereas subcritical crack propagation with rather low crack propagation rates yields rough fracture patterns.

3.8. Methodological critique

Controlling fracture tests on constant J -integral should ideally yield a uniform loading state at the crack tip. The crack driving force, pushing the crack to propagate further, is constant over the whole test. In this case, one would expect a constant crack propagation rate, resulting from a stationary fracture process. Instead of this, varying crack propagation rates were observed due to scattering in the crack resistance of the different samples with dissimilar quasi-static critical mode I fracture energies. If a less tough specimen (No. 2, 3, 6) is tested with the chosen setpoint value of $J = 2.2 \text{ kJ/m}^2$, the applied external energy exceeds the quasi-static fracture energy that would be necessary for a creep crack propagation. The consequence is a higher crack propagation rate with higher viscous overstresses and higher viscous dissipation in the adhesive to keep the adjusted crack driving force. If a relatively tougher specimen (No. 1, 4, 5, 8) is tested with the chosen setpoint value of $J = 2.2 \text{ kJ/m}^2$, the applied external energy is adequate for causing a creep crack propagation with lower crack propagation rates with lower viscous overstresses and lower viscous dissipation.

To provide the best fitting setpoint value of J , one could implement a method in which the crack driving force is gradually increased until the crack starts propagating. The corresponding value of J would then represent the quasi-static critical mode I fracture energy of the current specimen and could be held constant until complete fracture. This procedure would allow better comparability regarding the loading at a creep state with equally minor viscous effects but would lead to further challenges. In this case, the samples are dissimilarly loaded and the individual setpoints depend on the properties of the pre-crack. Consequently, different crack propagation rates can also occur here, if the properties of the pre-crack with its geometric imperfections are not representative for the whole specimen. Thus, the adjusted crack driving force might lead to higher crack propagation rates as well or might not be high enough to lead to a complete fracture of the whole specimen, especially in the presence of an R-curve behaviour.

From that point of view, it was practicable to use the iteratively found setpoint value of $J = 2.2 \text{ kJ/m}^2$ to guarantee the complete fracture of all samples within a tolerable period of some hours. To remind on this, some pretests with a value of J below 2.2 kJ/m^2 did end in equilibrium

in some cases, not yielding fracture almost exclusively, so that the tests were stopped after days without any further crack propagation.

It should also be stated that the width of 5 mm and the height of 3 mm of the adhesive layer may not lead to a plane strain state due to the possibility of distinct lateral contractions, in contrast to the case of thin and wide adhesive layers. Specimens with a width of 15 mm were used in preliminary investigations, but it was not possible to manually locate the major crack tip with the presented methodology, as the forming of minor cracks behind the major crack tip was pronounced to such an extent that distinguishing between major and minor cracks became impossible.

Furthermore, the authors spent a lot of time trying to automate determining the crack tip position in a similar way as described by Lahuerta et al. [21]. While the automatic evaluation of the major crack tip position for constant crosshead speeds proved to be unproblematic, the occurrence of minor cracks led to the crack tip no longer being reliably detectable by an algorithm. The use of a digital image correlation tool with deformation field measurement from both sides of the specimen akin to the methods of Sun and Blackman [22] might be advantageous, even if a four-camera system was needed for this purpose. This might open up possibilities to define criteria for the location of the crack tip position such as maximum strain, the loss of a specific speckle pattern, or criteria based on the shape of the process zone, which could additionally be investigated with this method.

The observed scatter within the experimental results can be found to be attributed to deviations in the fracture resistance between the substrates. As the controller deviation was shown to be very close to zero in the regions of constant J , it can be concluded that the proposed method of evaluation can be considered repeatable.

4. Conclusions and outlook

Within the limitations of this study, the following conclusions can be drawn:

- With the experimental setup shown, a uniformly loaded crack tip based on constant J -integral was achieved during the performed tests. The iteratively chosen setpoint value of $J = 2.2 \text{ kJ/m}^2$ was found to be close to quasi-static loading conditions with small viscous effects and ongoing creep fracture as time progressed. A value of J below 2.2 kJ/m^2 ended in equilibrium without subsequent crack propagation in some cases.
- For thick rubber-like adhesive layers, it is difficult to measure a reliable value for the crack tip position. Optical location cannot consider internal effects like viscous softening or micro-damage in the material, whereas crack extension measurements from the specimen compliance according to the enhanced simple beam theory can be a good approximation without the need for elaborate optical measurements.
- Forming of minor cracks within the adhesive layer was visible through surface tearing during crack propagation. This effect was quantified by counting the amount of “damaged pixels” within the captured images as well as building the difference between optically measured crack extension and the one coming from the compliance method. The herein obtained similar results showed that minor cracks away from the major crack tip in direction of crack propagation are the reason for the difference between the optical and compliance-based determined crack extension.
- The observed minor cracks correlate inversely with the observed crack propagation rate, which means that a pronounced existence of minor cracking yields decreasing crack propagation rates and vice versa. This indicates that minor cracks reduce the stress intensity in the macroscopic major crack tip, leading to an entirely higher crack resistance of the structure.

We advise that further research is undertaken in the following areas:

- The fracture behaviour of the investigated thick rubber-like adhesive is subject to large material scattering. Future studies should investigate this statistically, which may provide valuable information on the responsible processes.
- Next to the investigation of constant levels of J , one could expose the material on arbitrary curves such as sinusoidal loads to achieve fatigue tests controlled on an oscillating crack driving force. It would also be conceivable to design the setpoint curve in a way that increasing J -plateaus could be approached followed by a resting period until complete fracture.
- Carrying out the proposed experiments with measurement of the deformation behaviour using digital image correlation could provide information about the length of the process zone during crack propagation under constant crack driving force and, hence, yield better criteria for determination of an equivalent crack tip position such as maximum strain or the loss of a specific speckle pattern.
- In the regions of the fracture surface where the crack propagated under constant crack driving force, chevron patterns occurred to a significant extent. The background for the formation of those patterns is currently unclear and some insights on this might be interesting.

Funding sources

The work has been partially funded by Federal State Hessen, Germany, within the internal program “Strategischer Forschungsfonds” of TH Mittelhessen. The financial support is gratefully acknowledged.

Author contributions

Peer Schrader: Methodology, Investigation, Software, Formal Analysis, Writing – Original Draft, Writing -Review & Editing, Visualization.

Christopher Schmandt: Conceptualization, Methodology, Investigation, Writing – Original Draft, Writing -Review & Editing.

Stephan Marzi: Conceptualization, Supervision.

Acknowledgments

This article is part of P. Schrader’s doctoral thesis at the Doctoral Center for Engineering Sciences of the Research Campus of Central Hessen under the supervision of the Justus-Liebig-University Giessen in cooperation with the University of Applied Sciences of Central Hessen (Technische Hochschule Mittelhessen).

The authors would like to thank Sabine Wenig (SIKA Automotive AG, Romanshorn, Switzerland) for supplying the adhesive. Furthermore, the authors want to thank Prof. David A. Dillard for our fruitful discussion of the study during the 2021 Adhesion Society Meeting.

Appendix A. Supplementary data

Supplementary data to this article can be found online at <https://doi.org/10.1016/j.ijadhadh.2021.103079>.

References

- [1] Loureiro AL, da Silva LFM, Sato C, Figueiredo MAV. Comparison of the mechanical behaviour between stiff and flexible adhesive joints for the automotive industry. *J Adhes* 2010;86(7):765–87. <https://doi.org/10.1080/00218464.2010.482440>.
- [2] Richter C, Abeln B, Geßler A, Feldmann M. Structural steel–glass facade panels with multi-side bonding – nonlinear stress–strain behaviour under complex loading situations. *Int J Adhesion Adhes* 2014;55:18–28. <https://doi.org/10.1016/j.ijadhadh.2014.07.004>.
- [3] Meshgin P, Choi K-K, Reda Taha MM. Experimental and analytical investigations of creep of epoxy adhesive at the concrete–FRP interfaces. *Int J Adhesion Adhes* 2009; 29(1):56–66. <https://doi.org/10.1016/j.ijadhadh.2008.01.003>.
- [4] Puigvert F, Crocombe AD, Gil L. Fatigue and creep analyses of adhesively bonded anchorages for CFRP tendons. *Int J Adhesion Adhes* 2014;54:143–54. <https://doi.org/10.1016/j.ijadhadh.2014.05.013>.

- [5] Mostovoy S, Ripling EJ. Fracture toughness of an epoxy system. *J Appl Polym Sci* 1966;10(9):1351–71. <https://doi.org/10.1002/app.1966.070100913>.
- [6] Lefebvre DR, Dillard DA, Brinson HF. The development of a modified double-cantilever-beam specimen for measuring the fracture energy of rubber to metal bonds. *Exp Mech* 1988;28(1):38–44. <https://doi.org/10.1007/BF02328994>.
- [7] Dillard DA, Wang JZ, Parvatareddy H. A simple constant strain energy release rate loading method for double cantilever beam specimens. *J Adhes* 1993;41(1–4):35–50. <https://doi.org/10.1080/00218469308026553>.
- [8] Dillard DA. Stresses between adherends with different curvatures. *J Adhes* 1988;26(1):59–69. <https://doi.org/10.1080/00218468808071274>.
- [9] Chang Y-S, Lai Y-H, Dillard DA. The constrained blister—a nearly constant strain energy release rate test for adhesives. *J Adhes* 1989;27(4):197–211. <https://doi.org/10.1080/00218468908048453>.
- [10] Dillard DA, Bao Y. The Peninsula blister test: a high and constant strain energy release rate fracture specimen for adhesives. *J Adhes* 1991;33(4):253–71. <https://doi.org/10.1080/00218469108026498>.
- [11] Srilakshmi R, Ramji M, Chinthapenta V. Fatigue crack growth study of CFRP patch repaired Al 2014-T6 panel having an inclined center crack using FEA and DIC. *Eng Fract Mech* 2015;134:182–201. <https://doi.org/10.1016/j.engfracmech.2014.12.012>.
- [12] Eaton M, May M, Featherston C, Holford K, Hallet S, Pullin R. Characterisation of damage in composite structures using acoustic emission. *J Phys: Conf Ser* 2011;305:12086. <https://doi.org/10.1088/1742-6596/305/1/012086>.
- [13] Blackman B, Kinloch AJ, Paraschi M. The determination of the mode II adhesive fracture resistance, GIC, of structural adhesive joints: an effective crack length approach. *Eng Fract Mech* 2005;72(6):877–97. <https://doi.org/10.1016/j.engfracmech.2004.08.007>.
- [14] Rice JR. A path independent integral and the approximate analysis of strain concentration by notches and cracks. *J Appl Mech* 1968;35(2):379. <https://doi.org/10.1115/1.3601206>.
- [15] Škec L, Alfano G, Jelenić G. Enhanced simple beam theory for characterising mode-I fracture resistance via a double cantilever beam test. *Compos B Eng* 2019;167:250–62. <https://doi.org/10.1016/j.compositesb.2018.11.099>.
- [16] Paris AJ, Paris PC. Instantaneous evaluation of J and C. *Int J Fract* 1988;38(1):R19–21. <https://doi.org/10.1007/BF00034281>.
- [17] Andersson T, Stigh U. The stress–elongation relation for an adhesive layer loaded in peel using equilibrium of energetic forces. *Int J Solid Struct* 2004;41(2):413–34. <https://doi.org/10.1016/j.ijsolstr.2003.09.039>.
- [18] Allan DB, Caswell T, Keim NC, van der Wel CM, Verweij RW. *soft-matter/trackpy: trackpy v0.5.0*. Zenodo; 2021.
- [19] Schmandt C, Marzi S. Effect of crack opening velocity and adhesive layer thickness on the fracture behaviour of hyperelastic adhesive joints subjected to mode I loading. *Int J Adhesion Adhes* 2018;83:9–14. <https://doi.org/10.1016/j.ijadhadh.2018.02.028>.
- [20] Schmandt C, Marzi S. Effect of crack opening velocity on fracture behavior of hyperelastic semi-structural adhesive joints subjected to mode I loading. *Procedia Struct Integr* 2018;13:799–805. <https://doi.org/10.1016/j.prostr.2018.12.154>.
- [21] Lahuerta F, Westphal T, Nijssen R, van der Meer FP, Sluys LJ. Measuring the delamination length in static and fatigue mode I tests using video image processing. *Compos Part B* 2014;(63):1–7.
- [22] Sun F, Blackman B. A DIC method to determine the Mode I energy release rate G, the J-integral and the traction-separation law simultaneously for adhesive joints. *Eng Fract Mech* 2020;234:107097. <https://doi.org/10.1016/j.engfracmech.2020.107097>.

Paper B:

Mode III testing of structural adhesive joints at elevated loading rates

Peer Schrader, Stephan Marzi

Reprinted from International Journal of Adhesion and Adhesives, Volume 113, P. Schrader, S. Marzi, *Mode III testing of structural adhesive joints at elevated loading rates*, 103078, 2022, <https://doi.org/10.1016/j.ijadhadh.2021.103078>, with permission from Elsevier

Author Contributions:

The author conceptualized, designed and built the test setup, manufactured the tested specimens, and planned and conducted the experiments. The development of the evaluation methods as well as the evaluation of the test data was performed by the author. The author planned and wrote the paper. S. Marzi was responsible for funding acquisition, supervised the work and proofread the paper.



Contents lists available at ScienceDirect

International Journal of Adhesion and Adhesives

journal homepage: www.elsevier.com/locate/ijadhadh

Mode III testing of structural adhesive joints at elevated loading rates

Peer Schrader, Stephan Marzi*

Institute of Mechanics and Materials, Technische Hochschule Mittelhessen, Wiesenstrasse 14, 35390, Giessen, Germany

ARTICLE INFO

Keywords:

Epoxides
Aluminium and alloys
Destructive testing
Mechanical properties of adhesives
Rate-dependency

ABSTRACT

The Out-of-plane loaded Double Cantilever Beam (ODCB) test has proven to be a well-suited test method for determining both energy release rate and cohesive law of adhesive layers in mode III under quasi-static conditions. As the rate-dependency of the fracture behaviour of adhesive layers in shear is still a topic of ongoing research, we aim to investigate, whether the ODCB test can be modified to be applicable at elevated loading rates. For this purpose, the experimental setup of the ODCB test was modified to allow testing at elevated loading rates. Tests were performed on an epoxy adhesive at outer loading rates over several orders of magnitude, ranging from quasi-static conditions up to the maximum possible test speed of the used servo-hydraulic test machine. The results of these experiments are discussed thoroughly to gain insight into the applicability of the ODCB test at moderate loading rates. Furthermore, the experimental challenges associated with an increase in loading rate are highlighted to identify limitations of the experimental setup that need to be addressed when transitioning to impact testing.

1. Introduction

According to Machado et al. [1], a considerable body of literature has investigated the strain rate sensitivity of adhesives in bulk with the conclusion that tensile and shear properties were mostly found to increase with strain rate accompanied by increasingly brittle behaviour. The fracture energy of adhesive joints at increasing rates, as stated by Borges et al. [2], presents limited research, with most of the studies focusing on the fracture behaviour in pure mode I.

Especially regarding the rate-dependent fracture behaviour of adhesive joints in pure shear and mixed-mode, only a limited amount of studies are available: Carlberger et al. [3] studied the energy release rate (ERR) of an epoxy adhesive system in pure mode II at moderate loading rates using the End-Notched Flexure (ENF) test and found that the fracture energy decreased with loading rate whereas the peak stress increased. In contrast, Marzi [4] and May et al. [5] used the Tapered End-Notched Flexure (TENF) test for investigation and found an increase in fracture energy and peak stress. Borges et al. [2] investigated the fracture behaviour of two epoxy systems at different loading rates in pure mode II and in mixed mode I + II. During the ENF tests performed in their study, however, plastic deformation of the adherends was observed at increased loading rates, hindering the evaluation of the fracture energy. It should be noted that all of the mentioned studies focused on data reduction schemes based on linear elastic fracture

mechanics, which, as stated by Stamoulis and Carrere [6], could be problematic when investigating the fracture behaviour of adhesive systems at increasing loading rates because of a possibly non-negligible influence of viscoelastic and plastic effects on the adhesives' fracture behaviour.

A major difficulty of the ENF and TENF test setups is that, due to the large deformations of the adherends and high loading velocities needed to achieve sufficient elongations at the crack tip when testing at elevated loading rates, the adherends tend to deform plastically (as observed in the study of Borges et al. [2]), which hinders the determination of the ERR. Testing of highly ductile adhesive systems is, hence, also a difficult task due to the large amount of crack tip deformation required to initiate crack growth. Furthermore, an evaluation of the ENF test with the use of nonlinear fracture mechanics is deemed problematic at elevated loading rates, as the rotations at the load introduction points must be measured in real-time. An additional drawback of the ENF test is that, as stated by Stigh et al. [7], for most specimen configurations, a compressive load is applied to the process zone, which influences the evaluated fracture energy.

The Out-of-plane loaded Double Cantilever Beam (ODCB) test, which was proposed by Loh and Marzi [8] in 2018, is a valuable alternative to the ENF and TENF tests for the investigation of the shear behaviour of adhesive joints under quasi-static conditions. In this test, an external moment is applied to the substrates, leading to an out-of-plane

* Corresponding author.

E-mail address: stephan.marzi@me.thm.de (S. Marzi).<https://doi.org/10.1016/j.ijadhadh.2021.103078>

Received 5 October 2021; Accepted 14 December 2021

Available online 18 December 2021

0143-7496/© 2021 Elsevier Ltd. All rights reserved.

displacement, and thus resulting in a mode III loading of the crack tip. Later studies by Loh and Marzi [9,10] showed that the ODCB test (and modifications thereof), next to the investigation of epoxy adhesives, even allow the experimental investigation of ductile hyperelastic adhesive joints [11], enabling the determination of the ERR in mode III based on the J -integral and, hence, non-linear fracture mechanics.

This study aims to investigate, whether the ODCB test can be modified to also allow the determination of the ERR in shear when investigating increased loading rates. Furthermore, we wish to evaluate the feasibility of using the ODCB test at moderate loading rates to possibly enable the transition to dynamic testing. To illuminate this uncharted area, we performed ODCB experiments on an epoxy adhesive (SikaPower® 498, Sika Automotive, Hamburg, Germany) at a quasi-static and two elevated angular velocities (0.05 deg/s, 10 deg/s, and 120 deg/s) and wish to discuss the experimental results in greater detail. Hence, the current study aims to extend the application of the ODCB test to increased loading rates to allow the rate-dependent investigation of the fracture behaviour of adhesive layers undergoing shear deformation whilst also highlighting the intricacies of the test setup that need to be addressed to allow testing at even larger loading rates in future investigations.

To answer the arisen questions, we begin by taking a closer look at the used evaluation methods, the specimen preparation, and the experimental setup. Thereafter, we will present and discuss the experimental results, including the deformation behaviour of the adherends, the obtained crack opening displacement (COD), and the thereof calculated ERR. From this, the cohesive law is derived to approximate the shear strength of the adhesive. At last, the advantages and limitations of the test setup are discussed, and a summary of the results is given.

We will show that a distinctive novelty of the presented experimental setup is that it allows determining both ERR and cohesive law in mode III over several orders of magnitude in loading rate based on nonlinear elastic fracture mechanics, which has not yet been possible to the authors' knowledge. Furthermore, it is assumed that the experimental setup will enable future testing of thick, hyperelastic adhesive layers under shear deformations at different loading rates, which has also not been possible to date. The work will thus make an important contribution to enable further investigation of the rate-dependent fracture behaviour of adhesive joints under shear loads more closely.

2. Theory

As stated, the original ODCB test per the methods of Loh and Marzi [8], who discussed the theoretical background of the performed test in detail in their original paper, was modified within the context of this study. Whereas in the studies of Loh and Marzi [8–11] the axis of rotation around the upper point of load introduction was unconstrained to allow rotation of the specimen, the rotational degree of freedom was constrained within the framework of this study. This was done for multiple reasons: Firstly, modifying the boundary conditions and constraining the rotational degree of freedom allows the mass of the test setup to be reduced significantly, which minimizes transient effects during testing at increased loading rates. Secondly, a higher overall stiffness of the test setup can be achieved, which leads to an increased natural frequency of the setup so that it will not influence the measurements. Thirdly, constraining the rotational degree of freedom leads to the specimen being loaded purely by external bending moments, which, when using strain gauges to determine the local components of the applied moment acting on the crack tip, is advantageous for the evaluation of the J -integral at increased loading rates. However, it should be strongly emphasized in advance that traverse moments occur during testing with this modified setup which could potentially damage the testing machine if these are not sufficiently small and cannot be absorbed by the load frame.

Consider a specimen with the applied loads as displayed in Fig. 1.

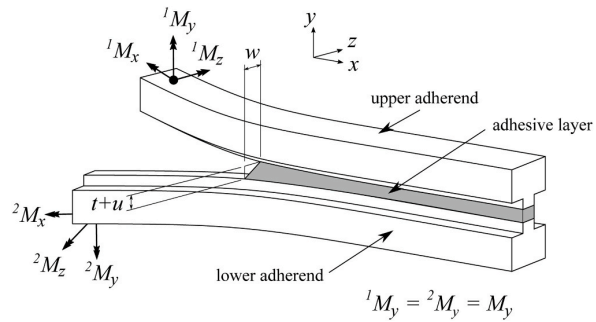


Fig. 1. Schematic representation of an ODCB specimen with applied loads.

Briefly, if this specimen is loaded in pure mode III, Loh and Marzi [8] found that the J -integral yields a value of

$$J_{III} = -\frac{M_y \kappa}{b} \quad (1)$$

with the moment M_y acting on the crack tip, the curvature κ in the lever arm of the adherends, and the width of the adhesive layer b under the assumptions stated above. As the beam curvature can be calculated from the externally applied moment $M_y = -\kappa EI_y$ with the bending stiffness EI_y of the adherends under the assumption of linear elastically deforming beams, Loh and Marzi [8] reduced Eq. (2) to

$$J_{III} = \frac{M_y^2}{b} \frac{1}{EI_y} \quad (2)$$

One should note, however, that the external measurement of the moment M_y acting on the specimen with an external load cell is likely subjected to oscillations at rising loading rates due to transient effects within the experimental setup, necessitating a local measurement of M_y . It is therefore useful to compute the moment applied to the crack tip from measuring the strain ϵ in the marginal fibres of the adherends. As ϵ can directly be related to the curvature κ with the adherend's width c via $\kappa = 2\epsilon/c$, Eq. (2) can be rewritten as

$$J_{III,loc} = \frac{4\epsilon^2 EI_y}{bc^2} \quad (3)$$

yielding a possibility to compute the mode III ERR without having to rely on an external load cell. It should be mentioned that the strain measurement of a linear elastic beam is insensitive to the location of measurement due to loading by pure external moments provided that the location is neither too close to the clamping nor the initial crack tip. Within this study, the bending stiffness EI_y is computed via linear regression between externally applied moment and the measured curvature of the lever arms before the evaluation of J_{III} and $J_{III,loc}$.

In a later study by Loh and Marzi [11], it was found that other (unintended) contributions to J occur during the runtime of an ODCB test if the specimen is not loaded in pure mode III. For the modified experimental setup used in this present study, these equate to

$$J_I = \frac{{}^1M_x^2 + {}^2M_x^2}{2b} \frac{1}{\mu I_{yz}}, \quad (4)$$

which is an “out-of-plane mode I” contribution due to the specimen twisting, and

$$J_I = \frac{{}^1M_z^2 + {}^2M_z^2}{2b} \frac{1}{EI_z}, \quad (5)$$

a contribution in pure mode I. Here, μ denotes the shear modulus of the adherends, and I_{yz} and I_z denote the torsional second moment of area and the second moment of area of the adherend around the bending axis

z , respectively. Hence, if the load is not introduced in pure mode III, J equates to

$$J = J_{III} + J_I + J_{I'} \quad (6)$$

As a pure mode I load is introduced by the moments around the z -axis, the specimen is, strictly speaking, loaded in mixed-mode I + III. The mixed-mode ratio can be derived from

$$\chi = \tan^{-1} \left(\frac{J_{III}}{J_I} \right) \quad (7)$$

as stated by Loh and Marzi [10]. For a pure mode III load the value of χ equates to 90° , for a pure mode I the value is 0° .

We also would like to mention that in the setups of Loh and Marzi [9–11], J_I had to be determined by measuring the angle of rotation around the z -axis, which is not required for the modified setup presented here. Furthermore, a contribution to J in mixed-mode I + II occurred in their set of boundary conditions, which resulted from shear deformations due to the finite width of the specimen. Due to the symmetric boundary conditions of the modified setup presented here, the contribution in modes I + II is therefore eliminated from the total value of the J -integral. In addition, as stated earlier, by loading the specimen purely with external bending moments, the present setup makes it possible to determine all contributions to the J -integral locally on the specimen by using strain gauges. This may be advantageous for the evaluation at increased loading rates, especially if investigations in mixed-mode I + III are to be carried out in subsequent studies.

The components of the COD vector are denoted by u , v , and w in cartesian coordinates, corresponding to the COD in direction of the fracture modes I, II, and III, respectively (cf. Fig. 1). Through measuring the COD, the cohesive traction can be determined during monotonic loading by taking the derivative of J to the displacements [12], yielding

$$\tau = \frac{dJ_{III}}{dw} \quad (8)$$

for the shear stress with the mode III COD. Within this study, to minimize numerical errors during differentiation, the experimental results of τ vs. w are obtained via taking the spectral derivative of J with respect to w and filtering with a low pass filter in the frequency range.

3. Experimental setup

The experiments performed in this study were conducted on the structural elastic-plastic adhesive SikaPower® 498. The adherends were aluminium substrates with the dimensions described by Loh and Marzi [8] and highlighted in Fig. 2, $E = (70 \pm 1)$ GPa and $I_y = (4271 \pm 59)$ mm⁴. Before applying the adhesive, the bonding surfaces of the adherends were sandblasted with corundum (grain size of 100–150 μ m), wipe-cleaned with lint-free paper wipes and methylethylketone, and then rinsed with the solvent. The adhesive and the adherends were then pre-heated to 55 °C before applying the adhesive with an electric caulking gun. To define the adhesive thickness, Teflon tape with a nominal thickness of 0.3 mm was placed at the beginning and the end of the adhesive layer. During the curing process (30 min at an exposure temperature of 175 °C), the substrates were held in place with screw

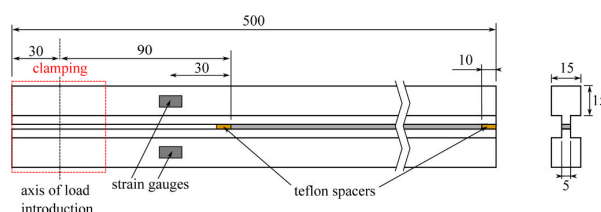


Fig. 2. Nominal dimensions of the tested specimens (dimensions in mm).

clamps. For lateral fixation during the curing process, a screw clamp was placed both at the beginning and the end of the adhesive layer on the side of the specimen; normal to the adhesive layer, the substrates were clamped directly at the positions of the Teflon tape. With the described preparation, an initial crack length of (90.3 ± 0.4) mm and a layer thickness of (0.29 ± 0.02) mm were achieved.

The experimental setup is depicted in Fig. 3. The tests were performed in a biaxial tension-torsional servo-hydraulic test machine (MTS Landmark Bionix, MTS Systems, Eden Prairie, USA). Within this study, the specimens were loaded at angular velocities of 0.05 deg/s, 10 deg/s, and 120 deg/s. To avoid lateral forces on the specimen, the bottom clamping device was mounted on two orthogonally placed linear slides. Furthermore, the axial force on the specimen was controlled to be nought by the control system of the test machine, which lead to the specimen being loaded predominantly with bending moments. The strain in the lever arms of the aluminium substrates was measured with strain gauges (FLAB-2-23, Tokyo Sokki Kenkyujo Co., Tokyo, Japan) in a quarter bridge circuit. On each substrate, one strain gauge was applied centrally between clamping and crack tip (cf. Fig. 2).

During the experiments at 0.05 deg/s, the moments on the specimen were measured with two six-axis load cells directly above the upper clamping device and below the bottom clamping device at each support of the specimen, allowing the determination of the contributions to J in mode I, mode III and the unintended contribution $J_{I'}$. For the external measurement of the applied moment M_y , at the velocities of 10 deg/s and 120 deg/s, a biaxial load cell, which was placed below the orthogonal linear slides, was used. A transient recorder (MS220R/T16, J.E.T Systemtechnik GmbH, Norderstedt, Germany) was used to capture the measured values with 8 kHz at the loading velocity of 10 deg/s and 80 kHz at 120 deg/s.

Unfortunately, the contribution to J in pure mode I and the unintended contribution $J_{I'}$ could only be measured in the quasi-static tests

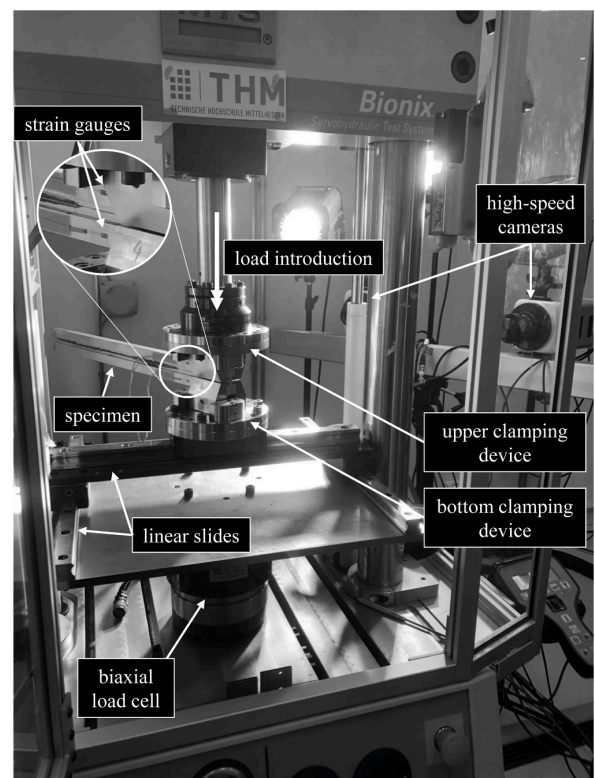


Fig. 3. Experimental setup at increased loading rates.

because the bandwidth of the available measuring amplifiers of the six-axis load cells was not sufficient to measure the moments at increased test velocities. Furthermore, an external measurement was also refrained from to avoid potential damage to the measuring equipment as the six-axis load cells are moving parts within the setup.

To determine the COD, a greyscale speckle-pattern was applied on the specimen with a speckle roller (Correlated Solutions Inc., Irmo, USA) which was later tracked by digital image correlation (DIC) software (GOM Correlate, GOM GmbH, Braunschweig, Germany for the quasi-static tests; VIC-3D, Correlated Solutions, Irmo, USA for the tests at increased loading rates) to calculate the displacements u and w . The COD was obtained by measuring the distance between the coordinates of two subsets, one on each adherend close to the initial crack tip. Before the evaluation of the COD, the measurements were adjusted for rigid body rotation.

For the quasi-static tests, an ARAMIS 3D Motion and Deformation Sensor (GOM GmbH, Braunschweig, Germany) with an image resolution of 12 MP was used to measure the components u and w of the COD at a sampling rate of 5 Hz. During the experiments at elevated loading rates, the specimens were filmed with two high-speed cameras (Photron FASTCAM Nova S6, Photron USA, San Diego, USA) with an image resolution of 1 MP at image acquisition rates of 2 kHz (loading velocity of 10 deg/s) and 20 kHz (loading velocity of 120 deg/s), respectively. For the evaluation, subset sizes of 19 pixels were used. With the given DIC-systems, physical pixel sizes of approx. 0.028 mm/px for the quasistatic experiments and 0.18 mm/px for the experiments at increased loading rates were achieved. Blank measurements of the unloaded specimens yielded an out-of-plane variance error (temporal standard deviation of measurement noise of the mode III COD w) of approx. $\pm 1.9 \mu\text{m}$ for the low-velocity experiments and $\pm 3.4 \mu\text{m}$ for the high-velocity experiments, and an in-plane variance error (temporal standard deviation of the measurement noise of the mode I COD u) of approx. $\pm 0.4 \mu\text{m}$ and $\pm 0.8 \mu\text{m}$, respectively. To combine the COD measurement with the other measured signals, the synchronization signals between the two high-speed cameras were recorded by the transient recorder, allowing synchronizing the measured values in post-processing.

Eleven experiments were conducted as part of this study: 3 tests were conducted at 0.05 deg/s, 4 specimens were tested at 10 and 120 deg/s each. We would like to emphasize that no plastic deformations of the adherends were found after testing.

4. Results and discussion

4.1. Quasi-static tests at 0.05 deg/s

The locally measured values of $J_{III,loc}$ obtained from the specimens' curvature are displayed in Fig. 4 alongside the measured value of J computed from the external moments and the absolute error between both evaluation methods. It can be observed for all tested specimens that the locally determined value for $J_{III,loc}$ matches well with the value of J determined from the external moments at the support points and that the error between both evaluation methods is of negligible magnitude. These observations allow the conclusions that the mode III contribution is dominant in the given load condition and that measuring $J_{III,loc}$ during the experiment will give a sufficiently accurate estimate of the total value of the J -integral.

This observation is further undermined by Fig. 5 in which the obtained mixed-mode ratio χ is displayed over the tests' runtime. The results show that the specimens are loaded in mode I initially before the mixed-mode ratio rapidly tends towards pure mode III. This, hence, implies that the contribution in pure mode I is insignificant at fracture, further strengthening the observation that the fracture process can be regarded as mode III fracture and that the local measurement of $J_{III,loc}$ gives a sufficiently accurate estimate for J at crack initiation. During the experiments, the unintended contribution J_{I^*} according to Eq. (4) was found to take up $(0.14 \pm 0.04) \%$ of J at the start of crack propagation, which is also deemed insignificant.

These findings are consistent with the previous studies in which

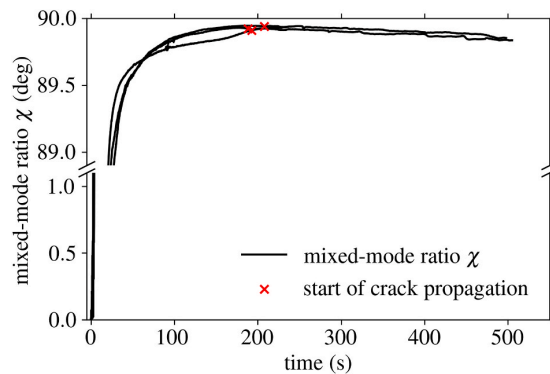


Fig. 5. Mixed-mode ratio obtained during the experiments.

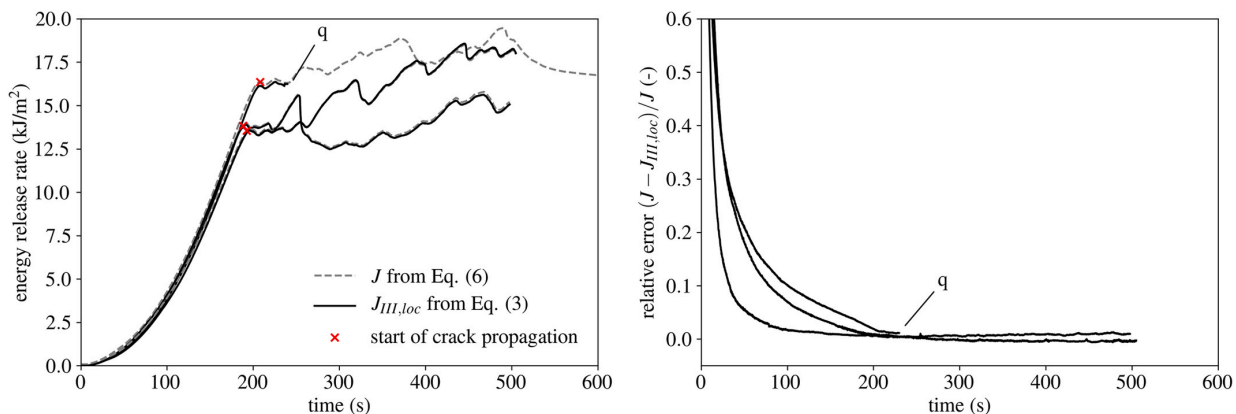


Fig. 4. Comparison between $J_{III,loc}$ obtained from specimen curvature and J obtained from external load cells (left) and relative error between $J_{III,loc}$ and J (right). Test indicated with q: error in local measurement, corresponding curves have been cut accordingly.

ODCB tests were conducted, as, in the studies from Loh and Marzi [9–11], the contributions to J other than the mode III contribution were also negligible at fracture. Furthermore, it was shown in a subsequent simulative study by Bödeker and Marzi [13] that the unintended contributions to J do not influence the thereof derived cohesive laws significantly. Based on our findings and the aforementioned studies, we extrapolate this to remain at least limitedly valid at increased loading rates, wherefore approximating J through solely measuring $J_{III,loc}$ and determining the cohesive law from the measurements should be possible with the used experimental setup at higher loading rates.

The measured components of the COD in mode I and mode III (u and w) are displayed in Fig. 6 until the start of crack propagation. As can be observed, the component in mode I is, in fact, inequal to nought in all cases, which is, as found by Loh and Marzi [8], due to lateral contraction of the adhesive. However, the mode III component is significantly larger and, hence, dominating the displacement at the crack tip, which agrees with the measured small unintended contributions to J . It should be emphasized that the moments acting in x - and z -direction during loading will influence the measured value of the mode I COD u . Positive moments iM_z will open the joint causing an increase in u , whereas a twisting of the adherends due to the moments iM_x can potentially cause opening on one side of the joint and closing on the opposite side. Therefore, we must also note that the measurement of u only on one side of the specimen cannot be a complete indication of the relative dominance of mode III over mode I in the displacement field. The twisting of the adherends and subsequent warping of their cross-section due to iM_x can also result in a mode II COD v . However, as Loh and Marzi [8] already stated, this component cannot be easily determined using DIC measurements due to the non-linear deformation field of the adhesive layer at the crack tip.

It is important to also mention that the traverse moments iM_x and iM_z , which are responsible for the contributions J_I and J_{II} , could potentially damage the testing machine. If one wishes to replicate the proposed setup, it should be checked in advance whether the load line can absorb these traverse moments without the testing machine being damaged. For this reason, the maximum values of the measured traverse moments are given in Appendix A so that these can be used as a guideline when designing a test setup.

4.2. Tests at 10 deg/s and 120 deg/s

In Fig. 7, the absolute value of the measured strain at the upper and lower adherend is demonstrated for one representative specimen at each loading velocity. As can be observed, the strain of the upper and lower adherend is almost congruent in both cases, indicating that the adhesive layer is loaded symmetrically. Only slight oscillations can be observed in the measured strain of the adherends at the highest loading rate, wherefore it is indicated that the inertia of the bottom clamping device does not influence the deformation behaviour of the specimens

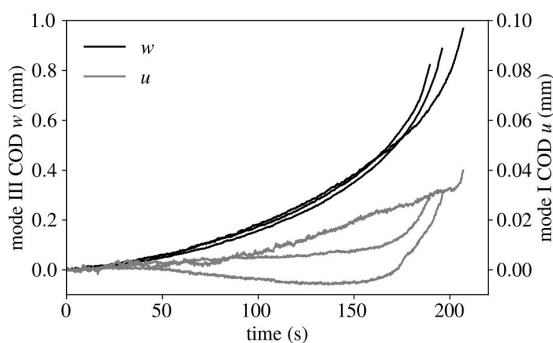


Fig. 6. Mode I and mode III components of crack opening displacement until crack propagation during the quasi-static tests at 0.05 deg/s.

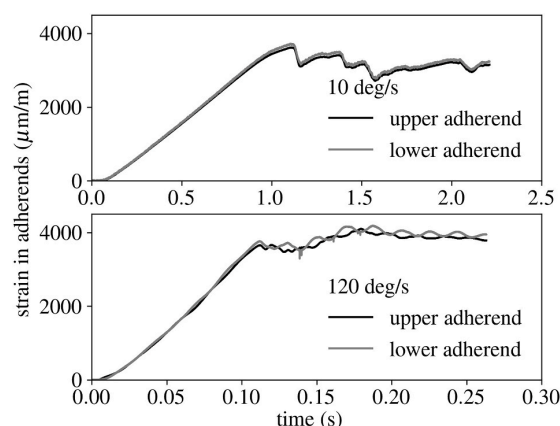


Fig. 7. Strain measured in the marginal fibres of the adherends for a representative specimen at 10 deg/s (top) and 120 deg/s (bottom).

significantly in the tested ranges of angular velocity.

We also want to note that the strain rate in the adherends is constant in good approximation between the end of the specimens' acceleration process and the start of crack propagation. This, in effect, also means that the externally applied moment increases at a nearly constant rate within this region, and as a result, crack initiation occurs under a constant external moment rate.

As described in Section 2, the bending stiffness of the adherends was determined before the evaluation of J_{III} via regression between the specimen curvature and the externally measured moment M_y . From this, a specimen stiffness of $(313.60 \pm 5.96) 10^6$ Nmm² was determined from the measurements at both increased loading velocities, which is congruent with the theoretical bending stiffness $EI_y = (298.97 \pm 8.46) 10^6$ Nmm² of the substrates.

In Fig. 8, the externally measured ERR according to Eq. (2) and the locally determined ERR according to Eq. (3) are shown at each loading velocity. It can be observed that both methods of evaluation yield

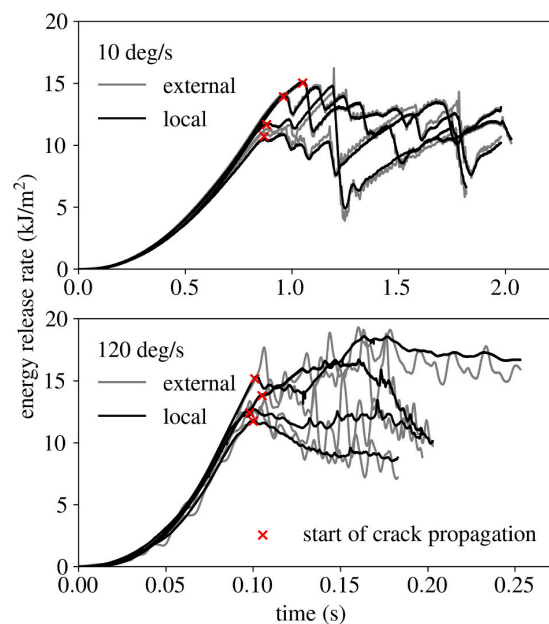


Fig. 8. Comparison between the locally and externally measured energy release rate at the loading velocities of 10 deg/s (top) and 120 deg/s (bottom).

equivalent results at the loading velocity of 10 deg/s, although small oscillations can already be observed in the external measurement. At the loading rate of 120 deg/s, these oscillations are very pronounced in the external measurement of the ERR, whereas the locally determined ERR is devoid of oscillations. Thus, it must be concluded that the local measurement of the mode III contribution to J using strain gauges is necessary at elevated loading rates, as the external measurement seems to be influenced by transient effects within the experimental setup. It can also be observed in Fig. 8 that the ERR at crack initiation in both the experiments at 10 deg/s and 120 deg/s lies in the range between 10 and 15 kJ/m²; the values at crack initiation during the quasi-static tests were found to be slightly larger (cf. Fig. 4). However, due to the large scattering of the values, it can already be stated that the ERR seems to be largely independent of loading rate in the view of material scattering.

The components u and w of the COD vector of a representative specimen at each loading velocity are displayed in Fig. 9. The time regime between the end of the acceleration process of the specimen and the start of crack propagation (indicated by a constant strain rate of the adherends) is highlighted by using solid lines. Initially, the mode III COD increases linearly in approximation. However, when reaching a COD between 0.1 and 0.2 mm, w begins to accelerate, although the outer moment rate remains constant. As highlighted in the figure, this point of acceleration coincides with the first local maximum of the shear stress according to the obtained cohesive laws. This indicates that the acceleration of w can likely be attributed to damage processes near the crack tip reducing the stiffness of the adhesive layer, leading to an increase in crack opening velocity. To determine a representative crack opening velocity for each test, linear regression is performed in the linearly increasing region between the end of the specimens' acceleration process and the first local maximum of the cohesive law as indicated by the displayed regression line.

In the performed experiments at elevated loading rates, the mode I component of the displacement vector is also unequal to nought and, compared to the quasi-static tests, larger in proportion to the mode III component. This could be an indicator for increased contributions in mode I, which means that the approximation of the total value of J by solely measuring the mode III contribution locally could lose accuracy. Especially in the region up to the maximum shear stress, the contribution in mode I is comparatively large, indicating a mixed-mode I + III loading during crack initiation in the linear region of the traction separation law. With the beginning acceleration of w , however, the contribution in mode I then becomes comparatively smaller. Therefore, we conclude that the mode III component w of the COD is still dominating the deformation at the initial crack tip. This, in effect, supports

the hypotheses that the crack is initiated close to pure mode III even at increased loading rates, contributions to J in other modes are present but comparatively small during crack initiation, and the cohesive law can be determined from Eq. (8) with a minor error.

4.3. Rate dependency of ERR and cohesive law

The progression of $J_{III,loc}$ over w for all tested specimens is displayed in Fig. 10 with the corresponding cohesive laws obtained by calculating the mean and standard deviation curves of the derivatives of J with respect to w according to Eq. (8). As it was already hinted at earlier, it can be observed that the obtained maximum of the ERR at crack initiation seems to be largely independent of loading rate in the view of material scattering. However, the slope of ERR vs. COD increases with the loading rate, which correspondingly also leads to an increase in shear strength. Furthermore, whereas the cohesive law during the quasi-static tests is of tri-linear shape, a tendency of the cohesive law to approach a bi-linear shape with increased loading rate can be observed. Hence, the stress state at the crack tip during the crack initiation phase seems to be depending on the loading rate regardless of the observed rate-independency of the ERR. The obtained tri-linear cohesive law during the quasi-static tests is consistent with previous studies focusing on the shear behaviour of the tested adhesive at quasi-static loading velocities such as Loh and Marzi [8,10] and Marzi et al. [14]. We want to mention that oscillations in the obtained cohesive laws can be observed, which likely result from the numerical derivation of the measurement data. The measurement noise in both quantities J and w significantly complicates numerical derivation, resulting in numerical errors and, hence, probably yielding the observed oscillations.

As stated earlier, the representative crack opening velocity for each test is determined from a linear regression within the linear region of the mode III COD between the end of the specimens' acceleration process and the first local maximum of the obtained shear stress. This yields representative crack opening velocities of $(1.66 \pm 0.34) \cdot 10^{-3}$ mm/s at 0.05 deg/s, (0.29 ± 0.02) mm/s at 10 deg/s, and (2.50 ± 0.75) mm/s at 120 deg/s in the initially elastic range of the adhesive traction, approximately equating to nominal strain rates, i.e. the quotient between representative crack opening velocity and initial adhesive layer thickness, of $(5.44 \pm 1.11) \cdot 10^{-3}$ 1/s, (1.05 ± 0.05) 1/s and (8.74 ± 2.68) 1/s.

In Fig. 11, the obtained values for the ERR at crack initiation and during crack propagation as well as shear strength (obtained from the first local maximum of τ and the slope of the J - w -curves as a comparative figure) are displayed over the representative crack opening velocity. The

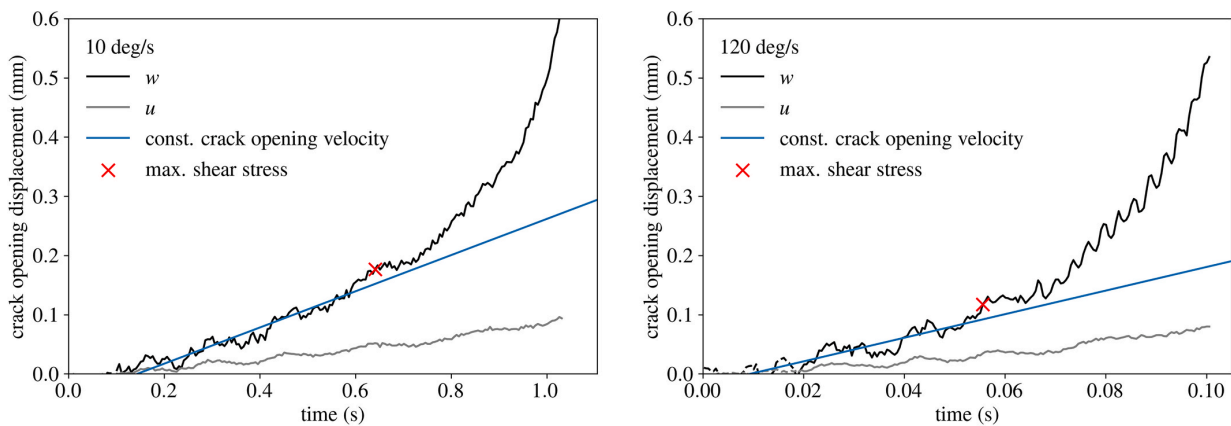


Fig. 9. Measured mode I and mode III components of crack opening displacement of a representative specimen at the loading rates of 10 deg/s (left) and 120 deg/s (right).

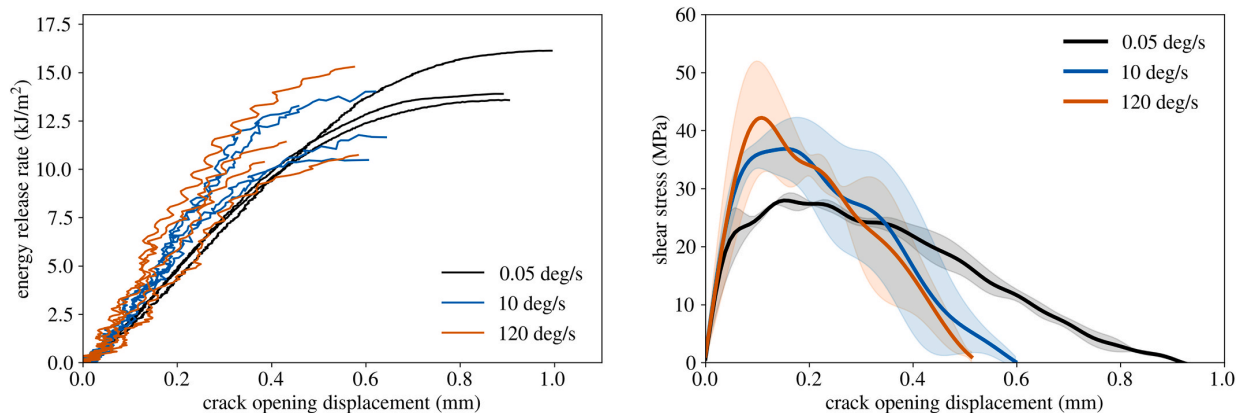


Fig. 10. Energy release rate (left) and mean curves of cohesive traction (right) with their corresponding standard deviation determined from the experiments.

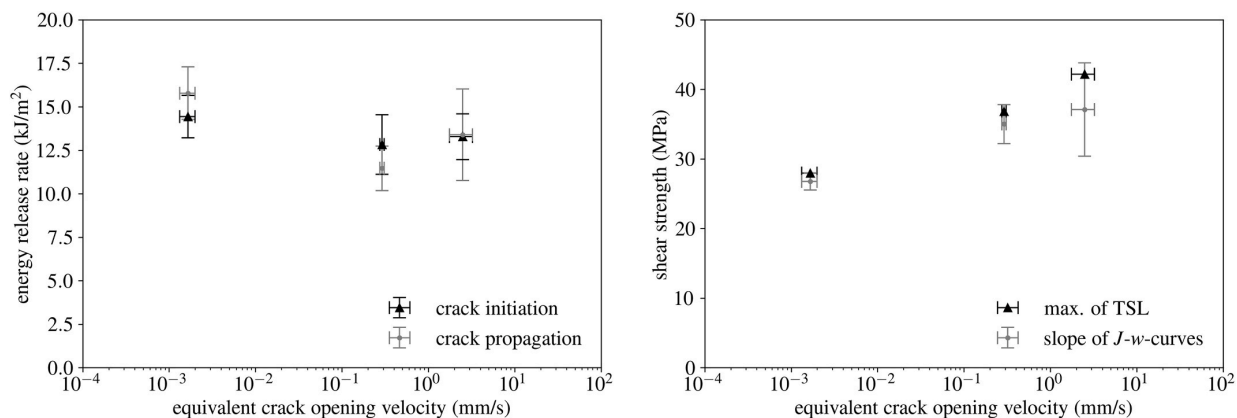


Fig. 11. Dependency of energy release rate (left) and shear strength (right) on the crack opening velocity.

results further undermine that the ERR of the tested adhesive is largely independent of loading rate given the observed material scattering. However, an increase in shear strength with crack opening velocity can be observed clearly from the performed experiments. It can also be observed that the shear strength obtained from the maximum of τ begins to slightly overestimate the shear strength according to the slope of the J - w -curves with increasing crack opening velocity. However, this is to be expected, as numerical differentiation of two signals with increasing amounts of measurement noise will, as stated previously, lead to oscillations and numerical errors. However, the good agreement between both methods of determination is deemed to be an indicator of the validity of the derived traction separation laws. Furthermore, considering the shape of the cohesive law, which was identified as tri-linear during quasi-static tests both in the present study as well as in the studies of Marzi et al. [14] and Loh and Marzi [8,10], the results of our study imply that the cohesive law approaches a bi-linear shape with an increase in loading velocity. This could be an indicator of a decrease in plastic deformations at the crack tip during crack initiation, leading to an increasingly brittle failure. A similar result was found in a study by Stamoulis and Carrere [6] during Arcan tests with SikaPower® 498, in which an increase in yield strength and failure stress of the joint was observed.

4.4. Fracture surfaces

The fracture surfaces of one representative specimen for each loading

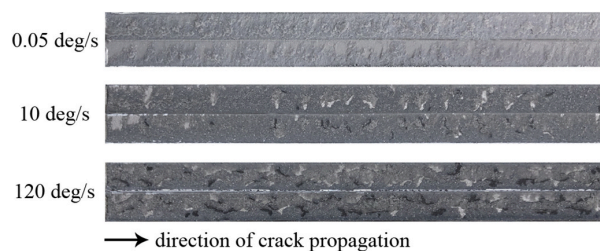


Fig. 12. Fracture surfaces of representative specimens at each loading velocity.

velocity are shown in Fig. 12. As it can be observed, the crack seems to initiate in the middle of the adhesive layer in all cases. In the quasi-static case, the crack seems to grow at an angle between the two interfaces, with the bond failing cohesively and, partially, close to the interface. It can also be observed that the fracture surface from the quasi-static experiment appears to be whiter, which could be an indicator for crazing and, hence, plastic deformations. This also correlates with the observed tri-linear cohesive traction (cf. Fig. 10), as the trapezoidal shape of the cohesive law could be an indicator for plastic flow at the crack tip. With increasing loading velocity, however, an increasing number of darker spots emerges on the crack surface, indicating that the initially observed failure close to the interface gradually evolves into

partly adhesive failure. This indicates that the crack tip changes position within the adhesive layer during crack propagation and could also be a reason for the observed increasingly brittle fracture behaviour according to the cohesive laws, which, as stated earlier, tend towards a bi-linear shape at increased loading rates. In conclusion, the fracture surfaces, in combination with the derived cohesive traction, indicate that the extent of plastic flow at the crack tip during crack initiation decreases and the fracture behaviour becomes more brittle, although the ERR remains constant.

4.5. Discussion of the experimental setup

Although local measurement of the applied moments 1M_x , 2M_x , 1M_z , and 2M_z from the specimen curvature with strain gauges was not possible during the performed tests, as only a limited amount of measurement channels was available at the used transient recorder, by using other measuring equipment, it should be possible to determine these quantities in the experiments as well in future studies. A more detailed investigation with DIC could be helpful for this purpose as well. However, as the investigation at the lowest loading rate showed that the crack tip is loaded in pure mode III during crack initiation and crack propagation, and the contribution to J in mode I and the unintended contribution J_I were negligibly small, measurement of these quantities is not considered mandatory in future investigations regarding the mode III fracture behaviour. A greater emphasis could be placed on determining the moments 1M_x , 2M_x , 1M_z , and 2M_z at elevated loading rates in future investigations, if one wants to perform the experiments in mixed-mode I + III, as it was done by Loh and Marzi [9–11] quasi-statically in previous studies.

We again want to point out that these traverse moments acting on the load line can potentially damage the testing machine. Therefore, special care should be taken when carrying out experiments with the proposed setup. If one wishes to reproduce the proposed setup, it must be checked in advance whether the load frame can withstand the traverse moments without taking damage.

A distinctive, novel feature of the presented setup is that testing of the selected adhesive in mode III was possible over four orders of magnitude of crack opening velocity. We assume that even larger rates could be achieved if the experimental setup were redesigned to be integrated into a drop tower, or rotary impact tester. However, we want to point out that further simplifications of the experimental setup might be necessary when transitioning into impact, as the application of an external moment on one support point with a simultaneous slide bearing of the other support point of the specimen is likely to be a major challenge during the design of the test setup. Especially for use in a drop tower, which is probably more common in industrial practice than rotary impact testers and Split Hopkinson bars, it may therefore make sense to modify the mode III test setup in such a way that it can be carried out with an uni-axial out-of-plane load.

As the ODCB test was also found to be suitable for the investigation of hyperelastic adhesives by Loh and Marzi [11], we assume that another great advantage of the presented modified ODCB setup is that investigating the fracture behaviour of such ductile adhesives in shear at different loading rates is also possible. In comparison to other shear tests such as the ENF and TENF tests, the presented approach would allow such ductile hyperelastic adhesives to be characterized even at larger adhesive layer thicknesses, which has not been possible to this point in time. Furthermore, a data-reduction scheme based on the J -integral was applied within this study. Especially considering the study of Stamoulis and Carrere [6], in which the authors found that data reduction schemes based on linear elastic fracture mechanics could be a potential source of error during testing at increased loading rates, this is a distinct advantage compared to other common methods used to investigate the

rate-dependent fracture behaviour of adhesive joints such as the ENF and TENF tests at moderate loading rates. Plastic deformations of the adherends, which can occur when conducting ENF tests at increased loading rates such as in the study of Borges et al. [2], were also not observed within the performed mode III tests.

Hence, we conclude that the proposed modification to the ODCB test can, next to the quasi-static investigation of adhesive joints, also be used to investigate the shear fracture behaviour of adhesives at elevated loading rates in mode III.

5. Conclusions

In our study, we presented modifications to the original Out-of-plane loaded Double Cantilever Beam test which enable the investigation of the energy release rate of adhesive joints in pure mode III at elevated loading rates. Experiments were performed on the epoxy adhesive SikaPower® 498 quasi-statically and at two elevated loading rates. Within the limitations of the present study, the following conclusions can be drawn:

1. The presented test setup can be used to determine both the energy release rate and the cohesive law of adhesive layers at increasing loading rates. Local measurement of the deformation behaviour of the specimen is necessary for this purpose, as effects of inertia influence the measurements obtained by external load cells. The adhesive layer was still loaded symmetrically in mode III within the tested range of loading rates.
2. The critical mode III energy release rate of the tested adhesive seems to be independent of the loading rate within the range of material scattering. More experiments should be conducted in the future to investigate this more closely.
3. With increasing loading rate, the traction separation law of the tested adhesive tends from a tri-linear to a bi-linear shape accompanied by an increase in shear strength. This could be a sign of a decrease in plastic deformations at the crack tip during crack initiation, leading to an increasingly brittle failure. This was also indicated by the fracture surfaces, which showed signs of plastic deformations during the quasi-static tests but not during the tests at increased loading rates.

Funding sources

This project is supported by the Federal Ministry for Economic Affairs and Energy (BMWi) on the basis of a decision by the German Bundestag [grant number ZB-ZF4283703]. The financial support is gratefully acknowledged.

CRediT authorship contribution statement

Peer Schrader: Methodology, Investigation, Formal analysis, Writing – original draft, Writing – review & editing, Visualization.
Stephan Marzi: Conceptualization, Supervision.

Acknowledgements

This article is part of P. Schrader's doctoral thesis at the Doctoral Center for Engineering Sciences of the Research Campus of Central Hessen under the supervision of the Justus-Liebig-University Giessen in cooperation with the University of Applied Sciences of Central Hessen (Technische Hochschule Mittelhessen).

The authors would like to thank Sabine Wenig (SIKA Automotive, Switzerland) for supplying the adhesive and Hssane Kididane for his support during the experimental investigation.

Appendix A

Maximum transversal moments obtained during the experimental investigation (absolute values):

Transversal moment	iM_x	iM_z
Maximum value [Nm]	15.5	11.2

References

- [1] Machado JJM, Marques EAS, Da Silva LFM. Adhesives and adhesive joints under impact loadings: an overview. *J Adhes* 2018;94(6):421–52. <https://doi.org/10.1080/00218464.2017.1282349>.
- [2] Borges CSP, Nunes PDP, Akhavan A, Marques EAS, Carbas RJC, Alfonso L, et al. Influence of mode mixity and loading rate on the fracture behaviour of crash resistant adhesives. *Theor Appl Fract Mech* 2020;107:102508. <https://doi.org/10.1016/j.tafmec.2020.102508>.
- [3] Carlberger T, Biel A, Stigh U. Influence of temperature and strain rate on cohesive properties of a structural epoxy adhesive. *Int J Fract* 2009;155(2):155–66. <https://doi.org/10.1007/s10704-009-9337-4>.
- [4] Marzi S. Measuring the critical energy release rate in mode II of tough, structural adhesive joints using the tapered end-notched flexure (TENF) test. *Eur Phys J Spec Top* 2012;206(1):35–40. <https://doi.org/10.1140/epjst/e2012-01584-4>.
- [5] May M, Hesebeck O, Marzi S, Böhme W, Lienhard J, Kilchert S, et al. Rate dependent behavior of crash-optimized adhesives – experimental characterization, model development, and simulation. *Eng Fract Mech* 2015;133:112–37. <https://doi.org/10.1016/j.engfractmech.2014.11.006>.
- [6] Stamoulis G, Carrere N. Linear elastic analysis of the loading rate dependency of the fracture properties of structural adhesives in the mixed mode I+II plane. *Eng Fract Mech* 2020;225:106840. <https://doi.org/10.1016/j.engfractmech.2019.106840>.
- [7] Stigh U, Biel A, Walander T. Shear strength of adhesive layers – models and experiments. *Eng Fract Mech* 2014;129:67–76. <https://doi.org/10.1016/j.engfractmech.2014.07.033>.
- [8] Loh L, Marzi S. An Out-of-plane Loaded Double Cantilever Beam (ODCB) test to measure the critical energy release rate in mode III of adhesive joints: special issue on joint design. *Int J Adhesion Adhes* 2018;83:24–30. <https://doi.org/10.1016/j.ijadhadh.2018.02.021>.
- [9] Loh L, Marzi S. A Mixed-Mode Controlled DCB test on adhesive joints loaded in a combination of modes I and III. *Procedia Structural Integrity* 2018;13:1318–23. <https://doi.org/10.1016/j.prostr.2018.12.277>.
- [10] Loh L, Marzi S. A novel experimental methodology to identify fracture envelopes and cohesive laws in mixed-mode I + III. *Eng Fract Mech* 2019;214:304–19. <https://doi.org/10.1016/j.engfractmech.2019.03.011>.
- [11] Loh L, Marzi S. Mixed-mode I+III tests on hyperelastic adhesive joints at prescribed mode-mixity. *Int J Adhesion Adhes* 2018;85:113–22. <https://doi.org/10.1016/j.ijadhadh.2018.05.024>.
- [12] Sørensen BF, Jacobsen TK. Determination of cohesive laws by the J integral approach. *Eng Fract Mech* 2003;70(14):1841–58. [https://doi.org/10.1016/S0013-7944\(03\)00127-9](https://doi.org/10.1016/S0013-7944(03)00127-9).
- [13] Bödeker F, Marzi S. Applicability of the mixed-mode controlled double cantilever beam test and related evaluation methods. *Eng Fract Mech* 2020;235:107149. <https://doi.org/10.1016/j.engfractmech.2020.107149>.
- [14] Marzi S, Biel A, Stigh U. On experimental methods to investigate the effect of layer thickness on the fracture behavior of adhesively bonded joints. *Int J Adhesion Adhes* 2011;31(8):840–50. <https://doi.org/10.1016/j.ijadhadh.2011.08.004>.

Paper C:

Influence of loading rate on the cohesive traction for soft, rubber-like adhesive layers loaded in modes I and III

Peer Schrader, Dennis Domladovac, Stephan Marzi

Preprint submitted to International Journal of Adhesion and Adhesives, submitted April 21st, 2022

Author Contributions:

D. Domladovac and the author contributed equally to the work and share first authorship. The experimental setup was conceptualized and planned by D. Domladovac and the author. The author was responsible for specimen manufacturing. The optical fibres for the backface strain measurements were prepared by D. Domladovac. The experiments were performed by D. Domladovac and the author. The approach to the evaluation of the backface strain measurements was developed together with D. Domladovac, who then evaluated the backface strain measurements. The remaining data was analysed by the author. The paper was planned and written by D. Domladovac and the author. S. Marzi was responsible for funding acquisition, supervised the work and proofread the paper.

Influence of loading rate on the cohesive traction for soft, rubber-like adhesive layers loaded in modes I and III

Peer Schrader¹), Dennis Domladovac¹), Stephan Marzi^{*})

Institute of Mechanics and Materials, Technische Hochschule Mittelhessen, Wiesenstrasse 14, 35390 Giessen, Germany

Abstract

To date, the fracture behaviour of soft, polyurethane-based adhesive joints has rarely been investigated. This work contributes to the experimental investigation of such joints in modes I and III by performing Double Cantilever Beam and Out-of-plane loaded Double Cantilever Beam tests at various loading rates. The tests were evaluated using a J -integral method, which is well established for testing of stiff adhesive layers and is conventionally used to determine the cohesive traction at the crack tip. Additionally, fibre-optics measurements were conducted to provide crack extension, process zone length, and cohesive traction from the measured backface strain of the adherends. It was found that the energy release rate seems to be largely independent of the loading mode. However, differences were observed regarding process zone length and resistance-curve behaviour. Furthermore, the backface strain measurement allows the determination of the cohesive traction along with the complete adhesive layer as well as separation and separation rate, yielding rate-dependent traction separation laws. A comparison between the backface strain measurement and the J -integral method showed that the “conventional” method delivers inadequate results for the cohesive traction, because its underlying theoretical assumptions are violated for soft, rubber-like adhesive joints. Hence, the backface strain measurement method provides valuable insight into the fracture behaviour of soft, rubber-like adhesive joints.

Keywords: polyurethane, fracture mechanics, mechanical properties of adhesives, rate-dependency, cohesive traction

1. Introduction

The literature contains a large number of studies investigating the fracture behaviour of epoxy-based adhesives but comparatively few works investigating soft, rubber-like polyurethane-based adhesives. However, many authors agree that polyurethane adhesives have various advantages in terms of a more even load distribution of peel loads, higher elongation at break, good damping properties and fatigue resistance, and energy consumption during impact [1–3]. The latter is of particular importance in passenger protection, as increased fracture energy leads to a greater amount of energy being absorbed by the adhesive layer in the event of a crash accompanied by finite deformations in the adhesive layer, which could potentially help to minimise personal injuries. Despite these important factors, only a few studies have investigated the fracture behaviour of polyurethane-based adhesive joints, whereas numerous studies have been conducted on polyurethane adhesives in their bulk form. The determination of cohesive laws is of particular importance

in many industrial applications, because from these, by use of cohesive zone modelling, the behaviour of adhesively bonded joints can be predicted efficiently in finite element analyses. Commonly, an evaluation method based on the J -integral according to Rice [4], which we will discuss later on, is used for this purpose. The approach assumes a purely (nonlinear) elastic material behaviour with the crack tip being the only inhomogeneity in the body, which is generally problematic for testing soft, rubber-like adhesive systems because effects of loading rate and energy dissipation outside of the crack tip in the process zone are neglected. For pure mode I loading, Rosendahl et al. [5] showed that the approach can, indeed, approximately be used for thick, hyperelastic adhesive layers under quasi-static conditions using finite element analysis. However, this finding remains to be verified experimentally. Furthermore, in mode III testing of rubber-like adhesives, in which the process zones are significantly larger than in mode I [6], the approach has not yet been used. For this reason, we propose a methodology based on the deflection curve of the adherends in Double Cantilever Beam (DCB) and Out-of-

¹) The authors share first authorship and contributed equally to this work.

^{*}) corresponding author. Tel.: +49 641 309 2124, fax: +49 641 309 2905, mailto: stephan.marzi@me.thm.de

plane loaded Double Cantilever Beam (ODCB) tests to circumvent the underlying assumptions of rate-independent material behaviour and negligible effects of the process zone, allowing the determination of cohesive laws in both modes I and III at different loading rates.

The dependency on loading rate and mode on the fracture energy of rubber-like adhesives has also been investigated in some recent studies: In pure mode I testing, Schmandt and Marzi [7,8] investigated the effect of loading rate and adhesive thickness on fracture energy, cohesive strength, and joint stiffness of polyurethane-based adhesives with DCB tests using the above-mentioned method of evaluation and found that fracture energy and cohesive strength show dependencies on both loading rate and layer thickness. Boutar et al. [9] investigated quasistatic single mode I and mode II fracture of a polyurethane-based adhesive system and found a significant dependency of the obtained fracture energy on loading mode, with the mode II fracture energy being over three times larger than the mode I fracture energy at a layer thickness of 1 mm. In contrast, Loh and Marzi [6] investigated the mixed-mode I+III behaviour at a layer thickness of 3 mm and found that there could be an indication that the critical fracture energy of thick polyurethane-based joints does not depend on the mode-mix-ratio. However, they also stated that the experimental scatter in their results did not allow a definitive statement about this issue. Furthermore, because of a pronounced resistance-curve behaviour, they were unable to determine the cohesive traction in the adhesive layer.

As hinted at earlier, the determination of process zone length and crack tip position is also of interest for the investigation of the fracture behaviour of adhesive joints: Considering the determination of crack length, Schrader et al. [10] found that the crack extension measurement for rubber-like adhesive joints proved to be a difficult task with both optical methods of crack length measurement and the enhanced simple beam theory approach according to Skec et al [11], leading to the conclusion that other methods for determining an equivalent crack tip position could be advantageous. Hence, as an alternative, we rely on an approach based on strain measurements on the adherends backface within this study. Similar approaches have already been established in some other studies with a focus on pure mode I testing of stiff adhesive systems: Ben Salem et al. [12] used several strain gauges along the top surface of a DCB specimen bonded by a structural adhesive joint for crack tip detection and identified the crack tip position from the position of maximum bending strain. Similarly, Bernasconi et al. [13] and Lima et al. [14] used optical backscatter reflectometry to obtain the strain on the adherends' backface. Truong et al. [15] also calculated the resistance curve for a composite specimen from backface strain measurements. To obtain a deflection curve during DCB experiments, Reiner et al. [16] and Sun and Blackman [17] used Digital Image Correlation (DIC) to obtain the displacement profiles, enabling the calculation of the energy release rate from the obtained displacement data. Additionally, especially for the investigation of soft adhesive systems, a measurement of strain along the adherends allows the investigation of the process zone shape, as performed by Jumel et al. [18] for example.

Building on the mentioned studies, the present work aims to investigate the effects of crack opening velocity and loading mode on a soft, rubber-like polyurethane-based adhesive joint, especially considering the determination of cohesive laws. For this reason, we performed DCB and ODCB experiments on a

soft, polyurethane-based adhesive system (Wiko Ultimate Elongation GLUETEC Industrieklebstoffe GmbH & Co. KG, Greußenheim, Germany) in both DCB and ODCB tests at different loading rates, i.e., 0.05 mm/s, 0.5 mm/s, and 5 mm/s in mode I and 0.05 deg/s, 0.5 deg/s and 5 deg/s in mode III, respectively. In each of the test series, one experiment with a fibre-optics based backface strain measurement was performed to investigate the deformation behaviour of the adherends and to compare the results with the conventionally used evaluation methods for the determination of traction separation laws based on the J -integral.

We shall begin by presenting the necessary theoretical background on the evaluation methods of the DCB and ODCB experiments based on J -integral and backface strain measurement. After stating the materials and methods, we shall present and thoroughly discuss the most important experimental findings. This includes the observed fracture patterns, the bending strain measured by the optical fibres, the rate-dependency of the ERR in modes I and III, the obtained R-curves, the measured process zone lengths, and the cohesive traction. Furthermore, the fibre-optics measurements are compared to the globally measured data to verify the used approaches of evaluation. As we will show, the determination of traction separation laws from the deflection curve of the adherends is a valuable addition to testing, as the conventional J -integral method of determining the cohesive traction is prone to error because the underlying assumptions are violated for soft, rubber-like adhesive layers. Additionally, the presented method based on the backface strain measurement allows the determination of a rate-dependent traction separation law.

2. Theory

2.1 J -integral and cohesive traction

The J -integral of an arbitrary shaped, non-linear elastic body according to Rice [4] is defined as

$$J = \int_S \left(W dy - t_i \frac{\partial \Delta_i}{\partial x} ds \right), \quad (1)$$

where S describes an arbitrary path circumscribing the crack tip in a counterclockwise direction, t_i are components of the (nominal) traction vector, Δ_i are components of the displacement vector, and W is the strain energy density, see Fig. 1. The integration is performed in the reference configuration and, per definition, provides the sum of all inhomogeneities in the body.

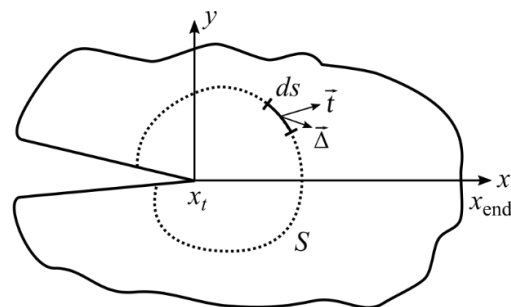


Figure 1 – Schematic representation of the line J -integral around a notch for a plane problem

Considering the testing of adhesive layers, determining the traction vector is of special interest for modelling the fracture behaviour of adhesive joints using cohesive zone models. Briefly, if the integration path is chosen around the boundary between the adherend and adhesive layer parallel to the x -axis ($dy = 0$) and exploiting the symmetry of a specimen (i.e., identical adherends), the above equation can be expressed as

$$J = 2 \int_{x_{\text{end}}}^{x_t} t_i(x) \frac{\partial \Delta_i(x)}{\partial x} dx = \int_{x_{\text{end}}}^{x_t} t_i(x) \frac{\partial \delta_i(x)}{\partial x} dx \quad (2)$$

where $\delta_i = 2\Delta_i$ are the components of the separation vector, i.e., the relative displacement of the upper and lower boundary, x_{end} is the (unloaded) end of the adhesive layer, and x_t is the crack tip position. This value obtained for the J -integral from Eq. 2 is in equilibrium with the sum of contributions from external loads (cf. Sec. 2.2) given that no energy is dissipated outside of the adhesive layer. The assumption of elastic behaviour of the adhesive layer implies that the traction depends solely on the deformation state, $t_i(\delta_i(x))$. Inserting this into the above equation and substituting $\frac{\partial \delta_i(x)}{\partial x} dx = \delta_i(x)$ then yields

$$J = \int_0^{\delta_i(x_t)} t_i(\delta_i(x)) d\delta_i(x). \quad (3)$$

under the assumption that the end of the adhesive layer x_{end} is unloaded. Using the crack opening displacement (COD) $\delta_{i,t} = \delta_i(x_t)$, the equation can be rewritten in differential form and rearranged for the cohesive traction

$$t_i(\delta_t) = \frac{dJ}{d\delta_{i,t}} \quad (4)$$

thus yielding the so-called cohesive law $t_i(\delta_t)$. This method is straightforward, as by measuring the J -integral over external loads (cf. Sec. 2.2) and the COD, traction separation laws can be determined directly by derivation of the measured quantities.

It should be highlighted, however, that it is difficult to justify the validity of the assumptions behind Eq. 4 for a soft polyurethane-based, rubber-like adhesive. For such adhesives, the assumption of purely elastic behaviour behind the presented derivations is deemed problematic: Firstly, the implication that the cohesive traction solely depends on the separation neglects the effects of loading rate on the material behaviour. Secondly, the assumption of a nonlinear elastic

body implies that the crack tip is the only material inhomogeneity in the body. This is also problematic, as soft adhesive layers will develop process zones of finite length before ultimate failure. As the J -integral provides the sum of all inhomogeneities in the elastic body, inhomogeneities in the process zone, e.g., plastic effects, viscoelasticity, and damage also contribute to the value of the J -integral and will falsely be ascribed to the crack tip when calculating the cohesive traction from Eq. 4.

Because the assumptions behind Eq. 4 are likely violated during the testing of soft, rubber-like adhesives, it can already be assumed that the approach of taking the derivative of the externally measured value of J for the COD can only yield an approximation of the traction at the crack tip. However, as this approach to the determination of traction separation laws is deemed very pragmatic and was used successfully in other studies considering the mode I fracture of polyurethane-based adhesive joints [5,7,8], it is worthwhile to check this approach with additional methods of measurement that allow a determination of the nominal traction in the adhesive layer to possibly assess the quality of the approximation.

2.2 Determination of energy release rate and cohesive traction from external measurements

Consider the DCB and ODCB specimens displayed schematically in Fig. 2. Briefly, if the specimen is loaded in pure mode I during a DCB test, as found by Paris and Paris [19], the J -integral according to Eq. 2 reduces to

$$J = \frac{F_y(\theta_1 + \theta_2)}{b} \quad (5)$$

For pure mode III loading during ODCB tests, Loh and Marzi [20] derived that the J -integral yields

$$J_{III} = \frac{M_y^2}{b} \frac{1}{EI_y} \quad (6)$$

with the applied moment M_y and the bending stiffness EI_y of the adherends. Loh and Marzi [21] found in a later study that unintended contributions to J can occur during testing in mode III, which result from a mode I contribution due to the specimen twisting under an out-of-plane deformation (J_{I*}) and a contribution in modes I and II due to the finite width of the adhesive layer (J_{I+II}):

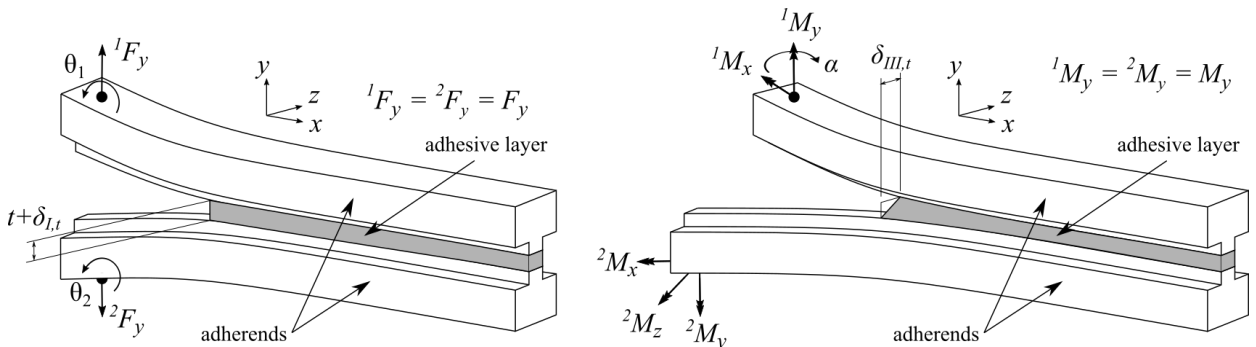


Figure 2 – Schematic representation of the used specimens with applied loads: DCB specimen (left) and ODCB specimen (right)

$$J_{I^*} = \frac{1}{2b} \frac{{}^1M_x^2 + {}^2M_x^2}{\mu I_{yz}} \text{ and } J_{I+II} = \frac{{}^2M_z^2}{2b} \frac{1}{EI_z} \quad (7)$$

Here, μ denotes the shear modulus of the adherends, and I_{yz} and I_z denote the torsional second moment of area and the second moment of area of the adherend around the bending axis z , respectively. From this, the total value of the J -integral is obtained from the sum of mode III and the artificial contributions:

$$J = J_{III} + J_{I^*} + J_{I+II} \quad (8)$$

However, it should be noted that in the subsequent studies by Loh and Marzi [6,21,22] and Schrader and Marzi [23], the contributions J_{I^*} and J_{I+II} were found to be negligible at the point of fracture during pure mode III investigations of both epoxy-based and polyurethane-based adhesive systems, i.e., $J \cong J_{III}$. The traction separation law can then be determined from Eq. 4 as the externally measured value of J is in equilibrium with the value of J in the adhesive layer given that the adherends do not deform plastically.

2.3 Determination of ERR and cohesive traction from the deflection curve

To gain better insight into the deformation behaviour of the specimen in each loading configuration, a measurement of the adherends' backface strain ε at discrete measuring points along with the specimen is used to determine the deflection curve at different times during the experiment. For each measurement in time, from the distance c between the position of strain measurement and the neutral axis of the adherend, which is assumed to be an Euler-Bernoulli beam, the beam curvature κ is obtained via $\kappa(x) = \varepsilon(x)/c$, ultimately yielding the bending moment

$$M_b(x) = -\kappa(x)EI \quad (9)$$

from the bending stiffness EI around the bending axis of interest (y -axis in the ODCB and z -axis in the DCB tests, respectively). From this, transverse force Q and line load q are obtained by differentiation of the bending moment for the x -position along the adherends, giving

$$Q(x) = \frac{dM_b(x)}{dx} \text{ and } q(x) = -\frac{d^2M_b(x)}{dx^2}. \quad (10)$$

Furthermore, integrating the curvature along the beam

provides the slope φ of one lever arm and the separation δ between the two adherends via

$$\begin{aligned} \varphi(x) &= -\int_{x_{end}}^{x_t} \kappa(x) dx \text{ and} \\ \delta(x) &= 2 \int_{x_{end}}^{x_t} \varphi(x) dx. \end{aligned} \quad (11)$$

It should be mentioned that, for a specimen with an unloaded end, it can be reasonably assumed that the integration constants for slope and deflection become nought, allowing the calculation of both quantities without further restrictions. As a result, a measurement of the beam curvature provides an additional possibility of obtaining the cohesive traction at discrete measuring points along with the length of the beam via

$$t(x) = \frac{q(x)}{b} \quad (12)$$

under the assumption that the load is distributed equally on the width of the adhesive layer for both peel and shear loads. Thus a comparison can be made to check the applicability of Eq. 4 can be checked with this measurement. Furthermore, considering Eq. 2, from the stress in the cohesive zone according to Eq. 12 and the relationship $\partial \Delta_i / \partial x = \varphi(x)$, the J -integral is obtained via

$$J = 2 \int_{x_{end}}^{x_t} t(x) \varphi(x) dx. \quad (13)$$

It is therefore evident that the measurement of the elongation at the marginal fibres of the adherends can be used to gain better insight into the fracture behaviour of the adhesive layer. By investigating the deformation behaviour at different times during the experiment and points along with the specimen, both traction, separation, and separation rate can be obtained.

3. Methods

3.1 Specimen manufacturing

Within this study, both DCB and ODCB tests were performed on the polyurethane-based adhesive system Wiko Ultimate Elongation (GLUETEC Industrieklebstoffe GmbH & Co. KG, Greußenheim, Germany) at various loading velocities. The tested adhesive system is a one-component, moisture-curing adhesive that exhibits a high elongation at break of about 800 % according to the manufacturer's data. The substrates of

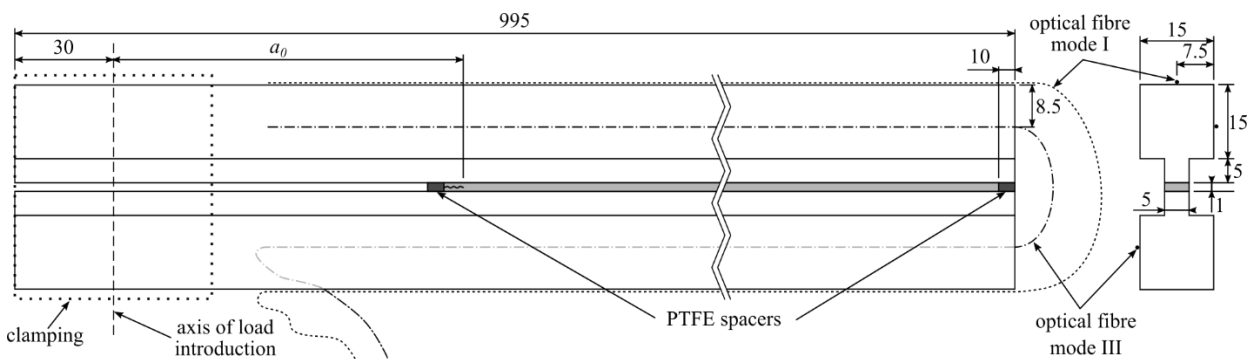


Figure 3 – Dimensions of the tested specimens; $EI_y = 2.98 \cdot 10^8 \text{ Nmm}^2$, $EI_z = 4.56 \cdot 10^8 \text{ Nmm}^2$, $\mu I_{yz} = 2.75 \cdot 10^8 \text{ Nmm}^2$

the used specimens were made of the high-strength aluminium alloy AlZn5,5MgCu (material grade number 3.4365, $E = 70$ GPa). The used specimens are displayed in Fig. 3 with the corresponding dimensions. The adherends had a T-shaped cross section to achieve a smaller adhesive layer width compared to the width of the adherends, avoiding plastification in the aluminum during the experimental investigation. Furthermore, the length of the specimens was chosen to be shortly below a meter, ensuring that the process zone did not reach the end of the specimen during the crack initiation phase even in the case of finite deformations at the crack tip, ensuring an unloaded end of the specimen.

Before applying the adhesive, the bonding surfaces of the substrates were sandblasted with corundum (grain size of 100-150 μm) and degreased with isopropyl alcohol. The adhesive was then applied with an electric caulking gun. To define the layer thickness, PTFE spacers with a nominal thickness of 1 mm were placed at the beginning and the end of the adhesive layer and removed after curing. Screw clamps were used to hold the substrates in place during the curing procedure at a room temperature of $(23 \pm 2)^\circ\text{C}$ and relative humidity of about $(50 \pm 5)\%$. The specimens were cured for 1 - 2 weeks. Before testing, a sharp pre-crack was introduced at the beginning of the adhesive layer by inserting a thin razor blade in the middle of the adhesive layer parallel to the bonding surfaces. With the described procedure, an initial crack length of (135.7 ± 1.2) mm, i.e., the distance between initial crack tip and axis of load introduction, and an adhesive layer thickness of (0.88 ± 0.08) mm were achieved.

3.2 Experimental setups and test matrix

The DCB and ODCB tests were performed in a biaxial tension-torsional servo-hydraulic test machine (MTS Landmark Bionix, MTS Systems, Eden Prairie, USA). The experimental setups are displayed in Fig. 4. To measure the rotations θ_1 and

θ_2 of the specimens at the load introduction points in the DCB tests, incremental rotary encoders (BDH 1P.05A320000-L0-5, Baumer AG, Frauenfeld, Switzerland) with a resolution of 320000 steps per full turn were used. The applied force was measured below the lower clamping device with a six-axis load cell (K6D110 4kN/250Nm, ME-Messsysteme GmbH, Hennigsdorf, Germany). To examine the rate-dependency of the adhesive, the DCB tests were performed at external loading rates of 0.05 mm/s, 0.5 mm/s, and 5 mm/s.

During the ODCB tests, the applied moments were measured using two of the above-mentioned six-axis load cells, one at each load introduction point of the specimen. To avoid lateral forces on the specimen, the bottom clamping of the specimen was mounted on two orthogonally placed linear slides. Throughout the ODCB tests, the axial force was controlled to be nought by the used testing machine. At the time of carrying out the experiments, it was assumed that the floating support would ensure that the transverse forces would not influence the experimental results akin to the results of Schrader and Marzi [23], wherefore the measurement of the transverse forces was omitted. As we will show later, however, it was found during the post-processing of the fibre-optics measurement that this assumption is problematic for the tested soft, rubber-like adhesive layer. The ODCB tests were performed at external loading rates of 0.05 deg/s, 0.5 deg/s, and 5 deg/s, respectively.

To investigate the deflection curve, the backface strain along with the specimen is measured using a fibre-optics system (ODiSI-B 5500, Luna Innovations Inc., Roanoke, USA, positional resolution of 2.5 mm). The fibre was bonded to the adherends along the upper and lower surface of the adherends for the DCB tests and on the tensile loaded outer surface of the adherends for the ODCB tests. As the experimental effort largely increases with the additional use of this measuring system, we refrained from increasing sample sizes with fibre-optics measurements for this pilot study. The results are evaluated following the procedure described in Sec. 2.3. It

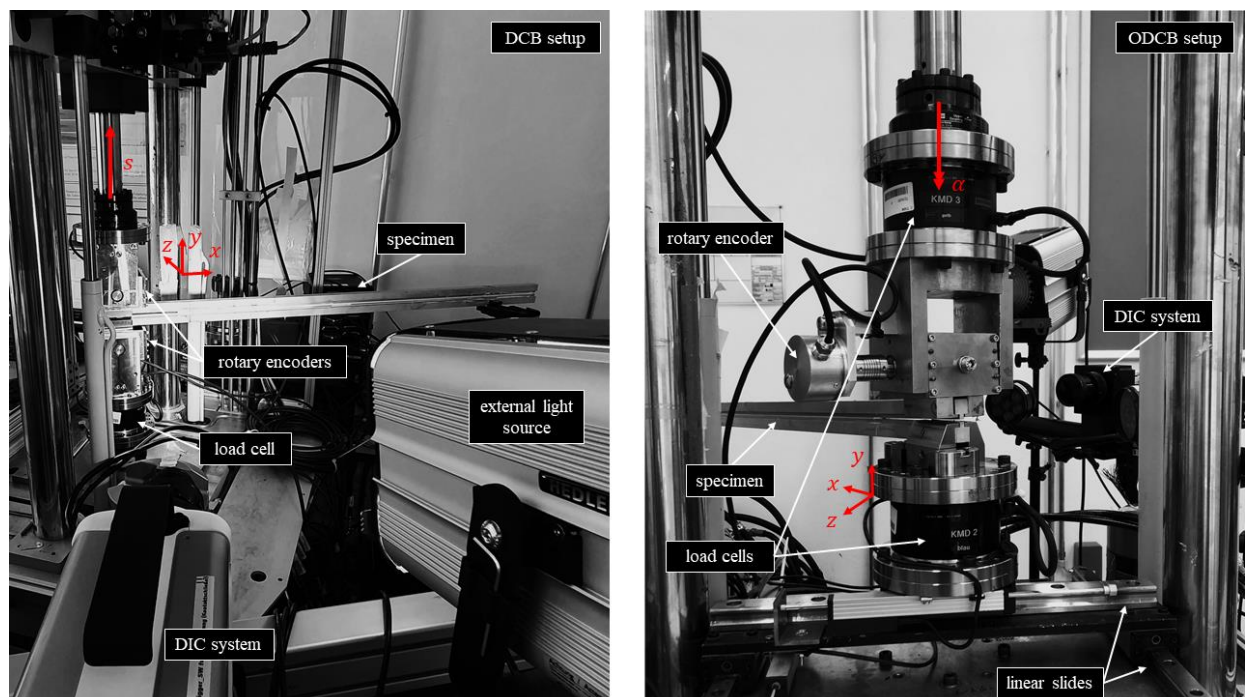


Figure 4 – Experimental setups: mode I DCB setup (left), mode III ODCB setup (right)

Table 1 – Test matrix and used DIC-systems

External loading rate		Sample size	DIC Camera	Image acquisition rate (fps)
Mode I (mm/s)	0.05	5	Aramis 3D Sensor ¹⁾	1
	0.5	4	Photron FASTCAM Nova ²⁾	30
	5	5	Photron FASTCAM Nova ²⁾	125
Mode III (deg/s)	0.05	4	ARAMIS 3D ¹⁾	1
	0.5	4	ARAMIS 3D ¹⁾	20
	5	4	Photron FASTCAM Nova ²⁾	125

Used DIC-setups:

¹⁾ ARAMIS 3D Motion and Deformation Sensor, GOM Correlate (GOM GmbH, Braunschweig, Germany)

²⁾ Photron FASTCAM Nova S6 (Photron USA, San Diego, USA), VIC-3D 8 (Correlated Solutions, Irmo, USA)

must be stated that numerically taking the derivative of the measured curvature for the x -position along the beam produces a large amount of numerical noise. To counteract this, the measurements were filtered with a Savitzky-Golay filter before each derivation step.

The COD was measured with stereo camera systems in all cases. To evaluate the COD, the relative distance between two measuring points at the position of the initial pre-crack was determined through DIC measurements, with one point being on the lower and one on the upper substrate. In the mode III experiments, the measurement of the COD was adjusted for the rigid body rotation of the specimens. Two DIC systems were used based on the desired rate of image acquisition: For the experiments at lower image acquisition rates between 1 and 20 fps ARAMIS 3D Motion and Deformation Sensor with corresponding evaluation software (GOM Aramis, GOM GmbH, Braunschweig, Germany) was used. For the tests with image acquisition rates between 30 and 125 fps, two 1 MP Photron FASTCAM Nova S6 (Photron USA, San Diego, USA) and the evaluation software VIC-3D 8 (Correlated Solutions, Irmo, USA) were used. Within the course of this study, to reduce numerical errors during differentiation, the experimental results of $t_i(\delta_t)$ are obtained with the procedure proposed by Biel [24], in which the experimental results of J vs. δ_t are fitted with a Prony series before taking the derivative.

For a better overview, the number of the performed experiments is summarized in Tab. 1 with the external loading rate, sample size, used DIC systems, and image acquisition rates. As stated earlier, in each of the conducted test series, one fibre-optics measurement was conducted.

3.3 Determination of crack extension and process zone length

From the backface strain measurement, crack extension and process zone length can also be determined using the Euler-Bernoulli beam theory (cf. Fig. 5). As it can reasonably be assumed that the transverse force in the lever arms of the adherends is constant during the DCB experiments, yielding a linear increase in the measured strain along with the optical fibre. Hence, to measure the crack extension, linear regression can be performed in the linear region of the measured strain and the point of 0.5 % deviation from linearity is defined as the crack tip position x_t . To determine the end of the process zone, the maximum fibre strain in the pressure zone is used. The end position of the process zone is then defined as the fibre position at which the threshold of 10% below the maximum fibre strain in the pressure zone is undercut. The process zone

length l_p is then computed from the difference between the current crack tip position and the end position of the process zone.

The procedure in the mode III experiments is analogous, with the difference that the beam curvature (and, hence, the bending strain in the optical fibre) in the lever arms before the crack tip is assumed to be constant under pure mode III loading from an external bending moment. Hence, linear regression is performed in the region of constant beam curvature. In this case, the crack tip position is defined as the point of 1 % deviation from linearity.

Additionally, the crack length is also calculated analytically under the assumption of simple beam theory, i.e., the assumption of the adherends being Euler-Bernoulli perfectly clamped at a point-like crack tip. A comparison is deemed worthwhile as the ERR for stiffer adhesive layers is often calculated from the crack length (e.g., akin to the methods standardised in ISO 25217 [25]) and analytically determining the crack length for soft, rubber-like adhesive layers instead of measuring it with great experimental effort could be beneficial in practice. For the DCB experiments, the crack length is calculated from the load-point separation s and the rotational angle θ at the load introduction points via

$$a_I = \frac{3s}{4\theta} \quad (14)$$

In the mode III ODCB experiments, the crack length is computed analytically via

$$a_{III} = \frac{\alpha E I_y}{2M_y} \quad (15)$$

with α being the rotational angle of the biaxial testing machine.

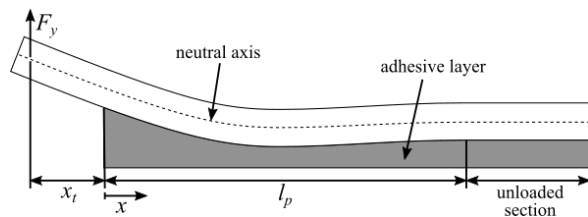


Figure 5 – Determination of crack tip position and process zone length

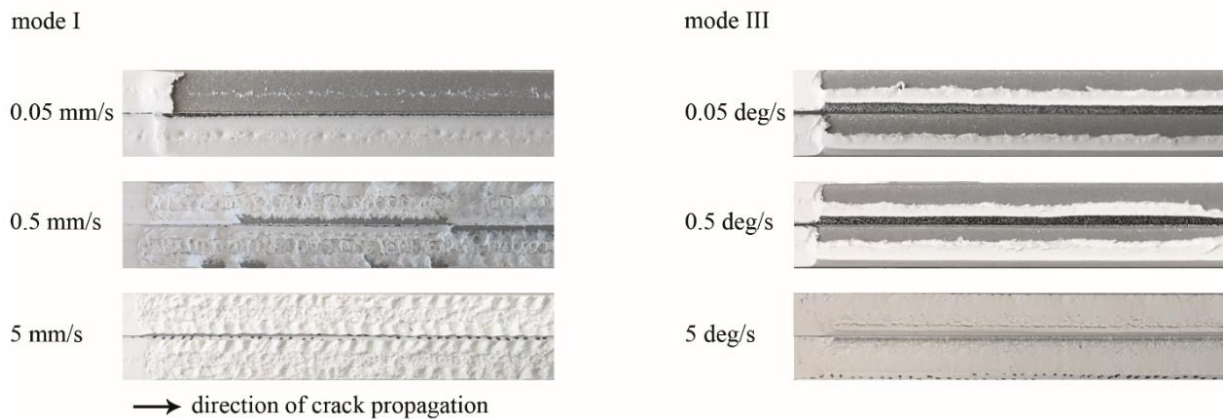


Figure 6 – Representative fracture surfaces obtained from the experiments

4. Results and Discussion

4.1 General observations and fracture surfaces

In all cases, large displacements at the initial crack tip are observed before the crack starts to propagate. During quasi-static mode I loading, the crack travels directly to the nearby interface, followed by adhesive failure, which is commonly observed regarding the quasi-static peeling of adhesive joints [8]. With increasing loading rate, the mode I failure becomes more cohesive (cf. Fig. 6). In the ODCB experiments, due to finite deformations at the crack tip, the mode III shear transitions into a peel load, accompanied by partly adhesive failure at highly stretched parts of the joint (cf. Fig. 7). Interestingly, the large displacement aspect during mode III loading indicates crack propagation perpendicular to the actual bonding surface, accompanied by partly adhesive failure at the outer edges of the adhesive layer. This is probably related to the general tendency of the adhesive to fail adhesively at particularly slow rates. It is assumed that during loading, highly stretched parts of the joint at the outer boundary fail adhesively, hence, reducing its effective width, before an ultimate cohesive failure occurs. However, this behaviour ceases at an increased rate of 5 deg/s, as the fracture surfaces show a tilted fracture surface with purely cohesive failure. In Fig. 7, it can also be observed that the outer edges of the adhesive layer opposing the side of partly adhesive failure are

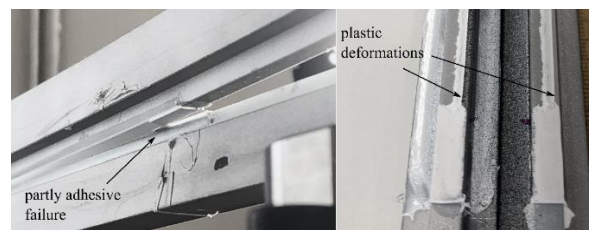


Figure 7 – Partly adhesive failure and plastically deformed, tilted side surfaces observed during mode III loading at the loading rates of 0.05 deg/s and 0.5 deg/s

tilted and plastically deformed.

4.2 Measured backface strain of the optical fibre

Fig. 8 shows the development of the bending strain in the optical fibre over the runtime of a DCB and an ODCB test at different selected times during the measurement. For better visualization, the zero value of the abscissa is set at the initial crack tip position. Independently from the loading mode, the process zone is already quite large at the beginning of the crack propagation, strongly indicating that the assumption of an infinitesimally small process zone is violated.

In the mode I experiments, the maximum strain first increases with the applied load and then begins to shift along with the specimen as the crack progresses. Furthermore, the bending

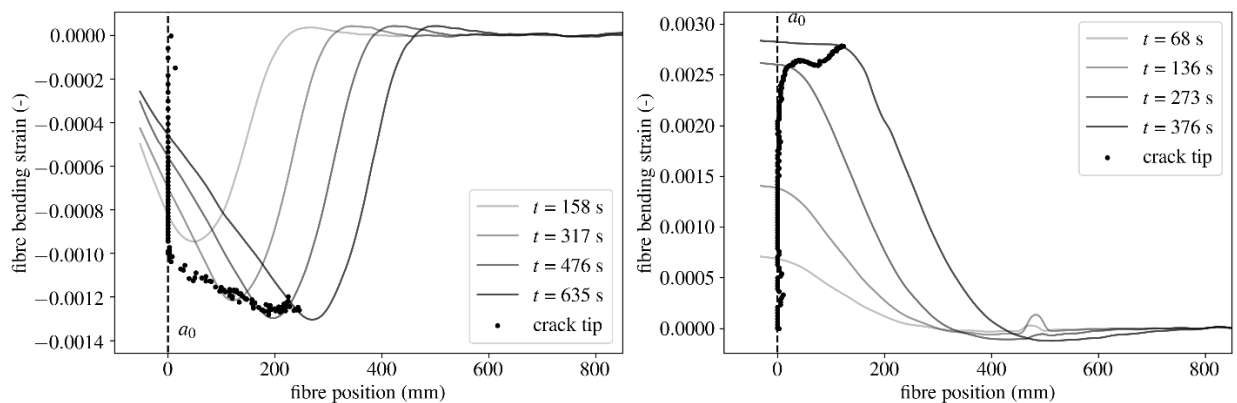


Figure 8 – Development of the bending strain of the optical fibre: quasi-static DCB test (left) and quasi-static ODCB test (right)

strain behaves linearly in front of the crack tip, indicating that a constant transverse force is applied in the lever arm. Deviations from linearity can hence be ascribed to the adhesive layer, indicating that the selected criterium for the detection of the crack tip position delivers satisfactory results.

In the mode III experiments, although one would expect a constant bending strain in the region of the lever arms because of the applied bending moment M_y , linear growth of the measured strain can be observed, indicating that an additional transverse force, probably due to friction in the lateral slides below the lower clamping device, acts on the specimen. The transverse force obtained from the fibre-optics measurement is displayed in Fig. 9 for the different loading rates. The assumption of friction being the main reason for the transverse forces is supported by the fact that the resisting force is relatively constant after a certain break-away force of the linear slides is reached. Because this resisting force is counter-directed to the applied moment component M_y , it will inevitably reduce the traction and the value of J in the adhesive layer. This result, which unfortunately only became apparent during post-processing, was rather unexpected. While this will not influence the fibre-optics evaluation, it must be assumed that the influence has a significant impact on the evaluation of J from the external measurements, as it cannot be considered with the used method of evaluation for the ODCB tests.

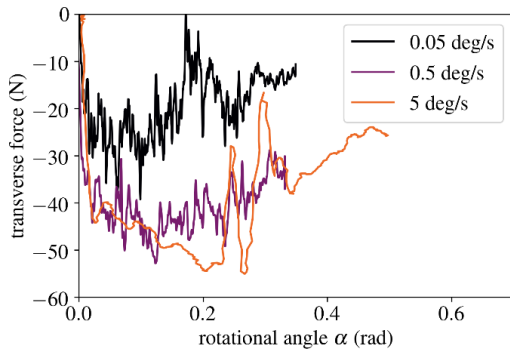


Figure 9 – Transverse forces obtained from the bending strain of the optical fibre during the ODCB tests

Comparison between fibre-optics, load and DIC measurements Before further investigating the fracture behaviour of the tested adhesive joints with the fibre-optics measurements, it shall be investigated whether the results can be verified with the globally measured data of COD and applied load. In

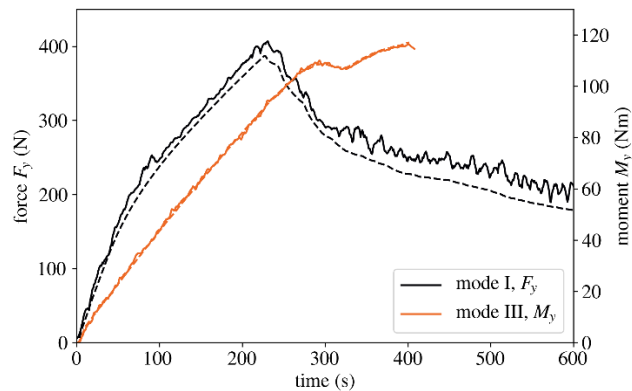
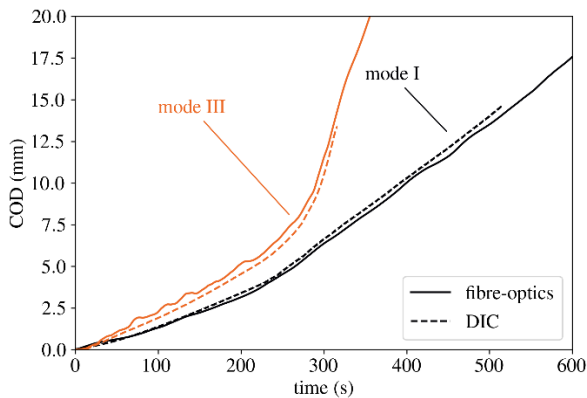


Figure 10 – Comparison between externally measured values and fibre-optics measurement: separation of the adherends at the crack tip (left), applied external force/bending moment (right)

Fig. 10, the results for two representative specimens (nominal adhesive layer thickness of 1 mm at the lowest loading rate) are shown for both the mode I and the mode III experiments. As can be observed, the separation at the initial crack tip obtained from both the DIC measurement as well as the values from the fibre-optics measurement show a good agreement, indicating that the separation of the adherends can be determined from the fibre-optics measurement with good accuracy. As the measurement data of the fibre-optics measurements are integrated along with the complete specimen to obtain the COD at the position of the crack tip x_t (cf. Eq. 11), this means that the separation at each measurement point along the adhesive layer can be determined reliably. As the shear force in mode I is constant in the lever arms in front of the crack tip, the values obtained by the fibre-optics measurement may be compared with the values measured on the external load cells as well, also showing a very good agreement. To compare the moments in mode III, the observed slope in the fibre bending strain in front of the crack tip is extrapolated to the point of load introduction. Here, the external moment measurement also agrees well with the moment obtained from the fibre-optics measurement. Overall, the good agreement of the external measurement of COD and applied load with the fibre-optics measurements indicate that the methodology proposed in Sec. 2.3 delivers valid results.

4.3 Influence of loading mode and loading velocity on the ERR

The mode I ERR obtained from Eq. 5 is shown in Fig. 11 over the measured rotational angle θ ; for a better overview, the tests conducted with fibre-optics measurements are highlighted. As expected, the measured values for J at fracture initiation are rising with the loading rate. The large discrepancy between the obtained ERR at 0.05 mm/s and 0.5 mm/s can be related to the adhesive failure observed during the quasi-static experiments. In Fig. 12, the mode III ERR according to Eq. 6 over the rotational angle α and the relative influence of the unintended contributions to J at the onset of fracture according to Eq. 7 are displayed for each loading rate. Here, it can be observed that, during the experiments at 0.05 deg/s and 0.5 deg/s, the ERR does not reach a steady plateau throughout the experimental investigation, already indicating that the ERR is rising with crack propagation, yielding a resistance curve (cf. Sec. 4.5). It can also be observed that the unintended contributions from

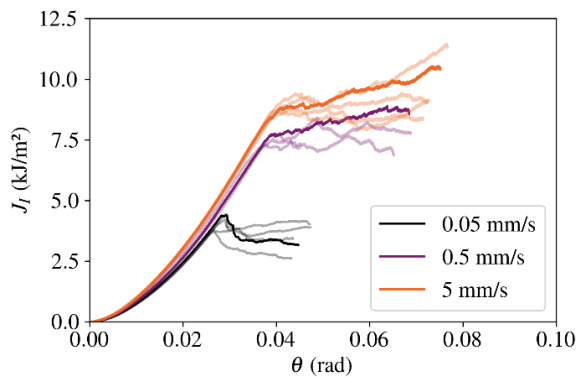


Figure 11 – Measured ERR during the mode I experiments; experiments with additional fibre-optics measurements are highlighted

the transverse moments are indeed negligible at the point of fracture, which is in good agreement with the results of prior investigations [6,21–23]. This also allows the conclusion that the fibre-optics measurement, although affected by a transverse force, is not influenced significantly by the moment components responsible for the unintended contributions to J . Fig. 13 presents the values for J obtained from Eq. 5 and 6 in comparison to the value obtained from the fibre-optics measurement according to Eq. 13 for the mode I and mode III experiments. Here, a good correspondence between both

methods of evaluation can be seen for pure mode I loading. For the mode III experiments, however, it can be observed that the value for J according to Eq. 6 and the fibre-optics measurement differ greatly from another, with the fibre-optics J being approx. 20 % lower than the externally measured value throughout the experiments. As hinted at earlier, this is due to the transverse force (cf. Fig. 9), which was observed during post-processing of the fibre-optics measurements but not recorded during the experiments. This is also undermined by the fact that both the transverse force and the difference between the evaluation methods are the smallest at the loading rate of 0.05 deg/s; for the tests at 0.5 deg/s and 5 deg/s, in which the transverse force is larger, the difference also increases. As the external measurement seems to be strongly influenced by the friction within the lateral slides, the results from the fibre-optics measurements clearly show that the evaluation of the ODCB test has to be revised for the testing of soft, rubber-like adhesive layers.

To estimate the dependency of J on loading rate and loading mode, the values of J at crack initiation are displayed over the representative crack opening velocity in Fig. 14. The representative crack opening velocity is determined from a linear regression of the COD vs. time in the initial linear region of $dJ/d\delta_{i,t}$ akin to the approaches of Schmandt and Marzi [7] and Schrader and Marzi [23], respectively. Here, a large discrepancy between the mode I and mode III results is visible if the externally measured values are considered. However, the

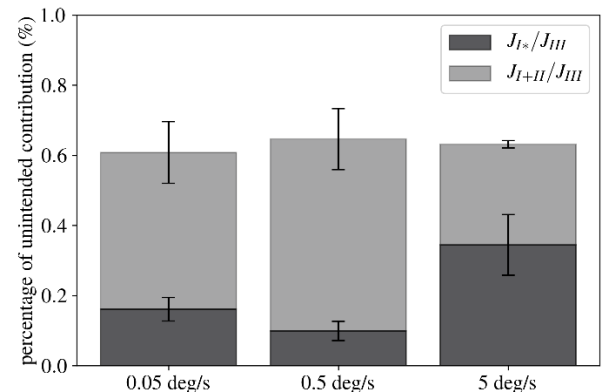
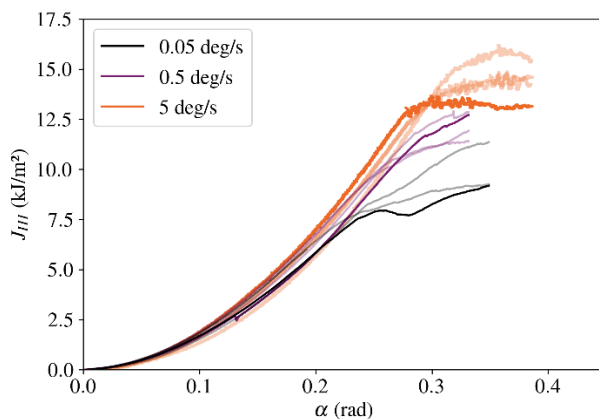


Figure 12 – Results of the ODCB experiments: measured ERR (left) and relative influence of the unintended contributions to J at the start of crack propagation (right); experiments with additional fibre-optics measurement are highlighted

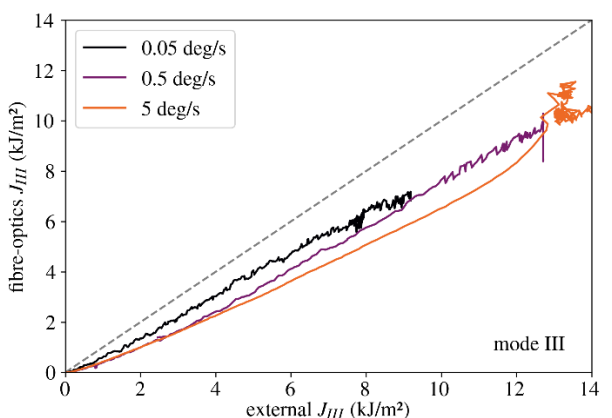
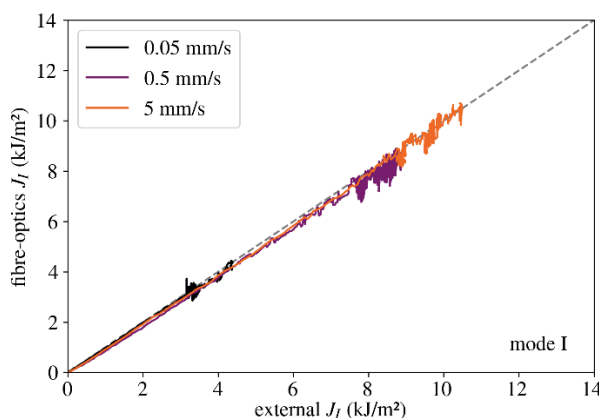


Figure 13 – Comparison between externally measured values and fibre-optics measurement of J

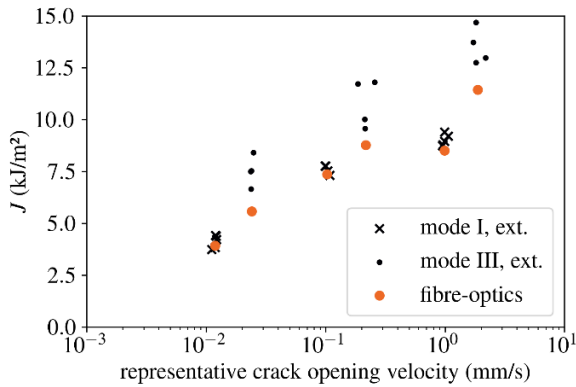


Figure 14 – Influence of loading mode and representative crack opening velocity on the externally measured ERR

values obtained from the fibre-optics measurements indicate that the differences between mode I and mode III mainly result from neglecting the transverse forces due to friction in the lateral slides. Hence, given the limitations of this study, a similar rate dependency is obtained for both modes I and III, indicating that the ERR could be independent of loading mode (as was also hypothesised by Loh and Marzi in [6]). This also correlates with the large deformations at the crack tip observed during the mode III experiments, which ultimately yield a local peel load at the crack tip at fracture initiation.

4.4 Crack propagation, resistance-curve behaviour and process zone length

The resistance curves for all tested specimens are shown in Fig. 15. Whereas a constant ERR can be observed in the mode I experiments during crack propagation, the ERR rises with crack extension in the mode III experiments at the lower loading rates of 0.05 deg/s and 0.5 deg/s. Due to the crack extension before reaching the critical value of J , the cohesive traction can not be calculated from $dJ/d\delta_{III,t}$ for these experiments, as, although the crack already started to propagate, the cohesive traction would be unequal to nought until the J -plateau was reached.

The process zone lengths obtained from the fibre-optics measurements are shown in Fig. 16 over the measured crack extension. Generally, the length of the process zone increases until the start of crack propagation and remains constant over the experiment in good approximation in all cases, indicating stationary conditions behind the crack tip even in the case of an observed R-curve. During mode I testing, the process zone length seems to be largely independent of the loading rate. In the mode III experiments, however, is noticeable that the process zone length drastically decreases at the loading rate of 5 deg/s, which can likely be ascribed to the partly adhesive failure during the experiments at 0.05 deg/s and 0.5 deg/s. In these experiments, the partly adhesive failure before cohesive crack propagation causes a decrease in stiffness of the joint and, hence, larger process zones. Additionally, it should be

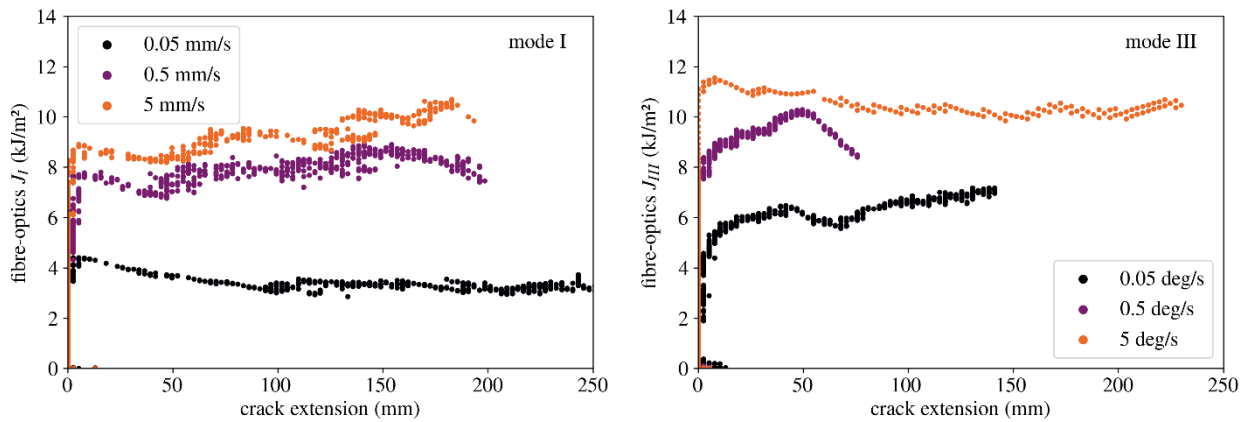


Figure 15 – Resistance curves obtained from the fibre-optics measurements

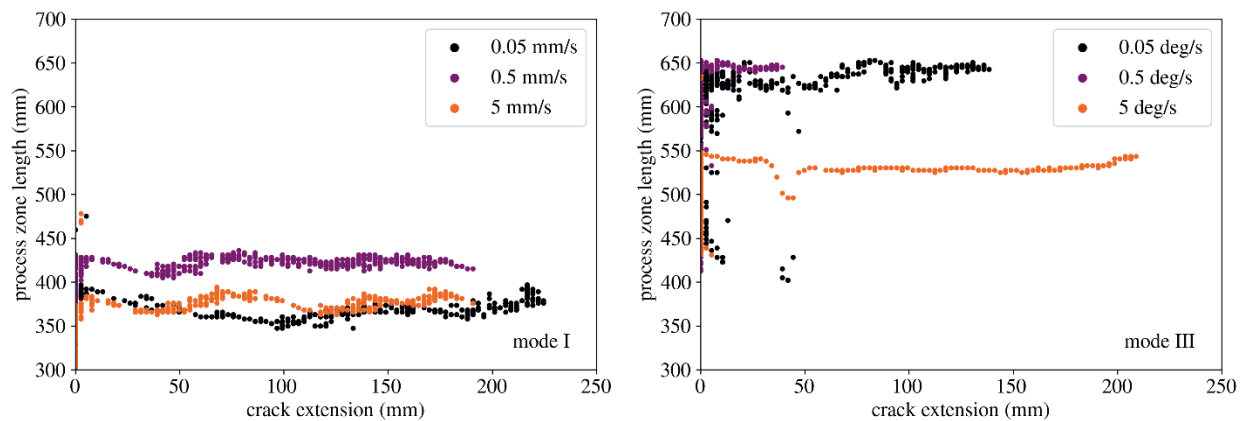


Figure 16 – Development of the process zone length during the experiments

noted that the process zone lengths in mode III are significantly larger than in mode I at the start of crack propagation, which can generally be related to a lower stiffness of the adhesive in shear than in peel.

As stated earlier, a comparison between the crack length obtained from the fibre-optics measurement and the analytical crack length according to simple beam theory is sought. In Fig. 17 the crack extension according to the fibre-optics measurement is displayed over the analytical crack extension during crack propagation. It can be observed that the slope of the curves is relatively close to one in the range of crack propagation in both modes I and III, which correlates with the results of Schrader et al. [10], who also found that the crack extension can be approximated for soft, rubber-like adhesive systems with simple beam theory assumptions. Fig. 17 also shows that the initial crack length is heavily overestimated by the analytical approach, with the error being around 160 mm in mode I and 180 mm in mode III, which, in all cases, is significantly larger than the initial crack length. As this offset seems to be constant, however, it could be argued that analytically calculating the crack length would be possible for

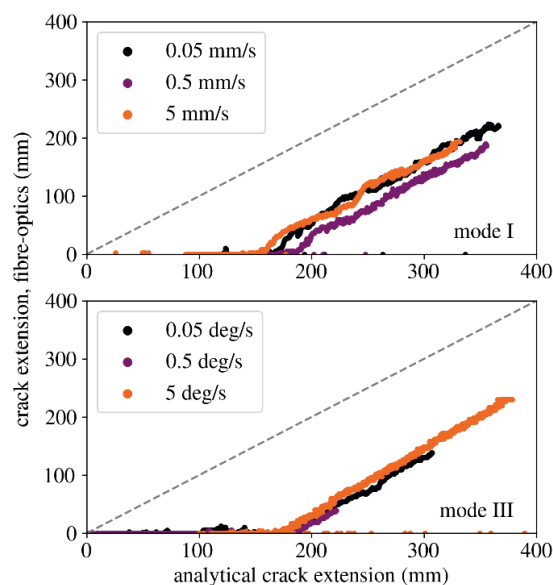


Figure 17 – Comparison between fibre-optics crack extension and analytical crack extension

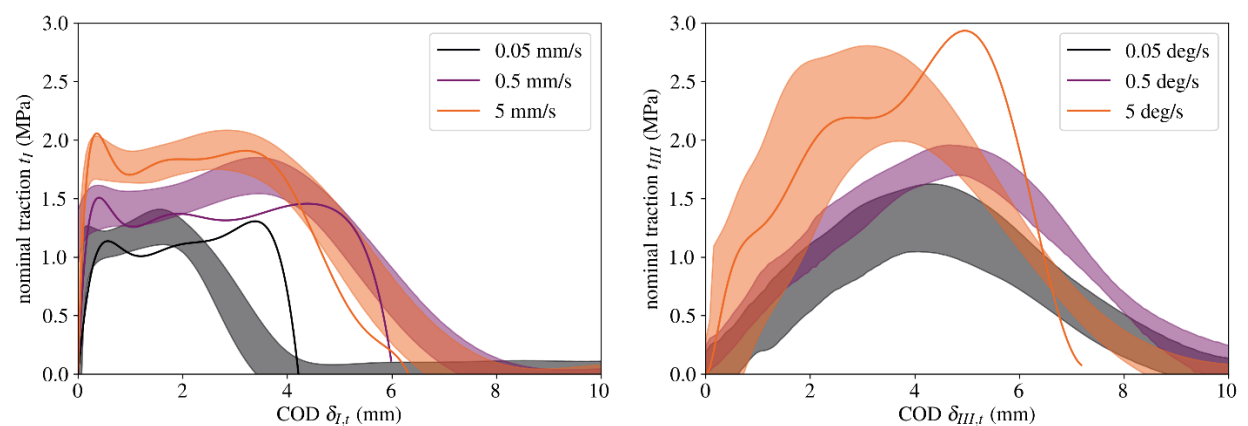


Figure 18 – Comparison between traction at the crack tip obtained from $dJ/d\delta_{I,t}$ (bold lines) and mean and standard deviation curves from the fibre-optics measurements (scatter bands)

the given soft, rubber-like adhesive system if the crack length were corrected for the determined offset.

4.5 Cohesive traction in the adhesive layer

The traction at the initial crack tip obtained from the “conventional” method according to Eq. 4 (bold lines) as well as the mean cohesive traction in the complete adhesive layer according to the fibre-optics measurements, cf. Eq. 12, (scatter bands) is shown in Fig. 18 for both modes I and III. It can already be observed that the measured cohesive traction changes with loading mode, as the initial stiffness of the joint is significantly lower in mode III than in mode I. Furthermore, the measured cohesive traction is dependent on the loading rate in both cases, already violating the underlying assumption of Eq. 4 that the cohesive traction must strictly depend only on the deformation and not on deformation rate. As can be observed, the traction obtained from $dJ/d\delta_{I,t}$ approximately correlates with the fibre-optics measurement in pure mode I, as both the stiffness of the adhesive layer and the plateau stress fit well with each other. For the lowest loading velocity, however, a clear discrepancy in the range of falling traction can be observed, which can probably be related to an increased influence of material inhomogeneities or creep effects in the process zone on the material behaviour. At the loading rates of 0.5 mm/s and 5 mm/s, their influence may be less pronounced in the process zone, which could explain the better agreement between the fibre-optics measurement and $dJ/d\delta_{I,t}$. Overall, the rough correspondence between methods of traction determination correlates with the investigations of Rosendahl et al. [5], who also found that calculating $dJ/d\delta_{I,t}$ can be used to approximate the cohesive traction of soft, rubber-like adhesive layers in pure mode I. For the mode III experiments at 0.05 deg/s and 0.5 deg/s, as hinted at earlier, the cohesive traction cannot be calculated from $dJ/d\delta_{III,t}$ due to the observed R-curve behaviour. In contrast, the fibre-optics measurement can still be used to calculate the cohesive traction within the adhesive layer in these experiments, which is a clear methodological advantage. Additionally, at the highest mode III loading rate of 5 deg/s, the traction obtained from $dJ/d\delta_{III,t}$ differs greatly from the fibre-optics measurements, allowing the conclusion that the determination of the cohesive traction from $dJ/d\delta_{III,t}$ is not feasible in mode III for such soft, rubber-like adhesive layers.

It is generally assumed that the differences between both methods of evaluation arise from violating the underlying theoretical assumptions behind the J -integral method. The fibre-optics measurement, however, can circumvent these assumptions and, by capturing the deformation behaviour of the complete specimen, allows the determination of the traction at the crack tip and along the complete cohesive zone from beam theory without neglecting the influences of energy dissipation in the process zone or influences of the loading rate on the cohesive traction. It can therefore be assumed that the determination of cohesive stresses using $dJ/d\delta_{i,t}$ for such soft, rubber-like adhesive layers is prone to error and can, within the limitations of this study, only be considered an approximation in pure mode I loading. Furthermore, the goodness of the approximation cannot be estimated a priori, as neither the rate-development nor the influence of dissipative effects in the process zone on the material behaviour is known if the traction is calculated from $dJ/d\delta_{i,t}$.

Another benefit of the fibre-optics measurement shall be noted: As stated earlier, the fibre-optics measurement also allows determining the separation of the adherends at each point of the optical fibre from the curvature of the adherends at discrete measurements in time. Hence, by calculating the time derivative of the measured separation at each measuring point along with the specimen, the separation rate within the complete adhesive layer is obtained, also allowing the investigation of the rate-dependency of the joint's behaviour. In Fig. 19, the cohesive traction at each point of measurement is displayed over separation and separation rate. Interestingly, the differences between the measurements at each measurement point seem to be very small, indicating that the cohesive traction is, in good approximation, independent of the position along with the specimen and that separation and separation rate are relatively similar for each point along with the specimen throughout the measurement. Hence, it can be concluded that modelling of the joint can theoretically be performed relatively straightforward with a rate dependent traction separation law.

Although we were unable to implement the traction obtained from the fibre-optics measurement into a cohesive zone model within the scope of this study, a future implementation is deemed worthwhile. With a rate-dependent cohesive zone model formulated from the measured values, it might be possible to better reproduce the behaviour of the adhesive joint. It is also assumed that, if observed, it might even be

possible to approximately reproduce stick-slip or R-curve behaviour due to the accurate determination of cohesive traction and separation rate from the fibre-optics measurement. However, these assumptions remain to be addressed in the context of a future simulative study.

4.6 Methodological Critique

As discussed earlier, a distinctive feature of the presented methodology using fibre-optics measurements for the investigation of the fracture behaviour of adhesive layers is that both the nominal traction within the adhesive layer as well as the current separation and the separation rate can be obtained for a large amount of measuring points along with the complete specimen. This is particularly important for the numerical modelling of the fracture behaviour using cohesive zone models, as the conventional method of using the J -integral to obtain the cohesive traction cannot be used for the soft, rubber-like adhesive layer under investigation, because, as shown, fundamental assumptions of the method are violated. Hence, the results of this study heavily imply that the use of fibre-optics for the investigation of adhesive joints may serve as a window to a better understanding of their fracture behaviour.

However, it has to be stated that the use of fibre-optics, especially for the almost 1 m long adherends used in this study, requires a very high experimental effort for specimen preparation and investigation. As there are separate measured values for each measurement point on the optic fibre, a large amount of data has to be evaluated. Furthermore, the numerical derivation of the measurement data to obtain the cohesive traction produces large amounts of numerical noise, which must carefully be removed using suitable filters before processing the data. As a result, the evaluation of the measurement data is very complex and time-consuming.

As just described, filtering of the fibre-optics measurement data for further processing is a major challenge in evaluation. It could therefore be appropriate to first approximate the measured beam curvature using an analytical relationship (polynomials, exponential functions, etc.) to facilitate numerical integration and differentiation. We have refrained from this in the context of this study to introduce as few assumptions as possible into the evaluation of the data a priori. In future studies, however, it is argued that the evaluation process could be simplified by carefully selecting appropriate

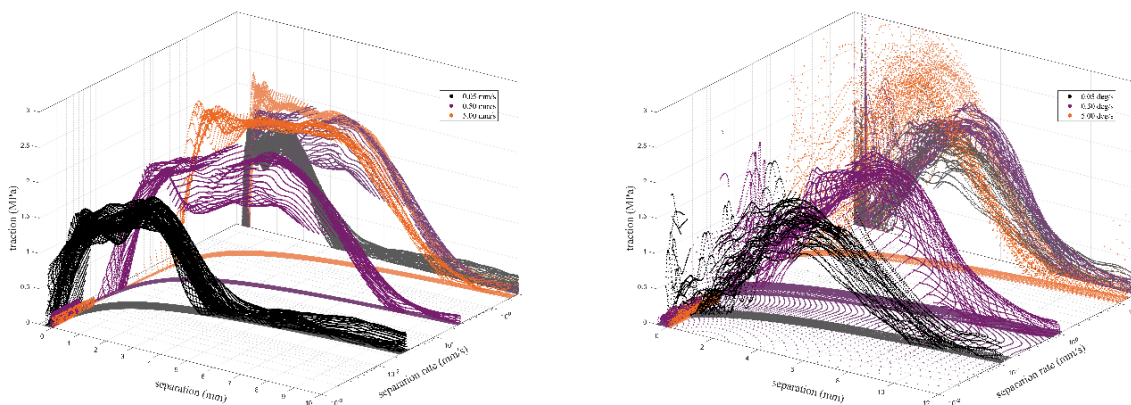


Figure 19 – Traction in the cohesive zone over current separation and separation rate: mode I (left) and mode III (right)

fit functions, e.g., [17,26].

At last, we would like to state that the determination of the beam curvature with fibre-optics offers additional possibilities in other areas of application within fracture mechanics testing, which have not – or only to a limited extent – been addressed in this study: It is argued that besides the primary focus of this work, i.e., the determination of the cohesive traction, changes in the beam curvature due to damage evolution behind the crack tip as observed by Schrader et al. [10] could be detected by fibre-optics measurements, allowing the researcher to gain better insight in the damage processes within the adhesive layer behind the major crack tip.

Especially for G -based approaches to determining the fracture energy of an adhesive layer, the current crack length must be measured with good accuracy. The determination of an equivalent crack length from the fibre-optics measurements was also shown to be possible in this study, which could allow the determination of crack tip position and crack propagation rate for adhesive systems or test setups in which optical methods for the evaluation of crack length fail due to lack of space or lack of visibility of the current crack tip position. Furthermore, compared to analytical methods for the determination of the equivalent crack length from load point displacement and/or applied loads, the approach presented here does not require any assumptions to be made about the boundary conditions of the substrates' beam bending such as cantilever beams that are perfectly clamped at the crack tip, which, considering the finite length of the process zone, was shown to be problematic in this work.

It was also shown within the course of this study that, in theory, fibre-optics measurements could even eliminate the need for other COD measurement systems such as DIC systems or COD gauges, as the system can also provide information about these quantities. Particularly if the entire process zone is to be examined, measurement employing DIC is very difficult, as a very large measurement window is required to cover the entire length of the specimen, which will negatively affect the accuracy of the DIC measurement. Furthermore, considering the mode III investigation, the large out-of-plane deformations are difficult to capture with DIC measurements due to limited depth of focus. A calculation of the COD from the beam deflection curve is therefore a worthwhile option for evaluation when investigating adhesive layers that exhibit finite deformations before ultimate failure.

Hence, overall, we believe that implementing the use of fibre-optics for the fracture mechanical investigation of adhesive joints could be a valuable addition to current research practice.

5. Conclusions

In our study, we investigated the effects of loading rate and mode on the fracture behaviour of a soft polyurethane adhesive joint subjected to peel and shear loading. The rate-dependency was investigated at external loading rates over three orders of magnitude in peel and shear. Next to the conventional evaluation methods employing the J -integral, crack extension, process zone length, and cohesive traction were determined from fibre-optics measurements. Within the limitations of this study, the following conclusions can be drawn:

- The results indicate that the ERR of the tested adhesive system may be largely independent of loading mode in pure modes I and III. This is probably due to the shear

loads in mode III testing ultimately transitioning into a peel load at finite deformations.

- The process zone can be investigated thoroughly by the use of fibre-optics measurements. It was observed that the process zone is fully developed at the start of crack propagation in all cases. During the mode III investigations, the process zones are significantly larger than in mode I, which is probably related to the stiffness of the adhesive being lower in shear than in peel.
- The fibre-optics measurements allow the determination of traction separation laws along with the complete adhesive layer based on the Euler-Bernoulli beam theory. Differences between the evaluation method using fibre-optics and the J -integral method were observed, which is likely due to a violation of the underlying theoretical assumptions of the J -integral method when investigating soft, rubber-like adhesive layers. Furthermore, from the fibre-optics measurement, the rate development along with the complete adhesive layer can be measured, which enables determining a rate dependent traction separation law.
- As the traction separation laws could not be determined reliably from the J -integral method in the mode III experiments, a determination of cohesive traction with fibre-optics measurements or similar methods is deemed mandatory for soft, rubber-like adhesive layers subjected to mode III loading.
- Although the ERR remains relatively independent of loading mode, the measured traction separation laws are not. Users should bear this in mind when designing and numerically investigating soft, rubber-like adhesive layers and must not assume that the traction separation laws in modes I and III are equivalent.

We were able to show that the investigation of the fracture behaviour of soft, rubber-like adhesive joints using the J -integral method involves complications that require investigation in more detail in future studies. For the time being, the fibre-optics measurements were used as proof of concept, from which, in future investigations, further insights can certainly be gained. Hence, we advise that further research is undertaken in the following areas:

- It became apparent from the fibre-optics measurements during the mode III investigations that transverse forces in the lateral slides influence the external determination of the ERR for the tested soft, rubber-like adhesive system. If ODCB experiments are conducted on similar adhesive systems in the future, the transverse forces should be included in the external evaluation of the J -integral.
- Although it was not possible to implement the measured traction separation laws in finite element analyses in the scope of this study, an implementation using cohesive zone models is deemed worthwhile. A simulative study could investigate whether the experimental results (and especially the observed R-curve behaviour) can be reproduced with the rate-dependent model.
- It should be investigated whether local effects, i.e., damage behind the crack tip in creep tests, or geometric influences due to defects in the adhesive layer can be investigated more thoroughly using the proposed methodology from fibre-optics measurements.

References

- [1] Loureiro AL, Da Silva LFM, SATO C, Figueiredo MAV. Comparison of the Mechanical Behaviour Between Stiff and Flexible Adhesive Joints for the Automotive Industry. *The Journal of Adhesion* 2010;86(7):765–87. <https://doi.org/10.1080/00218464.2010.482440>.
- [2] Banea MD, Da Silva LFM, Campilho RDSG. The Effect of Adhesive Thickness on the Mechanical Behavior of a Structural Polyurethane Adhesive. *The Journal of Adhesion* 2015;91(5):331–46. <https://doi.org/10.1080/00218464.2014.903802>.
- [3] Banea MD, Da Silva LFM. Mechanical Characterization of Flexible Adhesives. *The Journal of Adhesion* 2009;85(4-5):261–85. <https://doi.org/10.1080/00218460902881808>.
- [4] Rice JR. A Path Independent Integral and the Approximate Analysis of Strain Concentration by Notches and Cracks. *Journal of Applied Mechanics* 1968;35(2):379–86. <https://doi.org/10.1115/1.3601206>.
- [5] Rosendahl PL, Staudt Y, Odenbreit C, Schneider J, Becker W. Measuring mode I fracture properties of thick-layered structural silicone sealants. *International Journal of Adhesion and Adhesives* 2019;91:64–71. <https://doi.org/10.1016/j.ijadhadh.2019.02.012>.
- [6] Loh L, Marzi S. Mixed-mode I+III tests on hyperelastic adhesive joints at prescribed mode-mixity. *International Journal of Adhesion and Adhesives* 2018;85:113–22. <https://doi.org/10.1016/j.ijadhadh.2018.05.024>.
- [7] Schmandt C, Marzi S. Effect of crack opening velocity and adhesive layer thickness on the fracture behaviour of hyperelastic adhesive joints subjected to mode I loading: Special issue on joint design. *International Journal of Adhesion and Adhesives* 2018;83:9–14. <https://doi.org/10.1016/j.ijadhadh.2018.02.028>.
- [8] Schmandt C, Marzi S. Effect of crack opening velocity on fracture behavior of hyperelastic semi-structural adhesive joints subjected to mode I loading. *Procedia Structural Integrity* 2018;13:799–805. <https://doi.org/10.1016/j.prostr.2018.12.154>.
- [9] Boutar Y, Naïmi S, Mezlini S, da Silva LF, Ben Sik Ali M. Characterization of aluminium one-component polyurethane adhesive joints as a function of bond thickness for the automotive industry: Fracture analysis and behavior. *Engineering Fracture Mechanics* 2017;177:45–60. <https://doi.org/10.1016/j.engfracmech.2017.03.044>.
- [10] Schrader P, Schmandt C, Marzi S. Mode I creep fracture of rubber-like adhesive joints at constant crack driving force. *International Journal of Adhesion and Adhesives* 2022;113:103079. <https://doi.org/10.1016/j.ijadhadh.2021.103079>.
- [11] Škec L, Alfano G, Jelenić G. Enhanced simple beam theory for characterising mode-I fracture resistance via a double cantilever beam test. *Composites Part B: Engineering* 2019;167:250–62. <https://doi.org/10.1016/j.compositesb.2018.11.099>.
- [12] Ben Salem N, Budzik MK, Jumel J, Shanahan M, Lavelle F. Investigation of the crack front process zone in the Double Cantilever Beam test with backface strain monitoring technique. *Engineering Fracture Mechanics* 2013;98(18):272–83. <https://doi.org/10.1016/j.engfracmech.2012.09.028>.
- [13] Bernasconi A, Kharshiduzzaman M, Comolli L. Strain Profile Measurement for Structural Health Monitoring of Woven Carbon-fiber Reinforced Polymer Composite Bonded joints by Fiber Optic Sensing Using an Optical Backscatter Reflectometer. *The Journal of Adhesion* 2016;92(6):440–58. <https://doi.org/10.1080/00218464.2015.1043005>.
- [14] Lima R, Perrone R, Carboni M, Bernasconi A. Experimental analysis of mode I crack propagation in adhesively bonded joints by optical backscatter reflectometry and comparison with digital image correlation. *Theoretical and Applied Fracture Mechanics* 2021;116(10):103117. <https://doi.org/10.1016/j.tafmec.2021.103117>.
- [15] Truong HT, Martinez MJ, Ochoa OO, Lagoudas DC. Mode I fracture toughness of hybrid co-cured Al-CFRP and NiTi-CFRP interfaces: An experimental and computational study. *Composites Part A: Applied Science and Manufacturing* 2020;135(2):105925. <https://doi.org/10.1016/j.compositesa.2020.105925>.
- [16] Reiner J, Torres JP, Veidt M. A novel Top Surface Analysis method for Mode I interface characterisation using Digital Image Correlation. *Engineering Fracture Mechanics* 2017;173(1):107–17. <https://doi.org/10.1016/j.engfracmech.2016.12.022>.
- [17] Sun F, Blackman B. A DIC method to determine the Mode I energy release rate G, the J-integral and the traction-separation law simultaneously for adhesive joints. *Engineering Fracture Mechanics* 2020;234:107097. <https://doi.org/10.1016/j.engfracmech.2020.107097>.
- [18] Jumel J, Budzik MK, Shanahan ME. Process zone in the Single Cantilever Beam under transverse loading. *Theoretical and Applied Fracture Mechanics* 2011;56(1):7–12. <https://doi.org/10.1016/j.tafmec.2011.09.006>.
- [19] Paris AJ, Paris P. Instantaneous evaluation of J and C. *International Journal of Fracture* 1988(38):R19-R21.
- [20] Loh L, Marzi S. An Out-of-plane Loaded Double Cantilever Beam (ODCB) test to measure the critical energy release rate in mode III of adhesive joints: Special issue on joint design. *International Journal of Adhesion and Adhesives* 2018;83:24–30. <https://doi.org/10.1016/j.ijadhadh.2018.02.021>.
- [21] Loh L, Marzi S. A Mixed-Mode Controlled DCB test on adhesive joints loaded in a combination of modes I and III. *Procedia Structural Integrity* 2018;13:1318–23. <https://doi.org/10.1016/j.prostr.2018.12.277>.
- [22] Loh L, Marzi S. A novel experimental methodology to identify fracture envelopes and cohesive laws in mixed-mode I + III. *Engineering Fracture Mechanics* 2019;214:304–19. <https://doi.org/10.1016/j.engfracmech.2019.03.011>.
- [23] Schrader P, Marzi S. Mode III testing of structural adhesive joints at elevated loading rates. *International Journal of Adhesion and Adhesives* 2022:103078. <https://doi.org/10.1016/j.ijadhadh.2021.103078>.
- [24] Biel A. Constitutive behaviour and fracture toughness of an adhesive layer; 2019.
- [25] International Organization for Standardization. Adhesives — Determination of the mode I adhesive fracture energy of structural adhesive joints using double cantilever beam and tapered double cantilever beam specimens. 25217th ed. (ISO 25217); 2009.
- [26] Mao J, Nassar S, Yang X. An improved model for adhesively bonded DCB joints. *Journal of Adhesion Science and Technology* 2014;28(6):613–29. <https://doi.org/10.1080/01694243.2013.858387>.

Acknowledgements

This article is part of P. Schrader's doctoral thesis at the Doctoral Center for Engineering Sciences of the Research Campus of Central Hessen under the supervision of the Justus-Liebig-University Giessen in cooperation with the University of Applied Sciences of Central Hessen (Technische Hochschule Mittelhessen).

The authors would like to thank Maike Sapotta (GLUETEC Industrieklebstoffe GmbH & Co. KG, Germany) for supplying the

tested adhesive. Furthermore, we want to thank Jens Minnert and the Institute of Civil Engineering (Technische Hochschule Mittelhessen) for kindly lending us their fibre-optics system for the experimental investigation.

Funding Sources

This project is supported by the Federal Ministry for Economic Affairs and Climate Action (BMWK) on the basis of a decision by the German Bundestag [grant number ZB-ZF4283703]. The financial support is gratefully acknowledged.

Highlights

- Backface-strain measurements are conducted in mode I and III experiments
- Crack extension and process zone length are obtained from backface-strain
- The energy release rate of the tested adhesive is independent of loading mode
- Traction, separation, and separation rate are determined along the adhesive layer
- J -integral methods of evaluation deliver inadequate results for cohesive traction

CRedit authorship contribution statement

Peer Schrader:

Conceptualization, Methodology, Investigation, Formal analysis, Writing – Original Draft, Writing – Review & Editing, Visualization

Dennis Domladovac:

Conceptualization, Methodology, Investigation, Formal analysis, Writing – Original Draft, Writing – Review & Editing, Visualization

Stephan Marzi: Supervision, Funding acquisition

Paper D:

Novel mode III DCB test setups and related evaluation methods to investigate the fracture behaviour of adhesive joints

Peer Schrader, Stephan Marzi

Preprint submitted to Theoretical and Applied Fracture Mechanics, submitted August 25th, 2022

Author Contributions:

The author conceptualized, designed and built the test setup, manufactured the tested specimens, and planned and conducted the experiments. The development of the evaluation methods as well as the evaluation of the test data was performed by the author. The author planned and wrote the paper. S. Marzi was responsible for funding acquisition, supervised the work and proofread the paper.

Novel mode III DCB test setups and related evaluation methods to investigate the fracture behaviour of adhesive joints

Peer Schrader, Stephan Marzi*)

Institute of Mechanics and Materials, Technische Hochschule Mittelhessen, Wiesenstrasse 14, 35390 Gießen,
Germany

Abstract

In this work, two test setups in proximity to the familiar Double Cantilever Beam and Tapered Double Cantilever Beam tests are proposed which allow for determining the critical mode III energy release rate (ERR) of adhesive joints. The experiments are performed on an elastic-plastic adhesive (SikaPower® 498) and evaluated using data reduction schemes based on nonlinear elastic fracture mechanics (J -integral) and linear elastic fracture mechanics (Irwin-Kies equation). Next to the data reduction schemes based on linear elastic fracture mechanics in accordance with ISO 25217, crack length independent and corrected beam theory approaches are presented which incorporate measurements of the rotational angles of the load introduction points. Crack length and process zone length are measured during the experiments using backface strain measurements. Furthermore, a multi-specimen compliance calibration is employed to allow simplified testing in future studies. The obtained critical ERRs and cohesive laws are compared and discussed thoroughly to gain insight into the advantages and disadvantages of the different data reduction schemes. The results implicate that the J -integral evaluation method is the most reliable for evaluation of the mode III fracture energy, as no assumptions need to be made about the behaviour of the adherends when determining the mode III ERR.

Keywords: double cantilever beam, process zone length, cohesive laws, fracture toughness, linear elastic fracture mechanics, J -integral

Nomenclature

a	Measured crack length
a_{eq}	Equivalent crack length
$a_{eq,ESBT}$	Equivalent crack length from ESBT
$a_{eq,SBT}$	Equivalent crack length from Euler-Bernoulli Beam theory
$a_{eq,w/oF}$	Equivalent crack length from without force measurement
$a_{eq,\theta}$	Equivalent crack length from load point rotation
A	Cross-sectional area
b	Width of adhesive layer
C	Compliance of the adherend
CBT	Corrected Beam Theory
COD	Crack opening displacement
DCB	Double Cantilever Beam
DIC	Digital Image Correlation
ECM	Experimental Compliance Method
ESBT	Enhanced Simple Beam Theory
EI_y	Bending stiffness of the adherend in y -direction
ERR	Energy Release Rate
F_y	Applied force in coordinate direction y
G	Griffith ERR
G_{IIIc}	Critical mode III Griffith ERR
G_{ECM}	ERR from Experimental Compliance Method
$G_{SBT,E}$	G under SBT assumptions, Euler-Bernoulli Beam
$G_{SBT,T}$	G under SBT assumptions, Timoshenko Beam
$G_{SBT,eq}$	Crack length independent G with $a_{eq,SBT}$
$G_{SBT,\theta}$	Crack length independent G with $a_{eq,\theta}$
$G_{SBT,w/oF}$	Crack length independent G without force measurement
G_{ESBT}	Crack length independent G with $a_{eq,ESBT}$
G_{CBT}	G from CBT assumptions
$G_{CBT,ISO}$	G from CBT assumptions following ISO 25217
$G_{CBT,w/oF}$	G from CBT without force measurement
$G_{CBT,\theta}$	G from CBT using load point rotation θ
I_t	Torsional second moment of area of the adherends
J	J -integral ERR
J_{I*}	Unintended contribution to J
J_{III}	Mode III contribution to J
J_{IIIc}	Critical mode III fracture energy from J -integral evaluation
LEFM	Linear Elastic Fracture Mechanics
iM_x	Externally applied torsional moment around the axis of crack propagation x at load introduction point i
n	Slope of $\log(C)$ versus $\log(a)$ data
ODCB	Out-of-plane loaded Double Cantilever Beam
S_y	Statical moment of area of adherend in y -direction
SBT	Simple Beam Theory
TDCB	Tapered Double Cantilever Beam
TODCB	Tapered Out-of-plane loaded Double Cantilever Beam
UODCB	Uniaxial Out-of-plane loaded Double Cantilever Beam
w	Width of the adherend
x, y, z	Coordinate system
δ	Load point displacement
$\delta_{t,I}$	Mode I crack opening displacement
$\delta_{t,III}$	Mode III crack opening displacement
Δ	Virtual crack extension
θ	Rotational angle of load introduction point
κ_y	Shear correction factor
μ	Shear modulus of adherend material
τ	Nominal shear stress

1. Introduction

In the fracture mechanical investigation of materials, three distinct modes of fracture are assumed. When considering the state of research in the experimental investigation of these three failure modes, it is noticeable that mode I and mode II receive the utmost attention. In the case of pure mode I loading, the Double Cantilever Beam (DCB) and Tapered Double Cantilever Beam (TDCB) tests are standardized (e.g. in ISO 25217 [1]), very well established in research practice, and used in a variety of industrial applications because of its rather straightforward application. This also applies to the End-Notched Flexure test, which, for testing composite materials, is also standardized in ASTM D 7905 [2] and also frequently used for the mode II characterization of the fracture behaviour of adhesive layers, see Marzi et al. [3] or Stigh et al. [4] for example. Furthermore, the Tapered End-Notched Flexure and End-loaded split tests are also used frequently for the mode II characterization, see e.g., Marzi [5] and Blackman et al. [6]. However, considering the mode III testing of adhesive joints, only a few studies are available: In one of the first works regarding the mode III fracture of adhesive joints, Mai [7] proposed the edge-crack-line loaded test, in which two TDCB adherends were joined on their outer edge. Kinloch [8] later noted that, although this setup was originally designed for mode III testing, an indeterminate amount of mode I and II loading on the adhesive layer is almost certainly induced during testing. In a later work, Chai [9] proposed a mode III fracture specimen for testing adhesive joints as a derivative of the DCB test and evaluated the results by the use of simple Euler-Bernoulli beam theory. Almost simultaneously, Donaldson [10] proposed a very similar setup to characterize the interlaminar fracture toughness of different laminates and employed data reduction schemes based on Simple Beam Theory (SBT), the Experimental Compliance Method (ECM) and a work area method. Martin [11] later showed that the test setup of Donaldson [10] is significantly influenced by mode II loads, especially at the outer edges of the specimen. Johnston et al. [12] later presented modifications of Donaldson's [10] approach to determine the fracture energy of polymeric composites. Additionally, the mode III test setup of Yoshihara [13] shall be mentioned, who proposed a four-point bending test setup to determine the interlaminar mode III fracture toughness of wood.

All of the mode III studies mentioned so far were performed to determine the critical fracture energies based on linear elastic fracture mechanics and required using visual crack length determination methods or, as in the case of Johnston et al. [12], an FE-based data reduction procedure. Stigh et al. [14] proposed the split cantilever beam test, in which specimens consisting of thin-walled C-shaped beams (to achieve torsionless bending) and adhesive tape were investigated based on non-linear elastic fracture mechanics using the J -integral without the necessity of monitoring crack length. Loh and Marzi [15] later developed the Out-of-plane loaded Double Cantilever Beam (ODCB) test in which the adherend beams are loaded with an external moment instead of an axial force in a biaxial testing machine. Applying an external moment instead of force allowed a J -integral evaluation employing the Irwin-Kies equation in proximity to the experimental compliance method without the necessity of monitoring crack length. Schrader and Marzi [16], who performed ODCB tests at elevated loading rates, however, conclude in their recent

study that for testing at increased loading velocities a uniaxial test setup is deemed more practicable, as the ODCB test must be performed in a biaxial testing machine and requires a large experimental effort.

A J -integral evaluation of the fracture energy is generally deemed worthwhile: As found by Pérez-Galmés et al. [17] during mode II testing of composite materials, uncertainties in the crack length measurements lead to varying critical fracture energies when comparing different test setups, whereas J -integral approaches of data reduction yielded method independent ERRs. Furthermore, Stamoulis and Carrere [18], stated that using data reduction schemes based on linear elastic fracture mechanics may yield problems when investigating the fracture behaviour of adhesive systems at increasing loading rates, because the influence of viscoelastic and plastic effects on the adhesives' fracture behaviour may not be deemed negligible.

It should be mentioned that in the setups of Chai [9], Donaldson [10], and Stigh et al. [14], the tested adhesive layer widths were above 12 mm in all cases. As an unintended mode II load is induced during mode III loading [11] which occurs to be due to the finite width of the adhesive layer [19], it is considered desirable to further reduce the width of the adhesive layer when testing mode III fracture. Narrower adhesive layers are also deemed practicable for testing tougher materials, as the load at fracture is reduced with the layer width.

Hence, building on the previous works and given the limitations of these approaches, this study proposes two tests – with one being based on the familiar DCB test akin to the original ideas of Chai [9] and Donaldson [10] and one based on the TDCB test as a further development of Mai's edge-crack-line loaded test [7] – that allow an investigation of the mode III fracture behaviour of adhesive layers. The work aims to relate the previous test ideas, applying them to narrower adhesive layers and, above all, holistically comparing the methods of data reduction for the determination of critical ERR and cohesive laws on the same elastic-plastic adhesive system (SikaPower® 498). For the evaluation, G -based data reduction schemes in proximity to the methods of ISO 25217 [1] are applied to facilitate industrial application. Additionally, the Enhanced Simple Beam Theory (ESBT) approach by Škec et al. [20] is considered. Furthermore, in proximity to the study of Stigh et al. [14], a data reduction scheme based on the J -integral according to Rice [21] and its application to Double Cantilever Beam (DCB) tests as proposed by Paris and Paris [22] is employed as a benchmark. As the J -integral approach necessitates the measurement of the specimen's rotation at the points of load introduction, we also present novel Corrected Beam Theory (CBT) approaches which aim to also consider these rotation measurements. The crack length is monitored during the tests using fibre-optics strain measurements. The crack length measurements are then compared with various analytical approaches to crack length determination to possibly reduce the experimental effort in subsequent studies. Additionally, a multi-specimen compliance calibration method of data reduction is investigated. The results are discussed thoroughly to gain better insight into the influence of the different data reduction schemes on the obtained results.

2. Experimental

2.1 Specimen preparation

The experiments performed in this study were conducted on the structural elastic-plastic adhesive SikaPower® 498. The substrates used in this study were made of the aluminium alloy EN AW-7075 T6, $E = (70 \pm 1)$ GPa. The dimension of the adherends for both the UODCB and TODCB tests are shown in Fig. 1. The centre of area of the UODCB specimens is located at $y_S = 11.32$ mm and $z_S = 6.81$ mm, the shear centre of the beams is located 0.49 mm away from the centre of area in z-direction. The TODCB specimens were designed using finite element analysis so that an approximately constant external force is applied to the specimen during crack propagation.

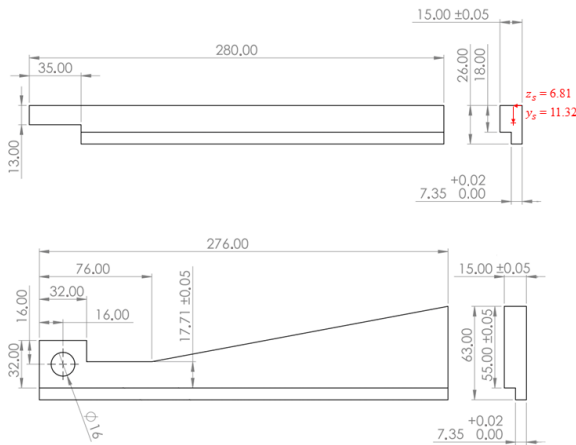


Figure 1 – Geometries of the used UODCB specimens (top) and TODCB specimens (bottom), dimensions in millimetres

The bonding surfaces of the adherends were prepared by sandblasting with corundum (grain size of 100 – 150 μ m), wipe-cleaning with methylethylketone and lint-free paper wipes and subsequent rinsing with the solvent. Both adhesive and adherends were then preheated to 55 °C. Then, one of the adherends was placed on custom aluminium spacers (Fig. 2) and the adhesive was applied with an electric caulking gun. The initial crack tip was defined by inserting a PTFE film (nominal thickness of 0.3 mm) at the beginning of the adhesive layer. The second substrate was placed on top of the first substrate and the adhesive layer followed by two additional

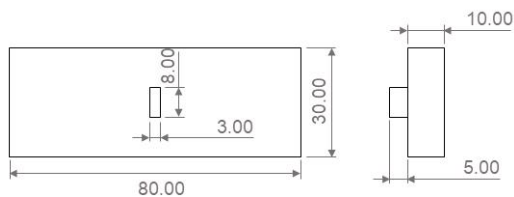


Figure 2 – Specimen preparation: aluminium spacers for defining adhesive width (left, dimensions in millimetres), specimens with screw clamps, aluminium spacers, and PTFE insert (right)

aluminium spacers, ensuring a parallel positioning of the adherend surfaces and defining the adhesive thickness. Screw clamps were used to hold adherends and spacers in place (Fig. 2). Then, excess adhesive was carefully removed with a spatula before the specimens were cured for 30 min at an exposure temperature of 175 °C. The PTFE insert was removed before testing. To obtain the adhesive thickness, the thickness of the aluminium substrates at the bonding surfaces (measured before applying the adhesive) was subtracted from the width of the complete specimen after curing.

2.2 Experimental setup

The experimental setups are shown in Fig. 3. The experiments were performed in a servo-hydraulic test machine (MTS Landmark Bionix, MTS Systems, Eden Prairie, USA) at a constant loading rate of 1 mm/min. To avoid lateral forces on the specimens, the lower clamping device was placed on orthogonal linear slides. Furthermore, the upper clamping was supported with axial ball bearings so that it was free to rotate around the tensile axis to avoid moments in the tensile direction. In effect, the specimens were loaded purely by a force component in the direction of the load train and a

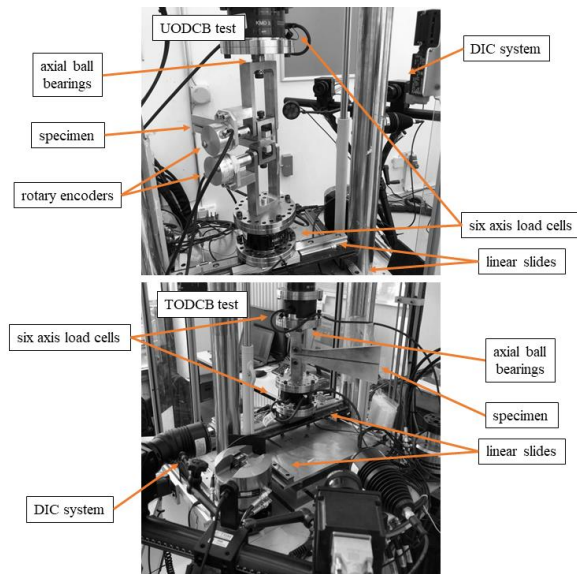


Figure 3 – Experimental setups: UODCB test setup (top) and TODCB test setup (bottom)



moment component around the axis of crack propagation, as the shear centre of the beams lies outside of the adhesive layer. To investigate the influence of this moment component on the results, six-axis load cells (K6D110 4kN/250Nm, ME-Messsysteme GmbH, Hennigsdorf, Germany) were placed above the upper and below the lower clamping of the specimens. During the UODCB tests, the rotational angle of the load introduction points is also measured with high-resolution rotary encoders (BDH 1P.05A320000-L0-5, Baumer AG, Frauenfeld, Switzerland).

Load point displacement δ and Crack Opening Displacement (COD) δ_t were determined utilizing Digital Image Correlation (DIC): Two 12 MP cameras (ARAMIS 3D Motion and Deformation Sensor, GOM GmbH, Braunschweig, Germany) were set up to capture the deformation at the crack tip and displacement of the load introduction points throughout the test (image acquisition rate of 2 fps). Before testing, a greyscale speckle pattern was applied to the specimens' surface and the clamping devices which was later tracked by DIC software (GOM Correlate, GOM GmbH, Braunschweig, Germany). The COD was then determined by measuring the distance between two subsets (subset size of 19 pixels), with each of them on one of the two adherends close to the initial crack tip. Before evaluation of the COD δ_t , the measurements were adjusted for rigid body rotation. With the used DIC setup, physical pixel sizes of approx. 0.08 mm/px were achieved. Blank measurements of an unloaded specimen yielded an in-plane variance error (temporal standard deviation of

measurement noise of the mode III COD $\delta_{t,III}$) of approx. $\pm 2.09 \mu\text{m}$ and an out-of-plane variance error (temporal standard deviation of the measurement noise of the mode I COD $\delta_{t,I}$) of approx. $\pm 3.75 \mu\text{m}$, respectively.

Because the visibility of the crack tip is limited for the presented test setups, although the crack tip position can in principle be determined visually during the experiment, a visual determination of the crack length is deemed rather unreliable. Hence, a fibre-optics system (ODiSI-B 5500, Luna Innovations Inc., Roanoke, USA) with a positional resolution of 0.653 mm along the optical fibre direction was used to measure the deformation of the specimen at the marginal fibre of the adherends at 2 Hz, which allows determining the position of the crack tip and the length of the process zone: Due to the stiff adhesive layer, it may reasonably be assumed that the crack tip is located at the position along the beam at which the bending strain reaches its maximum [23–26]. For convenient determination of the process zone length, the end position of the process zone is defined as the position along the optical fibre at which the threshold of 1% of maximum fibre strain is undercut. The optical fibres were adhesively bonded to the outer edges of the specimens in the middle of the adhesive layer. For a better overview, an example measurement with highlighted crack tip position and process zone length and the placement of the optical fibres are shown for a UODCB specimen in Fig. 4.

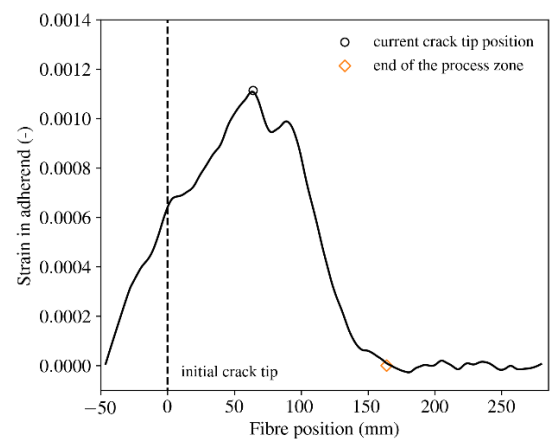
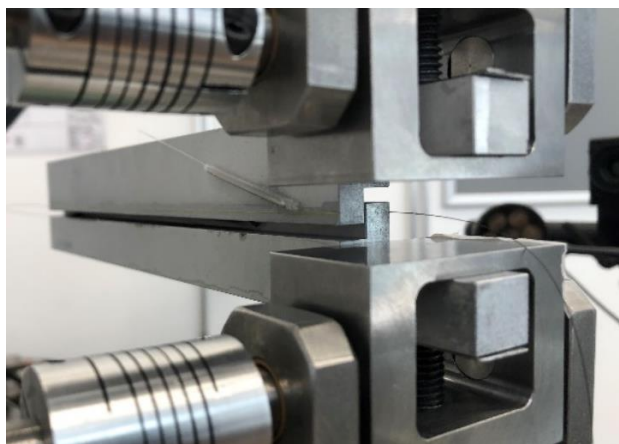


Figure 4 – Fibre-optics strain measurements: placement of optical fibre on a UODCB specimen (left) and sample measurement with highlighted crack tip position and process zone length, initial crack tip at zero-point (right)

Table 1 – Test matrix

Ref.	Test series	Initial crack lengths (mm)	Layer thickness (mm)	Number of performed tests (-)
UODCB-A	simultaneous crack length measurement	60.6 ± 0.4	0.31 ± 0.01	5
UODCB-B	multi-specimen compliance calibration	60.1 to 143.2	0.30 ± 0.01	10
TODCB-A	simultaneous crack length measurement	60.4 ± 0.5	0.37 ± 0.02	5
TODCB-B	multi-specimen compliance calibration	60.1 to 151.1	0.36 ± 0.01	9

2.3 Test Matrix

Within the context of this study, 5 experiments were conducted for each test configuration (UODCB and TODCB setup) with simultaneous crack length monitoring using fibre-optics strain measurements. Furthermore, additional UODCB and TODCB experiments were conducted with varying initial crack lengths to investigate whether a multi-specimen compliance calibration method of data reduction can be adopted. With the preparation process described in Sec. 2.1, the initial crack lengths and layer thicknesses summarized in Tab. 1 were obtained. It shall additionally be noted that in Tab. 1, short references to the test series are also given, which will be used for reasons of conciseness during this study.

3. Theory

3.1 J -integral evaluation of the ERR in UODCB tests

Within this study, the J -integral approach according to Rice [21] is used as a benchmark for the determination of the mode III ERR of the UODCB specimens. Consider the UODCB specimen shown in Fig. 5 with the applied loads. For the sake of completeness, the position of the optical fibre is also highlighted in the figure. Briefly, loading the specimen with an external force in the mode III direction yields a J_{III} of

$$J_{III}(F, \theta) = \frac{F_y(\theta_1 + \theta_2)}{b}, \quad (1)$$

which coincides with the J -integral solution for a DCB specimen as derived by Paris and Paris [22]. Here, θ_1 and θ_2 denote the rotational angles of the load introduction points, F_y is the applied force in y -direction, and b is the width of the adhesive layer. The moments applied around the axis of crack propagation at each load introduction point result in an unintended contribution to J , which, as derived by Loh and Marzi [19,27], is given via

$$J_{I^*} = \frac{1}{2b} \frac{{}^1M_x^2 + {}^2M_x^2}{\mu I_t}, \quad (2)$$

where μ is the shear modulus and I_t is the torsional second moment of area of the adherends, respectively. In principle, the

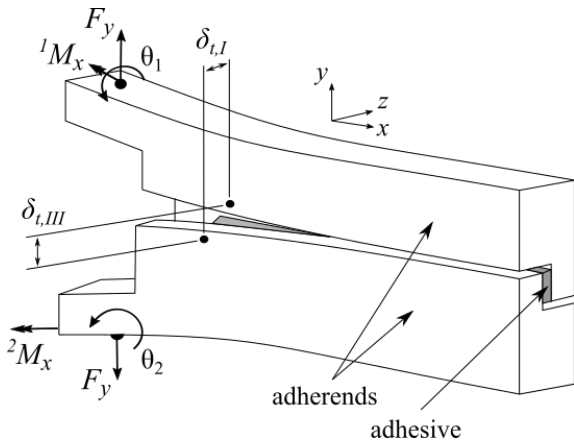


Figure 5 – Schematic representation of a UODCB specimen with applied loads and crack opening displacement

J -integral for the complete specimen is then obtained via

$$J = J_{III} + J_{I^*}, \quad (3)$$

but given that the unintended contribution is of a negligible order of magnitude, i.e., $J_{I^*}/J \ll 1$, the J -integral can be reasonably approximated via Eq. 1.

It shall be noted that, unfortunately, the J -integral evaluation cannot be adopted for the TODCB specimen, as an explicit dependence of the beam's cross-section on the direction of crack propagation leads to a path-dependence of J , thus prohibiting an evaluation with Eq. 1.

3.2 Irwin-Kies Equation and LEFM data reduction schemes

It shall be mentioned in advance that, due to the selected cross-section of the beams, the shear centre is not strictly in the line of action of the applied force for both the UODCB and TODCB specimens, which, in principle, induces a torsional load on the crack tip in the direction of crack propagation and ultimately results in a peel load on the adhesive layer. However, as the force is not applied ideally at a single point but along over a surface in the real experiment, both the centre of area as well as the shear centre of the adherends are still in the "axis" of load application, wherefore the resulting moment components in the direction of crack propagation are considered negligible. Hence, for the data reduction schemes discussed in the following sections, influences of uneven bending are neglected. As will be shown later, this assumption does not influence the experimental results significantly for the selected boundary conditions.

Generally, the fracture energy of an adhesive layer can be computed via the Irwin-Kies equation

$$G = \frac{F_y^2}{2b} \frac{dC(a)}{da} \quad (4)$$

from the applied force F , the width of the adhesive layer b , and the change of compliance $C(a)$ over the change of the lever arm a during crack propagation. The compliance is obtained from the beam's end deflection δ via $\delta = C(a)F_y$. Hence, to determine the fracture energy, assumptions must be made about the compliance of the adherends. For this purpose, three approaches can be distinguished: methods based on Simple Beam Theory (SBT) assume a perfectly built-in cantilever beam clamped at the crack tip, whereas Corrected Beam Theory (CBT) and Experimental Compliance Method (ECM) aim to consider the compliance of the adhesive layer based on experimental data.

3.2.1 Simple Beam Theory approaches

For example, using SBT and assuming a shear-rigid Euler-Bernoulli beam with the known bending stiffness EI_y of the lever arms of length a around the y -axis of the beam, the compliance is obtained via

$$C(a) = \frac{2a^3}{3EI_y}. \quad (5)$$

Derivation of this function with respect to a and inserting it into the Irwin-Kies equation then yields

$$G_{SBT,E}(F_y, a, EI_y) = \frac{F_y^2 a^2}{EI_y b}. \quad (6)$$

Next to the Euler-Bernoulli approach, Timoshenko Beam Theory is also used to accompany shear deformations in the cantilever beam of length a due to transverse force. For this approach, the compliance is given as

$$C(a) = \frac{a^3}{3EI_y} + \frac{a}{\mu\kappa_y A}. \quad (7)$$

with μ as the beam's shear modulus, κ_y as the shear correction factor, and A as the cross-sectional area of the beam. The shear correction factor is used to consider the change in cross-sectional area due to warping as a result of transverse shear and is, for arbitrary cross-sections, obtained via

$$\frac{1}{\kappa_y} = \frac{A}{I_y^2} \int_A \frac{S_y^2(z)}{w^2(z)} dA \quad (8)$$

with the statical moment of area over the beam's height $S_y(z)$ and its width $w(z)$. For the geometry used in this study, a value of $\kappa_y = 0.8481$ was obtained from Eq. 8, which is only slightly larger than the value for a rectangular cross-section ($\kappa_y = 5/6$). Consequently, the Timoshenko Beam Theory approach yields a fracture energy of

$$G_{SBT,T}(F_y, a, EI_y) = \frac{F_y^2}{b} \left(\frac{a^2}{3EI_y} + \frac{2}{\mu\kappa_y A} \right). \quad (9)$$

3.2.2 Approaches independent of crack length

In literature, the ERR according to simple beam theory is generally determined using the force, displacement, and crack length measurements. It should be noted that, depending on the case of application, some of these measurements cannot be performed with reasonable accuracy, e.g., if the crack length cannot be measured due to limited visibility. Hence, it is practical to substitute these quantities with other measurements and employ approaches with an equivalent crack length. For example, under the simple beam theory assumption that the load point displacement of a cantilever beam of equivalent crack length a_{eq} can be calculated via

$$\delta = \frac{2F_y a_{eq,SBT}^2}{3EI_y}, \quad (10)$$

an equivalent crack length of

$$a_{eq,SBT}(F, \delta, EI_y) = \sqrt[3]{\frac{3EI_y \delta}{2F_y}}. \quad (11)$$

is obtained. With this, Eq. 6 can be rewritten as

$$G_{SBT,eq}(F, \delta, EI_y) = \left(\frac{3}{2}\right)^{2/3} \frac{F_y^{4/3} \delta^{2/3}}{b^3 \sqrt[3]{EI_y}}, \quad (12)$$

delivering a method of determining the ERR without the necessity of monitoring crack length. We want to emphasize that, similarly, additional methods of determining the ERR can be obtained if the rotational angles θ of the adherends at the load introduction points are also measured and one assumes

that

$$\theta = \frac{F_y a_{eq,\theta}^2}{2EI_y}. \quad (13)$$

Inserting this into Eq. 6 interestingly gives

$$G_{SBT,\theta}(F_y, \theta) = \frac{2F_y \theta}{b}, \quad (14)$$

which coincides with the J -integral approach to determining the mode III ERR. As stated earlier, this approach has the additional advantage that one must not differentiate between Euler-Bernoulli or Timoshenko beam theory, as the rotational angle yields Eq. 13 for both beam theory approaches. An additional possibility of determining the equivalent crack length is obtained by equating Eqs. 10 and 13,

$$a_{eq,w/oF}(\delta, \theta) = \frac{3\delta}{4\theta}, \quad (15)$$

yielding a possibility of determining the equivalent crack length without relying on external force measurements. From this, the ERR can be calculated via

$$G_{SBT,w/oF}(\delta, \theta, EI_y) = \frac{64EI_y \theta^4}{9b\delta^2}. \quad (16)$$

This approach could be especially interesting for impact testing, in which the applied force may be difficult to measure, whereas the displacement and rotation of the load introduction points could be performed more reliably.

Additionally, the ESBT approach, which was recently developed by Škec et al. [20], shall be investigated. This approach also assumes a fully clamped shear deformable cantilever beam but with the addition of an initial beam root rotation at the crack tip. From this, they derived an equivalent crack length of

$$a_{eq,ESBT}(F_y, \delta, EI_y) = \sqrt[3]{\left(\frac{1}{\sqrt{\alpha}}\right)^3 + a_{eq,SBT}^3} - \frac{1}{\sqrt{\alpha}} \quad (17)$$

with $\alpha = \mu\kappa_y A / EI_y$ and a fracture energy of

$$G_{ESBT}(F_y, \delta, EI_y) = \frac{F_y^2}{b} \left(\frac{a_{eq,ESBT}^2}{EI_y} + \frac{1+2a_{eq,ESBT}\sqrt{\alpha}}{\mu\kappa_y A} \right). \quad (18)$$

3.2.3 Corrected Beam Theory approaches

Next to the SBT approaches that assume the adherends as perfectly built-in cantilever beams clamped at the crack tip discussed so far, the CBT approach attempts to also consider the compliance of the adhesive layer by assuming an Euler-Bernoulli beam with a slightly increased crack length of $a + |\Delta|$, yielding

$$C(a) = \frac{2(a+|\Delta|)^3}{3EI_y}. \quad (19)$$

The value for the correction factor $|\Delta|$ is determined experimentally as the zero-intercept of a linear regression between the cube root of the measured compliance versus the measured crack length. Substituting into the Irwin-Kies

equation then gives four additional methods of determining the ERR:

$$G_{CBT}(a, F_y, EI_y) = \frac{F_y^2(a+|\Delta|)^2}{EI_y b} \quad (20)$$

$$G_{CBT,ISO}(a, \delta, F_y) = \frac{3F_y \delta}{2b(a+|\Delta|)} \quad (21)$$

$$G_{CBT,w/oF}(a, \delta, EI_y) = \frac{9EI_y \delta^2}{4b(a+|\Delta|)^4} \quad (22)$$

$$G_{CBT,\theta}(a, \theta, EI_y) = \frac{4EI_y \theta^2}{b(a+|\Delta|)^2} \quad (23)$$

It shall be noted that Eq. 21 coincides with the approach following ISO 25217 [1], which is commonly used in practice. Eqs. 22 and 23 also have the interesting advantage that the force measurement can be excluded from the evaluation, which may be interesting for impact testing. It should be emphasized that by potentiating measured quantities, a corresponding error propagation results, which can be problematic especially for evaluation methods in which the crack length is included, already allowing the conclusion that G_{CBT} , $G_{CBT,w/oF}$, and $G_{CBT,\theta}$ (Eqs. 20, 22, and 23) may be more sensitive to measurement uncertainties in the crack length measurements. However, it can be assumed that these could still be advantageous compared to other approaches, e.g., when angle, rotation, or force measurements, depending on the case of use, cannot be deemed as reliable as others.

3.2.4 Experimental Compliance Method

A similar approach is taken by the Experimental Compliance Method (ECM), often also denoted as Berry's method [28], in which the compliance is assumed to be a power function:

$$C(a) = ka^n. \quad (24)$$

The value for n is then determined from experimental data as the slope of a linear regression between the logarithm of the obtained compliance and the logarithm of the measured crack length, ultimately yielding a fracture energy of

$$G_{ECM}(F_y, \delta, a) = \frac{nF_y \delta}{2ba}. \quad (25)$$

For the tests with tapered specimens, the Irwin-Kies equation (cf. Eq. 4) is used for the evaluation of the fracture energy with the experimentally determined $dC(a)/da$ (yielding the ECM according to ISO 25217 [1]). As stated earlier, the TODCB specimens are tapered with a linear increase in such a way that $dC(a)/da$ is approximately constant.

3.3 Experimental advantage of the J -integral approach

Before going further, some experimental advantages between the J -integral approach – and the approach according to $G_{SBT,\theta}$ (Eq. 14) which coincides with the J -integral evaluation – and the LEFM data reduction schemes shall be highlighted. With the J -integral approach, the mode III fracture energy is determined by measuring the rotational angles of the adherends at the force introduction points θ_1 and θ_2 under the assumption of linear elastically deforming adherends and small rotational angles. Although the angles of rotation of the substrates must additionally be measured to determine the fracture energy with this method, a measurement of the crack

length becomes superfluous. As the determination of the crack length is generally a difficult measurement task and is, hence, subject to corresponding measurement uncertainties [17], whereas the angle measurement is possible with a very high level of accuracy, the J -integral method is considered a benchmark for the determination of the fracture energy and method comparison within the framework of this study.

Furthermore, doing without the crack length measurement is likely advantageous for measurements in confined spaces (e.g., climate chambers) or during high-speed measurements, in which the determination of crack length becomes increasingly involved. Furthermore, neither must assumptions be made on the function $C(a)$ nor must the values of $dC(a)/da$ be determined experimentally to obtain the fracture energy, further reducing potential sources of error during evaluation. Additionally, when using the rotation of the load introduction points for evaluation, the J -integral results are not influenced by any assumptions on whether the adherends behave as Euler-Bernoulli or Timoshenko beams, whereas, for displacement measurements, which are currently used in most applications in fracture mechanical testing, a shear correction term would be introduced when using Timoshenko beam theory.

3.4 Determination of the cohesive traction

The cohesive traction until the start of crack propagation is determined during monotonic loading by taking the derivative of the fracture energy to the COD δ_t [29], yielding

$$\tau = \frac{dJ_{III}}{d\delta_{t,III}} \cong \frac{dG_{III}}{d\delta_{t,III}} \quad (26)$$

as the nominal shear stress within the adhesive layer. As found by Bödeker and Marzi [30], the unintended contributions to J typically do not influence the cohesive traction obtained from the experiments significantly. It should also be mentioned that the traction separation laws are obtained via the methods of Biel [31] by fitting the measured curves of ERR vs. $\delta_{t,III}$ with a prony series and taking the derivative of the fitted curve to reduce numerical errors.

4. Uniaxial Out-of-plane loaded Double Cantilever Beam tests

4.1 J -integral evaluation

In Fig. 6, the measured mode III ERR according to the J -integral approach is presented for the test series UODCB-A, showing very repeatable results. However, it should be emphasized that, although one would expect an approximately constant value of J during crack propagation, the value of the mode III ERR decreases rapidly after the start of crack propagation, leading to a falling resistance curve. This, as will be shown in the following sections, is related to the crack tip kinematics and can be attributed to an increasing mode I opening of the joint due to the selected boundary conditions. The point at which the process zone reaches the end of the adhesive layer according to the fibre-optics strain measurements (cf. Fig. 10) is also displayed, as this is the instant at which the end of the specimen cannot be considered unloaded anymore. Furthermore, the ratio between the unintended contribution J_{I*} and the mode III ERR is also

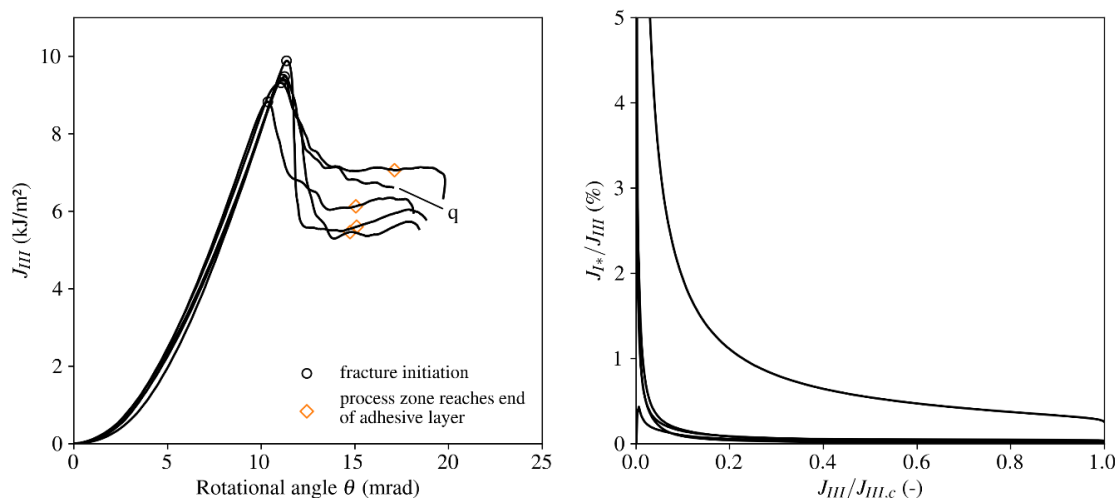


Figure 6 – J -integral evaluation of the UODCB tests, test series UODCB-A: measured mode III J -integral value (left), unintended mode I contribution until the start of crack propagation (right); test indicated with q: error in crack length measurement, the test is eliminated from the LEFM evaluations

displayed over $J_{III}/J_{III,c}$ until the start of crack propagation. The ratio is comparatively large at the beginning of the tests but rapidly tends toward much smaller values until ultimately falling well below 1% in every case at the start of crack propagation, indicating that fracture is initiated close to pure mode III.

It should additionally be mentioned that the dissipated frictional work in the linear slides obtained from the displacement of the lower clamping device and the lateral force acting on the specimen was found to reach a value of just (0.011 ± 0.004) J at the start of crack propagation, which is also considered a negligible influence on the ERR. Therefore, it can also be concluded that an evaluation of the critical ERR under the assumption of even bending is, indeed, practical, as the contributions due to the torsion of the specimens are negligible at the start of crack propagation.

4.2 Crack tip kinematics and cohesive traction

The mode I and mode III components of the COD until the start

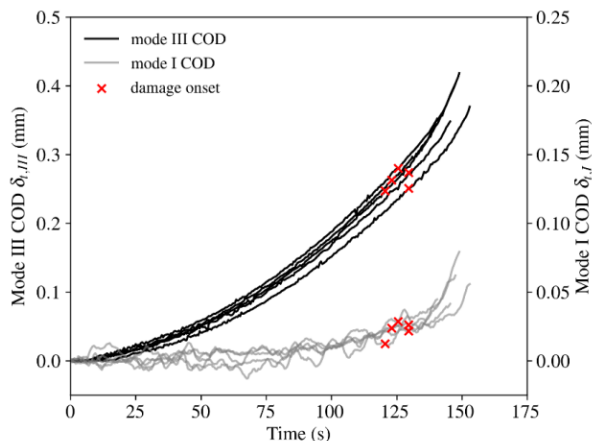


Figure 7 – Mode I and mode III COD measurements during UODCB tests

of crack propagation are displayed in Fig. 7 for test series UODCB-A. Here, it can be observed that the mode I component is generally smaller than the mode III component but unequal to nought. This is due to lateral contraction of the adhesive [15] and the transverse moments 1M_x and 2M_x , which will inevitably cause slight twisting of the adherends, hence opening the joint in mode I on one side of the joint and closing in the other [16]. It should also be noted that the twisting of the adherends due to the moments around the axis of crack propagation can also result in a mode II COD. However, this component is difficult to determine because of the limited visibility of the crack tip and the non-linear deformation field of the adhesive layer at the crack tip. It can also be observed that the mode I component of the COD $\delta_{I,t}$ increases relatively steadily until the start of damage initiation according to the traction separation law (cf. Fig. 9), after which $\delta_{I,t}$ rapidly accelerates: At this point, $\delta_{I,t}$ contributes approx. (8.1 ± 1.1) % to the total magnitude of the COD. At the start of crack propagation, the mode I COD $\delta_{I,t}$ contributes (14.9 ± 2.6) % to the magnitude of the COD.

After the start of crack propagation, as stated earlier, it was observed that the ERR decreases. As shown for a representative specimen in Fig. 8, with a growing crack, the relative influence of the mode I COD at the current crack tip increases, leading to a tilting of the specimen. To roughly quantify this, the tilting of the specimen around the axis of crack propagation (x -axis) as obtained by the DIC measurements is also shown in the figure. It can be observed that the rotation of the specimen around the axis of crack propagation increases with a propagating crack, implying that a mode I influence on the fracture behaviour is likely the cause for the falling resistance curve. Hence, it must be concluded that the proposed test is suitable for the determination of the critical mode III ERR at fracture initiation but does not allow the determination of the propagation value of J due to increased mode I influence on the fracture behaviour with crack growth, as mode I fracture is energetically favourable over mode III fracture.

The mean traction separation law obtained from Eq. 26 is displayed in Fig. 9 for test series UODCB-A. A comparison

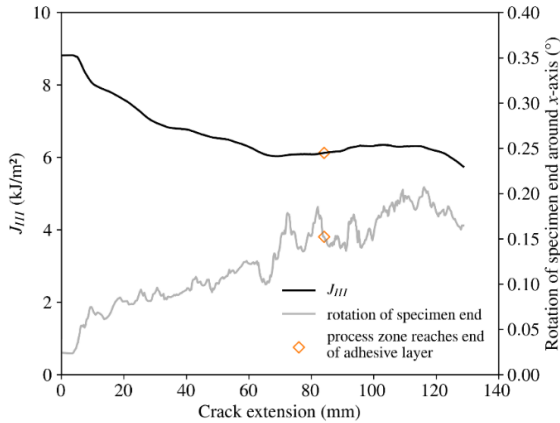


Figure 8 – Resistance curve obtained during a representative UODCB test in comparison to the end rotation of the specimen

with the mode III results of Loh and Marzi [32] (corrected in [33]) and the mode II results of Marzi et al. [3] shows that the proposed uniaxial setup delivers a tri-linear cohesive law with equivalent initial stiffness and plateau stress. Furthermore, the point of damage initiation according to the cohesive law fits well between the experimental setups. However, after damage initiation, the traction decreases more rapidly in the performed UODCB in comparison to the pure mode III tests of Loh and Marzi [32] or the pure mode II tests of Marzi et al. [3]. This can likely be attributed to the strongly increasing mode I influence on the total magnitude of the COD after damage initiation, as mode I fracture is energetically favourable. It shall, again, be highlighted that the obtained mode III fracture energy according to Eq. 1 – and $G_{SBT,\theta}$ (Eq. 14), respectively – and the obtained traction separation law shown in Fig. 9 shall be considered the benchmark values for the following method comparisons.

4.3 Crack growth and process zone length

The measured crack length and the equivalent crack length from Eqs. 11, 13, 15 and 17 are shown over the measured crack extension in Fig. 10 (test series UODCB-A). Furthermore, in

Tab. 2, the results from linear regressions of the shown curves are given. The intercept of the regression line with the ordinate corresponds to a virtual crack extension by which the initial crack length is overestimated by the equivalent crack length, a regression slope of 1 corresponds to a perfect agreement between the measured and equivalent crack extension. The results show that each method of determination yields a virtual crack extension before the crack starts to propagate, which is already an indicator that the SBT assumption of the adherends being perfectly built-in beams at the crack tip is violated. Whereas the methods according to Eq. 11, Eq. 13, and Škec et al. [20] (Eq. 17) yield a good agreement between measured and equivalent crack extension, the method based on Eq. 15, $a_{eq,w/oF}$, delivers comparatively poor results, as the equivalent crack extension underestimates the measured crack extension and the virtual crack extension shows significant scattering. It should be highlighted that $a_{eq,\theta}$ gives the most accurate approximation for the crack extension given that the slope of the regression lines is closest to 1. Hence, it can already be concluded that measuring the rotational angles of the load introduction points allows for a relatively precise determination of the crack extension, wherefore resistance curves can be approximated with very good accuracy without having to monitor the actual crack length. Furthermore, by utilizing the rotational angle for crack length determination, one must not differentiate between Euler-Bernoulli or Timoshenko beam theory assumptions.

Additionally, in Fig. 10, the length of the process zone is shown over the measured crack extension (test series UODCB-A). The length of the process zone is, given measurement noise, approximately constant from the start of crack propagation up to a crack extension of about 85 mm, after which the process zone reaches the end of the adhesive layer. It should be noted that the process zone length of approx. 100 mm at the start of crack propagation also indicates that the compliance of the adhesive layer will have a significant influence on the ERR evaluation methods, thus undermining the necessity of using either the J -integral evaluation, crack length independent methods of determining the ERR, or methods relying on a compliance calibration, e.g., CBT or ECM approaches. It shall also be mentioned that, if a more compliant adhesive was used for the investigation, the length

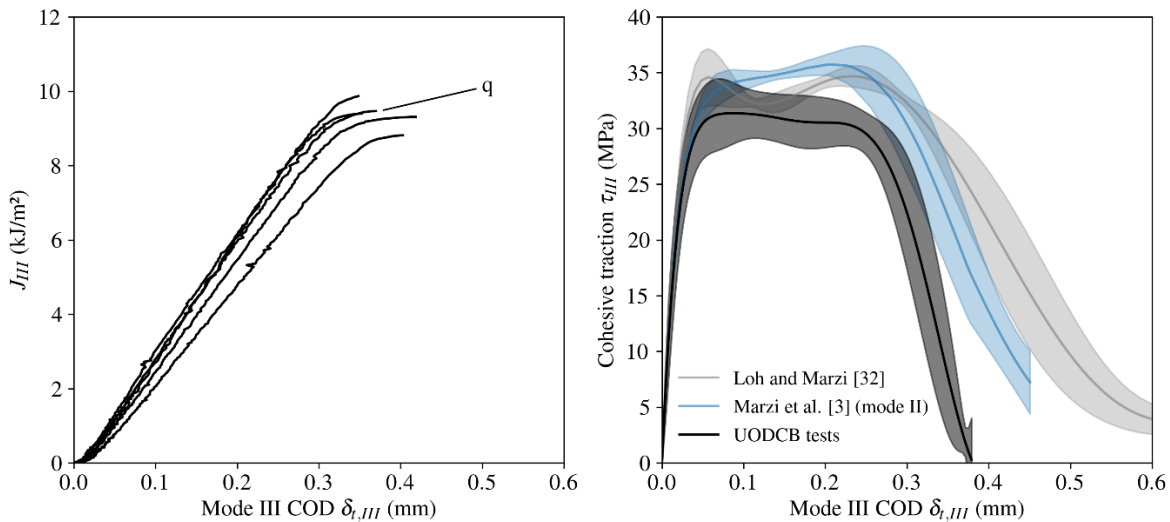


Figure 9 – ERR (left) and cohesive traction (right) obtained from the UODCB experiments

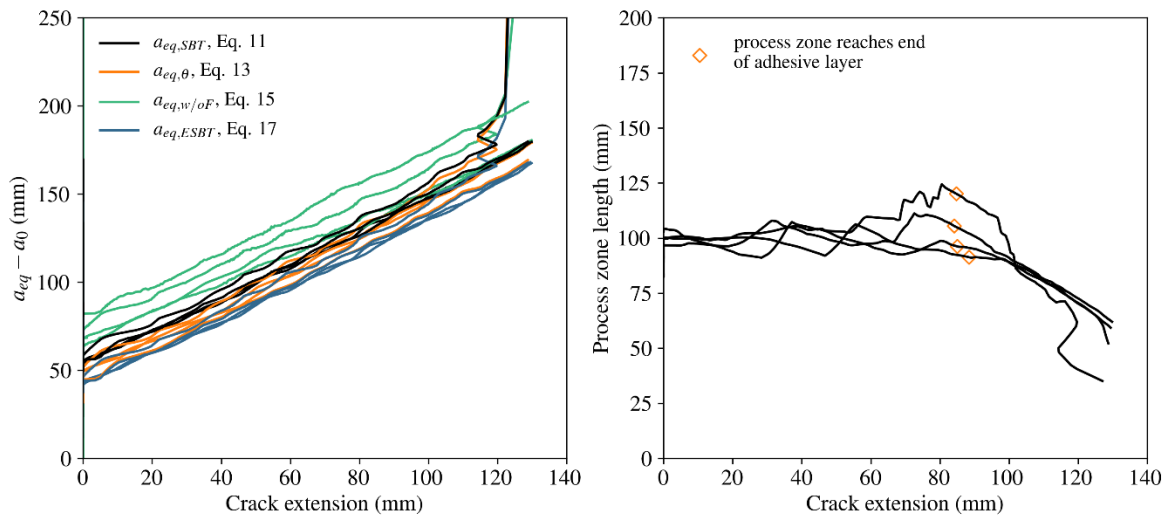


Figure 10 – Crack propagation: comparison between equivalent crack lengths and crack extension measurement (left), process zone length (right)

Table 2 – Comparison of methods for obtaining an equivalent crack length with crack length measurements

	$a_{eq,SBT}$ (Eq. 11)	$a_{eq,\theta}$ (Eq. 13)	$a_{eq,w/oF}$ (Eq. 15)	$a_{eq,ESBT}$ (Eq. 17)
Intercept	52.924 ± 1.960	44.613 ± 2.422	71.123 ± 5.426	40.884 ± 1.959
Slope	0.979 ± 0.017	1.015 ± 0.025	0.895 ± 0.043	0.978 ± 0.017

of the process zone may have a larger influence on the obtained results. The results indicate that investigating the influence of the process zone length on the experimental evaluation of the ERR and cohesive traction could be worthwhile, especially when testing soft, rubber-like adhesive layers.

4.4 Comparison with LEM Data Reduction Schemes for the determination of the critical ERR

As stated earlier, the virtual crack extension $|\Delta|$ for the CBT approaches to data reduction is generally determined from a linear regression between the measured crack length and the cube root of the measured compliance, whereas the ECM parameter n is determined from a linear regression between the logarithms of both quantities. In Fig. 11, both the experimental values from test series UODCB-A and UODCB-B are shown. For the test series UODCB-A, the regression is performed from the start of crack propagation up to the point at which the process zone reaches the end of the adhesive layer (cf. Fig. 10). Furthermore, for the test series with varying initial crack lengths (UODCB-B), both the compliance at the start of crack propagation as well as the compliance in the initial linear range of the force-displacement curves are displayed. It can be observed that – for both the CBT and the ECM approach – the determined regression lines generally show a very good agreement between the test series if the compliance is taken at the start of crack propagation. If the initial compliance of the specimen is considered, an “offset” can be observed, which is likely due to the compliance of the adhesive layer being smaller at this point because the process zone has not yet fully developed. This, in effect, affects the value of $|\Delta|$, as the intercept with the abscissa is sensitive to “offsets” in specimen compliance. When determining the ECM parameter n , this offset is insignificant, which is also indicated by the good agreement in regression slopes between the test series. The obtained parameters for $|\Delta|$ and n for all test series and

methods of evaluation are summarized in Tab. 3. It should be highlighted that the values for $|\Delta|$ and n obtained from the experiments at different initial crack lengths at the start of crack propagation in test series UODCB-B agree well with the values obtained during crack propagation in test series UODCB-A. From this, it can be concluded that the values for $|\Delta|$ and n may be approximated with reasonable accuracy from pretests with various initial crack lengths, allowing for a multi-specimen compliance calibration.

Table 3 – Determined parameters for CBT and ECM evaluation of the ERR (UODCB)

Test series	$ \Delta $	n
UODCB-A	62.305 ± 2.970	1.8026 ± 0.0352
UODCB-B, fracture initiation	59.811	1.8322
UODCB-B, linear range of F - δ -curve	53.687	1.8822

To compare the different methods of evaluation, in Fig. 12, the ERR until the start of crack propagation according to the individual methods as well as the obtained cohesive traction are displayed for one representative specimen from test series UODCB-A. It can be observed that the approaches containing the current crack length with underlying SBT assumptions deliver poor results in determining the ERR as was already implied in Sec. 4.3. Blackman et al. [34] also observed significant discrepancies between the SBT and other approaches in pure mode I testing, concluding that the other methods of evaluation are preferable. It seems that this discrepancy becomes even more prevalent in mode III testing, which is likely due to the adhesive layer being more compliant in shear than in peel and neglecting the effects of the adhesive layer’s compliance and beam root rotation is, hence, an even larger potential source of error.

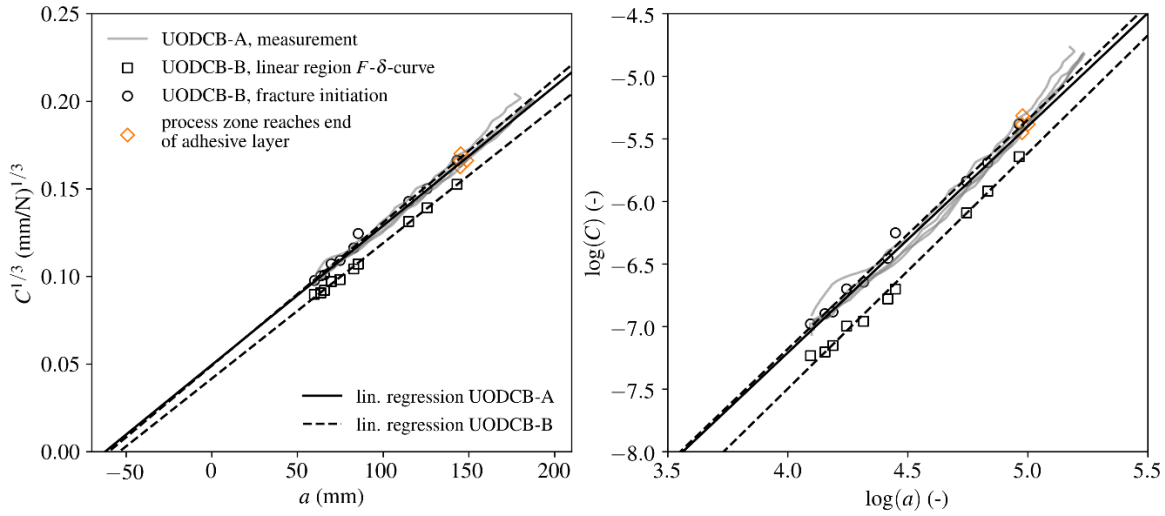


Figure 12 – Determination of virtual crack extension $[\Delta]$ and ECM parameter n for UODCB specimens

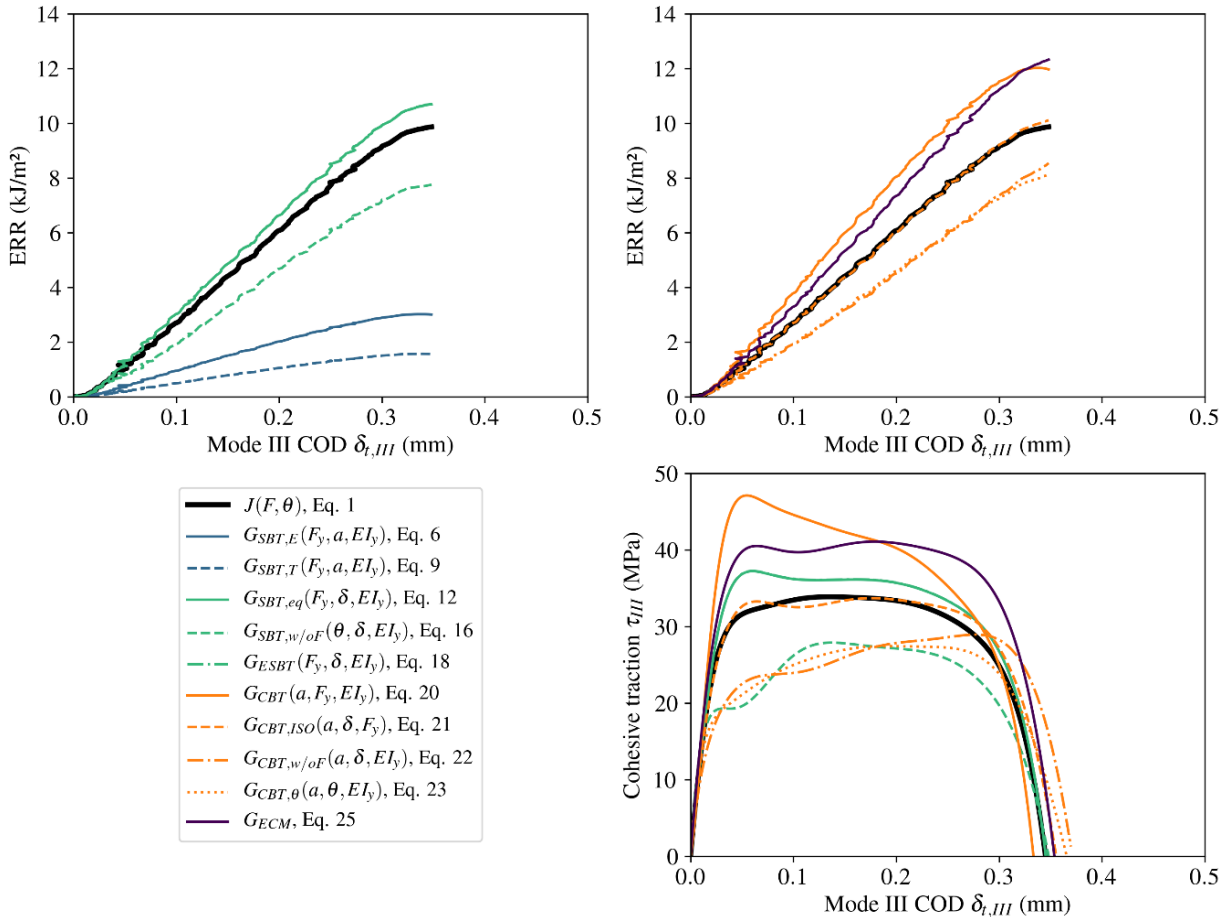


Figure 11 – Comparison of the different data reduction methods with the J -integral benchmark

The crack length independent approaches show a mixed performance in determining the critical ERR: whereas the method based on the applied force and displacement, $G_{SBT,eq}$ (Eq. 12), and the ESBT approach (Eq. 18) coincide and show results comparable to the J -integral benchmark, the crack length independent method from load point displacement and

rotational angles, $G_{SBT,w/oF}$ (Eq. 16), underestimates the critical ERR. For the CBT approaches, the CBT method standardized in ISO 25217 [1], $G_{CBT,ISO}$ (Eq. 21), gives the most accurate result for the determination of the critical ERR. The other CBT approaches, i.e., $G_{CBT,ISO}$, $G_{CBT,w/oF}$, and $G_{CBT,\theta}$ (Eqs. 20, 22, and 23), which also include potentiated

measured quantities such as crack length, displacement or rotational angles show less accurate results and deviate significantly from the J -integral benchmark. However, as stated earlier, depending on the case of use, e.g., when the force measurement cannot be deemed reliable during impact testing it is assumed that the methods of data reduction following Eq. 22 and 23 can still potentially be considered a viable alternative for determining the ERR. According to Biel [31], using the linear fit for determining the parameter n in the ECM method results in G_{ECM} (Eq. 25) overestimating the ERR for short cracks and underestimating it for long cracks. It is assumed that this is the reason for the ECM approach also not giving satisfying results when determining the critical ERR in comparison to the J -integral benchmark.

Considering the traction separation laws, it can be observed that all methods of determination yield an equivalent adhesive stiffness, implying that, as long as the material behaviour is mostly linear elastic, the different data reduction schemes deliver comparable results. Furthermore, the point of damage initiation is also very similar for all shown methods. However, the plateau value of the tri-linear traction separation law obtained from the J -integral evaluation method is only matched by the crack length independent approaches according to Eqs. 12 and 18 and the CBT evaluation method standardized in ISO 25217 [1] $G_{CBT,ISO}$ (Eq. 21).

5. Tapered out-of-plane loaded double cantilever beam tests

In Fig. 13, the measured force-displacement curves from the TODCB specimens as well as the determination of dC/da from the simultaneous crack length measurements and multi-specimen compliance calibration method are displayed. The obtained values for dC/da are summarized in Tab. 4. As can be observed, the applied force reaches a plateau during crack propagation until the process zone reaches the end of the adhesive layer. Akin to the compliance calibration from the UODCB tests, the values for dC/da agree with the simultaneous crack length measurement and the multi-specimen calibration method if the compliance is taken at the start of crack propagation.

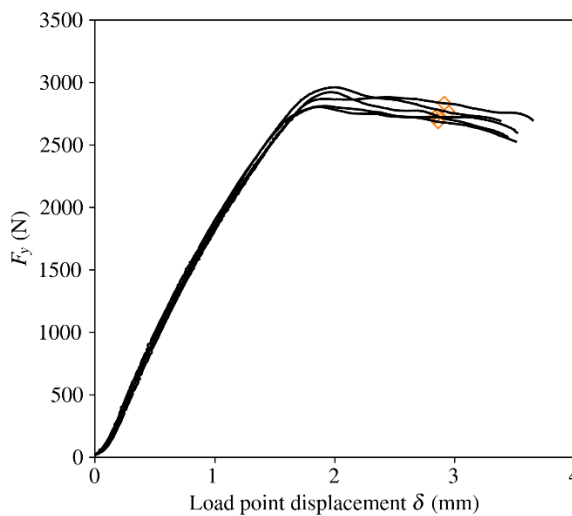


Table 4 – Determined parameters for CBT and ECM evaluation of the ERR (TODCB)

Test series	dC/da
TODCB-A	$(1.1637 \pm 0.1353) \cdot 10^{-5}$
TODCB-B, fracture initiation	$1.1959 \cdot 10^{-5}$
TODCB-B, linear range of F - δ -curve	$1.0624 \cdot 10^{-5}$

The mode I and mode III components of the COD until the start of crack propagation are displayed for test series TODCB-A in Fig. 14. Akin to the UODCB results for the crack tip kinematics (cf. Fig. 6), the mode I component of the COD $\delta_{I,t}$ increases relatively steadily until the start of damage initiation according to the traction separation law (cf. Fig. 16), with $\delta_{I,t}$ also accelerating after the damage onset. At the damage onset, $\delta_{I,t}$ contributes about $(8.4 \pm 2.1) \%$ to the total magnitude of the COD, which is comparable to the mode I influence during the UODCB tests. At the start of crack propagation, the mode I COD $\delta_{I,t}$ contributes $(11.4 \pm 2.1) \%$ to the total COD. This value is significantly smaller than in the UODCB tests, which may be an indicator that the mode I influence on the fracture

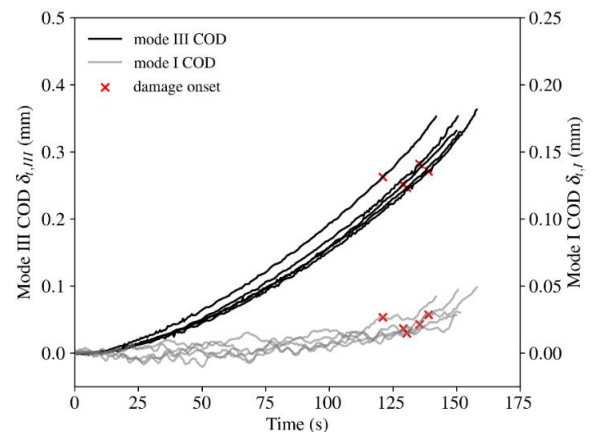


Figure 13 – Mode I and mode III COD measurements during TODCB tests

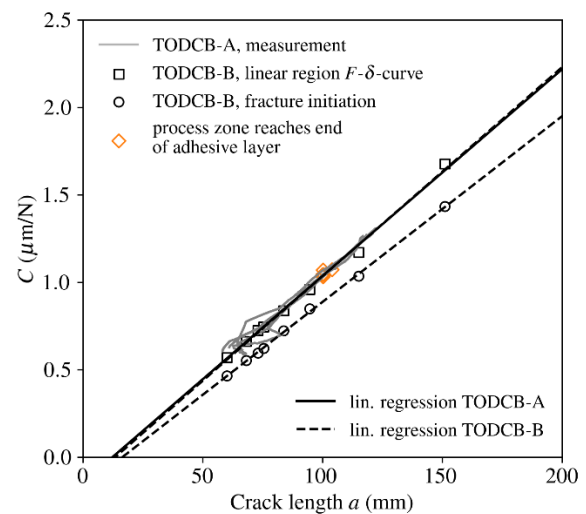


Figure 14 – Force-displacement and compliance results from the TODCB experiments

behaviour is less pronounced during crack propagation in the TODCB experiment, which correlates with the obtained force plateaus during crack propagation.

The length of the process zone is shown in Fig. 15 alongside the resistance curve and the specimen's rotation around the axis of crack propagation for a representative specimen. As can be observed, the process zone is larger than in the UODCB experiments. In effect, the crack may only propagate for approx. 40 mm before the process zone reaches the end of the adhesive layer. As can also be seen, the resistance curve shows an approximately constant ERR during crack propagation, with the end rotation of the specimen also being relatively constant. This indicates that, during the TODCB tests, the mode I influence on the fracture behaviour is more constant during crack propagation, hence yielding constant ERR during crack propagation.

In Fig. 16, the mode III ERR is displayed over the measured $\delta_{III,t}$ with the dC/da obtained from the test series TODCB-A. Furthermore, the mean traction separation law is displayed alongside the results from test series UODCB-A, showing a

very good agreement. It can therefore be concluded that both proposed test setups are suitable for determining traction separation laws and deliver equivalent results.

6. Discussion

6.1 Method comparison

The influence of the different methods of evaluation is highlighted in Fig. 17, in which the values of the ERR at the start of crack propagation are shown for each method of evaluation. As was already stated earlier, the critical ERR obtained from the J -integral is assumed to give the most accurate result as it is not influenced by any beam theory assumptions other than that the adherends shall behave as linear elastic beams and may be obtained from quantities that can be measured directly with very good accuracy. The LEFM approaches to determining the UODCB tests generally deliver mixed results in comparison to the J -integral benchmark, with

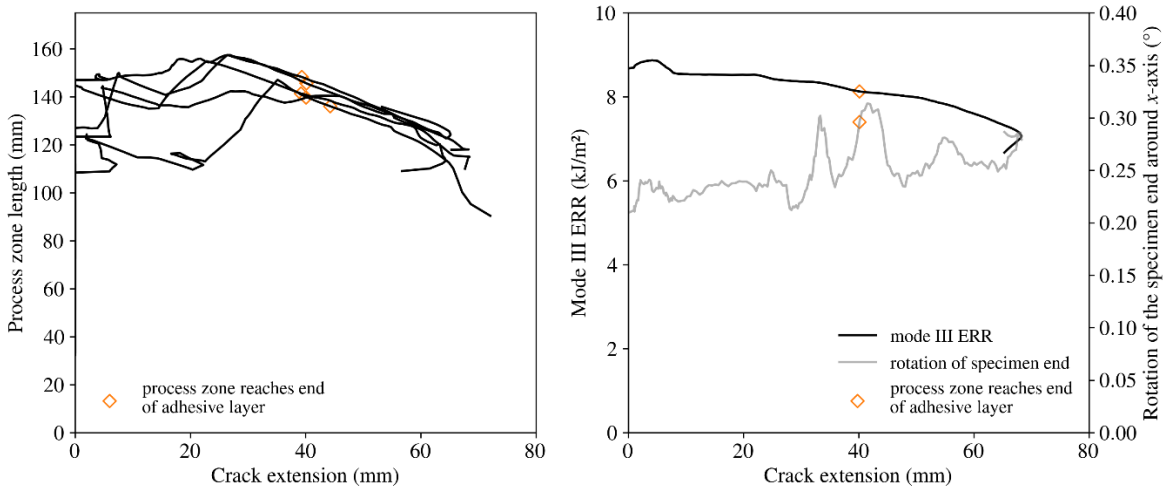


Figure 15 – Crack propagation during TODCB tests: process zone length (left), resistance curve obtained during a representative TODCB test in comparison to the end rotation of the specimen (right)

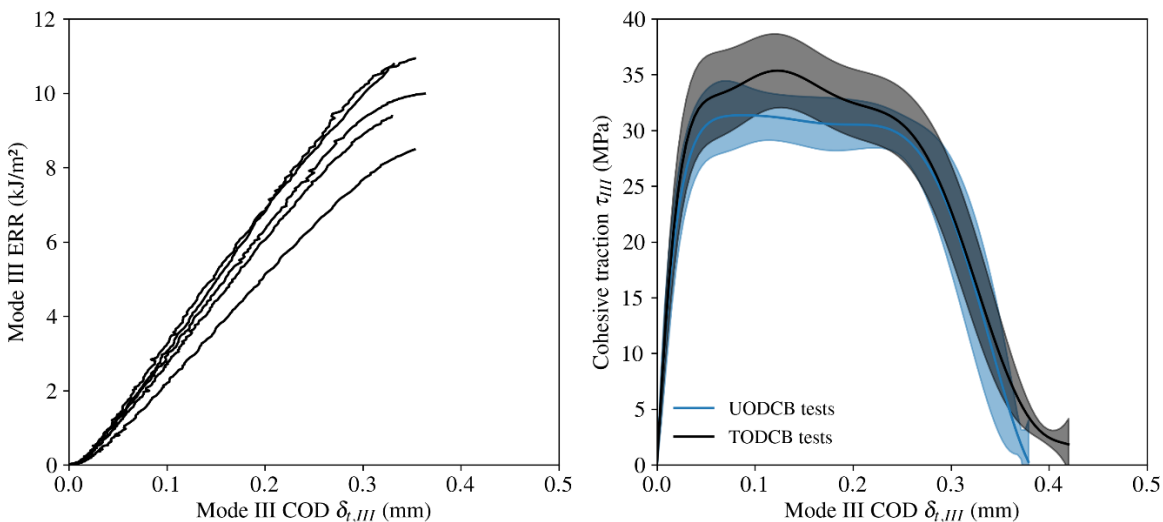


Figure 16 – Energy release rate (left) and cohesive traction (right) obtained from the TODCB experiments

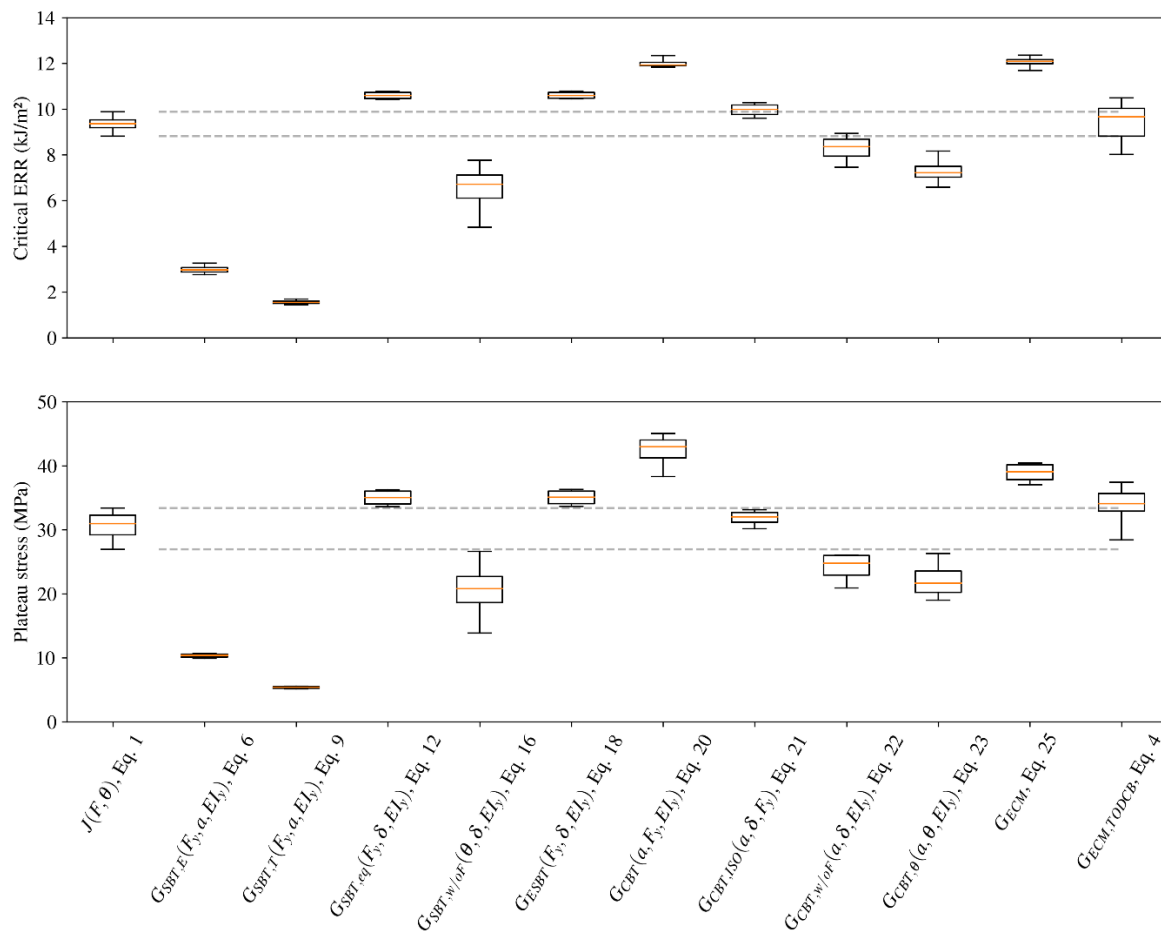


Figure 17 – Boxplot comparison between the evaluation methods; orange line denotes the median value, squares denote standard deviation, error bars denote minimum and maximum measured values

the CBT method standardized in ISO 25217 [1] $G_{CBT,ISO}$ and the crack independent methods using equivalent crack lengths obtained from SBT and ESBT, i.e., $G_{SBT,eq}$, $G_{SBT,\theta}$ (which coincides with the J -integral solution), and G_{ESBT} , delivering the most accurate results. This is also in agreement with the findings of Pérez-Galmés et al. [17], who compared the J -integral evaluation and LEFM approaches for various mode II test setups and found that the results varied strongly between the test setups when using LEFM evaluation methods due to inaccuracies in the crack length measurements, whereas the J -integral evaluation delivered a constant ERR. Especially the methods without force measurements, e.g., $G_{SBT,w/oF}$, $G_{CBT,w/oF}$, and $G_{CBT,\theta}$ (Eqs. 16, 22, and 23), will be affected increasingly by inaccuracies in the crack length measurements, because crack length and other measured quantities are included in higher orders, increasing the experimental scatter. Furthermore, erroneous values for the bending stiffness will also have a large influence on the obtained ERR for the LEFM methods, which may especially be problematic for testing composites.

It should be strongly highlighted that the crack length could be measured very accurately in this study by using fibre-optics strain measurements, which, however, requires a very large amount of experimental effort. If the crack length were to be determined visually, it should be emphasized that the LEFM

methods will inevitably deliver less accurate results when determining the ERR, as the determination of crack length is generally a difficult task. Hence, we strongly advocate for using the J -integral approach for the determination of the ERR, as it does not rely on assumptions on the compliance of the adherends and the crack length measurement is not necessary, minimizing the influence of measurement uncertainties and obviating the necessity of determining corrective factors such as $|\Delta|$ or n in the CBT and ECM approaches, respectively.

It should also be noted that the critical ERRs and the cohesive traction obtained from the UODCB and TODCB tests are in very good agreement. Interestingly, in comparison to the UODCB tests in which a falling resistance curve was observed, the TODCB test shows a relatively constant ERR during crack propagation. It is suspected that the increasing out-of-plane bending stiffness with crack length in the tapered specimens could counteract mode I deformations of the adhesive layer, which was observed by the approximately constant rotational angle of the specimen end around the axis of crack propagation (cf. Fig. 13). Furthermore, the larger process zone may cause the loads to act more evenly on the adhesive layer, which could also result in a reduced influence of mode I deformations at the crack tip during crack propagation.

6.2 Methodological Critique

Before we conclude, some methodological critique and a discussion of the potential of the proposed test setups shall be given: In this study, we relied on a floating bearing of the lower clamping of the specimen to minimize lateral moments, which could potentially damage the testing machine. Hence, in the context of this proof-of-concept study, we preferred to use a more complicated test setup and used DIC to determine the boundary conditions and the kinematics of the specimen instead of risking damage to the testing machine. Furthermore, the floating bearing and the negligible influence of the transverse forces on the mode III ERR in the UODCB tests may allow testing with a uniaxial load cell in future investigations. In comparison to the works of Chai [9], Donaldson [10], and Stigh et al. [14], in which great care was taken to design specimens that yield torsionless bending under mode III deformations, the necessity of using floating bearings to minimize these lateral moments is a disadvantage of the setups presented in this study. However, as the test setups of Chai [9], Donaldson [10], and Stigh et al. [14] were limited to wider adhesive layers and the design of the adherends represents an additional difficulty, the complex kinematics of the specimen were accepted in this study to enable testing of narrower adhesive layers. In future studies, however, it is deemed worthwhile to evaluate whether using a positionally fixed lower clamping could simplify the kinematics of the specimen, possibly yielding a more constant ERR during crack propagation in the UODCB tests. However, extreme care should be taken to not damage the testing equipment. Furthermore, using six-axis loads at the points of load introduction is considered mandatory in this case, as contributions to the fracture energy could otherwise not be determined.

Above all, it should also be admitted that for the method comparison, with the selected angle measurement of the load introduction points, it is not yet possible to distinguish reliably between loading with piano hinges or end-blocks, which is why the large displacement and end-block corrections according to ISO 25217 [1] were not implemented in the context of this study. In the future, the influence of this on the results should be investigated more closely to be able to make better estimates for comparison between the J -integral and LEFM approaches.

In a subsequent study [16], we found that it could be beneficial to develop a uniaxial test setup for mode III testing at elevated loading rates. It is believed that the presented UODCB and TODCB setups could prove useful especially in testing at increased loading rates, e.g., in drop towers or high-speed tensile test rigs. Furthermore, it is assumed that the proposed setups may be beneficially used in confined spaces such as climate chambers, enabling the investigation of environmental influences on the mode III fracture behaviour of adhesive joints.

Generally, we advise that the test setups are investigated numerically by the use of Finite Element Analysis in future simulative work to better understand the proposed test setups and their possibilities for use in industrial applications. Furthermore, we advise that the proposed CBT methods could also be applied for mode I testing, as depending on the given measured variables, advantages could be achieved in some test designs, for example by eliminating the force measurement from the ERR at high loading rates.

7. Conclusions

In the present study, two experimental setups, i.e., the Uniaxial Out-of-plane loaded Double Cantilever Beam Test (UODCB) and the Tapered Out-of-plane loaded Double Cantilever Beam test (TODCB), were proposed based on the works of Mai [7], Chai [9], Donaldson [10], and Stigh et al. [14] to determine the critical mode III ERR and cohesive laws of adhesive layers. Crack length and process zone length were evaluated using backface strain measurements. Various evaluation methods based on the J -integral and Irwin-Kies Equation are investigated for the determination of critical ERR and cohesive traction and thoroughly compared. Within the limitations of this study, the following conclusions can be drawn:

- The proposed UODCB and TODCB setups allow a simplified determination of the critical mode III ERR and cohesive laws in uniaxial test setups. The J -integral evaluation of the UODCB tests provides the most accurate value for the critical mode III ERR as the least measurement uncertainties or beam theory assumptions are necessary to obtain the critical ERR. When using CBT or ECM data reduction schemes, a multi-specimen compliance calibration is deemed reliable if the compliance is taken at the start of crack propagation.
- When using the applied force and rotational angle of the load introduction points for the evaluation of the UODCB experiments, the J -integral solution and Griffith ERR coincide, allowing for a determination of the ERR without having to monitor the current crack length.
- The equivalent crack extension in the UODCB tests determined using SBT and ESBT assumptions, despite an initial offset, matches well with the actual crack extension. The SBT method using force and rotational angle seems to deliver the most precise approximation for the actual crack extension.
- The backface strain measurements showed that the process zone lengths during crack propagation were well above 100 mm, implying that the process zone reaches the end of the specimen relatively early, especially in the TODCB experiments. A future, in-depth investigation on the influence of the process zone length on the determination of ERR and cohesive traction is therefore deemed worthwhile.

References

- [1] International Organization for Standardization, Adhesives — Determination of the mode I adhesive fracture energy of structural adhesive joints using double cantilever beam and tapered double cantilever beam specimens, 25217th ed., 2009.
- [2] D30 Committee, Test Method for Determination of the Mode II Interlaminar Fracture Toughness of Unidirectional Fiber-Reinforced Polymer Matrix Composites, ASTM International, West Conshohocken, PA.
- [3] S. Marzi, A. Biel, U. Stigh, On experimental methods to investigate the effect of layer thickness on the fracture behavior of adhesively bonded joints, *International Journal of Adhesion and Adhesives* 31 (2011) 840–850. <https://doi.org/10.1016/j.ijadhadh.2011.08.004>.
- [4] U. Stigh, A. Biel, T. Walander, Shear strength of adhesive layers – Models and experiments, *Engineering Fracture Mechanics* 129 (2014) 67–76. <https://doi.org/10.1016/j.engfracmech.2014.07.033>.

- [5] S. Marzi, Measuring the critical energy release rate in mode II of tough, structural adhesive joints using the tapered end-notched flexure (TENF) test, *Eur. Phys. J. Spec. Top.* 206 (2012) 35–40. <https://doi.org/10.1140/epjst/e2012-01584-4>.
- [6] B. Blackman, A.J. Kinloch, M. Paraschi, The determination of the mode II adhesive fracture resistance, GIIC, of structural adhesive joints: an effective crack length approach, *Engineering Fracture Mechanics* 72 (2005) 877–897. <https://doi.org/10.1016/j.engfracmech.2004.08.007>.
- [7] Y.W. Mai, Quasi-Static Adhesive Fracture, *The Journal of Adhesion* 7 (1975) 141–153. <https://doi.org/10.1080/00218467508075046>.
- [8] A.J. Kinloch, *Adhesion and Adhesives*, Springer Netherlands, Dordrecht, 1987.
- [9] H. Chai, Shear fracture, *International Journal of Fracture* 37 (1988) 137–159. <https://doi.org/10.1007/BF00041716>.
- [10] S.L. Donaldson, Mode III interlaminar fracture characterization of composite materials, *Composites Science and Technology* 32 (1988) 225–249. [https://doi.org/10.1016/0266-3538\(88\)90022-X](https://doi.org/10.1016/0266-3538(88)90022-X).
- [11] R.H. Martin, Evaluation of the Split Cantilever Beam for Mode III Delamination Testing, in: T.K. O'Brien (Ed.), *Composite Materials: Fatigue and Fracture (Third Volume)*, ASTM International, 100 Barr Harbor Drive, PO Box C700, West Conshohocken, PA 19428-2959, 1991, 243–243-24.
- [12] A.L. Johnston, B.D. Davidson, K.K. Simon, Assessment of split-beam-type tests for mode III delamination toughness determination, *Int J Fract* 185 (2014) 31–48. <https://doi.org/10.1007/s10704-013-9897-1>.
- [13] H. Yoshihara, Examination of the 4-ENF test for measuring the mode III R-curve of wood, *Engineering Fracture Mechanics* 73 (2006) 42–63. <https://doi.org/10.1016/j.engfracmech.2005.06.008>.
- [14] U. Stigh, A. Biel, D. Svensson, Cohesive zone modelling and the fracture process of structural tape, *Procedia Structural Integrity* 2 (2016) 235–244. <https://doi.org/10.1016/j.prostr.2016.06.031>.
- [15] L. Loh, S. Marzi, An Out-of-plane Loaded Double Cantilever Beam (ODCB) test to measure the critical energy release rate in mode III of adhesive joints: Special issue on joint design, *International Journal of Adhesion and Adhesives* 83 (2018) 24–30. <https://doi.org/10.1016/j.ijadhadh.2018.02.021>.
- [16] P. Schrader, S. Marzi, Mode III testing of structural adhesive joints at elevated loading rates, *International Journal of Adhesion and Adhesives* (2022) 103078. <https://doi.org/10.1016/j.ijadhadh.2021.103078>.
- [17] M. Pérez-Galmés, J. Renart, C. Sarrado, A.J. Brunner, A. Rodríguez-Bellido, Towards a consensus on mode II adhesive fracture testing: Experimental study, *Theoretical and Applied Fracture Mechanics* 98 (2018) 210–219. <https://doi.org/10.1016/j.tafmec.2018.09.014>.
- [18] G. Stamoulis, N. Carrere, Linear elastic analysis of the loading rate dependency of the fracture properties of structural adhesives in the mixed mode I+II plane, *Engineering Fracture Mechanics* 225 (2020) 106840. <https://doi.org/10.1016/j.engfracmech.2019.106840>.
- [19] L. Loh, S. Marzi, A Mixed-Mode Controlled DCB test on adhesive joints loaded in a combination of modes I and III, *Procedia Structural Integrity* 13 (2018) 1318–1323. <https://doi.org/10.1016/j.prostr.2018.12.277>.
- [20] L. Škec, G. Alfano, G. Jelenić, Enhanced simple beam theory for characterising mode-I fracture resistance via a double cantilever beam test, *Composites Part B: Engineering* 167 (2019) 250–262. <https://doi.org/10.1016/j.compositesb.2018.11.099>.
- [21] J.R. Rice, A Path Independent Integral and the Approximate Analysis of Strain Concentration by Notches and Cracks, *Journal of Applied Mechanics* 35 (1968) 379–386. <https://doi.org/10.1115/1.3601206>.
- [22] A.J. Paris, P. Paris, Instantaneous evaluation of J and C, *International Journal of Fracture* (1988) R19–R21.
- [23] A. Bernasconi, M. Kharshiduzzaman, L. Comolli, Strain Profile Measurement for Structural Health Monitoring of Woven Carbon-fiber Reinforced Polymer Composite Bonded joints by Fiber Optic Sensing Using an Optical Backscatter Reflectometer, *The Journal of Adhesion* 92 (2016) 440–458. <https://doi.org/10.1080/00218464.2015.1043005>.
- [24] R. Lima, R. Perrone, M. Carboni, A. Bernasconi, Experimental analysis of mode I crack propagation in adhesively bonded joints by optical backscatter reflectometry and comparison with digital image correlation, *Theoretical and Applied Fracture Mechanics* 116 (2021) 103117. <https://doi.org/10.1016/j.tafmec.2021.103117>.
- [25] H.T. Truong, M.J. Martinez, O.O. Ochoa, D.C. Lagoudas, Mode I fracture toughness of hybrid co-cured Al-CFRP and NiTi-CFRP interfaces: An experimental and computational study, *Composites Part A: Applied Science and Manufacturing* 135 (2020) 105925. <https://doi.org/10.1016/j.compositesa.2020.105925>.
- [26] N. Ben Salem, M.K. Budzik, J. Jumel, M. Shanahan, F. Lavelle, Investigation of the crack front process zone in the Double Cantilever Beam test with backface strain monitoring technique, *Engineering Fracture Mechanics* 98 (2013) 272–283. <https://doi.org/10.1016/j.engfracmech.2012.09.028>.
- [27] L. Loh, S. Marzi, Mixed-mode I+III tests on hyperelastic adhesive joints at prescribed mode-mixity, *International Journal of Adhesion and Adhesives* 85 (2018) 113–122. <https://doi.org/10.1016/j.ijadhadh.2018.05.024>.
- [28] J.P. Berry, Determination of Fracture Surface Energies by the Cleavage Technique, *Journal of Applied Physics* 34 (1963) 62–68. <https://doi.org/10.1063/1.1729091>.
- [29] B.F. Sørensen, T.K. Jacobsen, Determination of cohesive laws by the J integral approach, *Engineering Fracture Mechanics* 70 (2003) 1841–1858. [https://doi.org/10.1016/S0013-7944\(03\)00127-9](https://doi.org/10.1016/S0013-7944(03)00127-9).
- [30] F. Bödeker, S. Marzi, Applicability of the mixed-mode controlled double cantilever beam test and related evaluation methods, *Engineering Fracture Mechanics* 235 (2020) 107149. <https://doi.org/10.1016/j.engfracmech.2020.107149>.
- [31] A. Biel, Constitutive behaviour and fracture toughness of an adhesive layer, 2019.
- [32] L. Loh, S. Marzi, A novel experimental methodology to identify fracture envelopes and cohesive laws in mixed-mode I + III, *Engineering Fracture Mechanics* 214 (2019) 304–319. <https://doi.org/10.1016/j.engfracmech.2019.03.011>. Corrected in [33].
- [33] L. Loh, S. Marzi, Corrigendum to “A novel experimental methodology to identify fracture envelopes and cohesive laws in mixed-mode I+III” [Eng. Fract. Mech. 214 (2019), 304–319], *Engineering Fracture Mechanics* 263 (2022) 108294. <https://doi.org/10.1016/j.engfracmech.2022.108294>.
- [34] B. Blackman, A.J. Kinloch, M. Paraschi, W.S. Teo, Measuring the mode I adhesive fracture energy, GIC, of structural adhesive joints: the results of an international round-robin, *International Journal of Adhesion and Adhesives* 23 (2003) 293–305. [https://doi.org/10.1016/S0143-7496\(03\)00047-2](https://doi.org/10.1016/S0143-7496(03)00047-2).

Acknowledgements

This article is part of P. Schrader's doctoral thesis at the Doctoral Center for Engineering Sciences of the Research Campus of Central Hessen under the supervision of the Justus-Liebig-University Giessen in cooperation with the University of Applied Sciences of Central Hessen (Technische Hochschule Mittelhessen).

The authors would like to thank Sabine Wenig (SIKA Automotive, Romanshorn, Switzerland) for supplying the adhesive. Furthermore, we want to thank Dennis Domladovac for his support during the experimental investigation with the fibre-optics system and Jens Minnert and the Institute of Civil Engineering (Technische Hochschule Mittelhessen) for kindly lending us their device for the experimental investigation.

Highlights

- Two mode III test setups are proposed for determining ERR and cohesive traction
- SBT and CBT methods using rotational angle of load introduction points are proposed
- Backface strain measurements for measuring crack extension and process zone length
- J -integral evaluation allows the most accurate determination of critical ERR

Funding Sources

This project is supported by the Federal Ministry for Economic Affairs and Climate Action (BMWK) on the basis of a decision by the German Bundestag [grant number ZB-ZF4283703]. The financial support is gratefully acknowledged.

CRediT authorship contribution statement

Peer Schrader: Conceptualization, Methodology, Formal Analysis, Investigation, Writing – Original Draft, Writing – Review & Editing, Visualization

Stephan Marzi: Resources, Supervision, Funding acquisition